CHAPTER ONE:

INTRODUCTION

1.1 Pyrazine

Pyrazine **[1]** is a stable and colourless compound which is soluble in water. It is a heterocyclic aromatic organic compound with the chemical formula $C_4H_4N_2$. The molecular structure is symmetrical with a point group of D2h. Its derivatives such as phenazine are well known for their antitumor, antibiotic and diuretic activity. Pyrazine is less basic in nature than the other heterocyclics which are pyridine, pyridazine and pyrimidine.

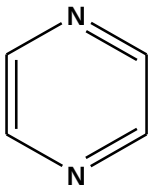

[1]

These three parents heterocyclic, unlike pyridine, are expensive and not readily available and so are seldom used as starting materials for the synthesis of their derivatives. One striking aspect of physical properties of pyrazine is the high boiling point i.e. 118 °C. The high boiling point of pyrazine is attributed to the polarisability of the N-N unit which results in extensive dipolar association in the liquid. The first recorded synthesis of pyrazine was that of tetraphneylpyrazine **[2]** by Laurent in 1855. In this preparation α-phenyl-α-(benzlideneamino)acetonitrile, PhCH=NCHPhCN (benzoylazotid prepared from crude benzaldehyde that is benzaldehyde containing hydrogen cyanide by treatment with ammonia) was subjected to dry distillation to give

amarone. Amarone is a group of simple pyrazine derivatives that has been synthesized. Example of amarone compounds are ketine and glycolin.[1]

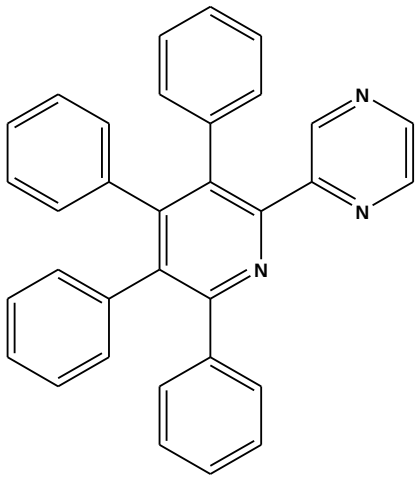

[2]

Many methods exist for the organic synthesis of pyrazine and derivatives and some of them very old. An earliest process that has been reported is in the year 1876, where the pyrazine has been synthesized through Staedel-Rugheimer scheme. This scheme involves the participation of 2-chloroacetophenone with ammonia. The product is amino ketone, which is then condensed and followed by oxidation process that leads to a pyrazine.[2] A variation is the Gutknecht pyrazine synthesis in 1879 as shown in **Figure 1.1** was also based on this self condensation but differing in the way the alpha-ketoamine is synthesized, where the chlorine compound in the above method is a lachrymatory agent.[3]

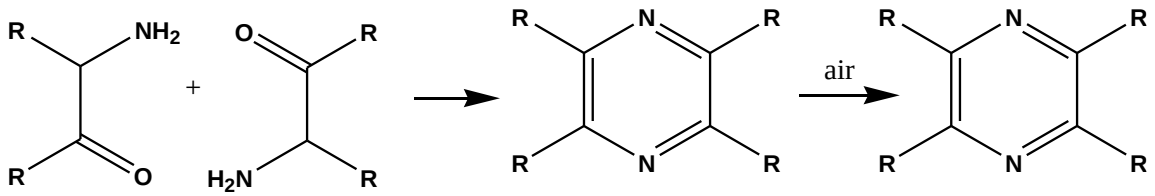

Figure 1.1: Gutknecht pyrazine synthesis

Commercially, the high temperature cyclodehdrogenation of precursor such as *N*-hydroxyethyl ethane-1,2-diamine is used. Symmetrical pyrazines result from the spontaneous self condensation of two moles equivalents of a 2-aminoketone, or 2-aminoaldehyde, followed by an oxidation. In order to produce symmetrical pyrazines, 1,2-dicarbonyl compounds undergo double condensation with 1,2-diamines; an oxidation is then required.[4] An ingenius modification of the general method uses 5,6-diamonouracil as a masked unsaturated 1,2-diamine. The products can be hydrolysed with cleavage of the pyrimidone ring finally arriving at amino-pyrazine acids as products. The pyrazine ring system is found in the fungal metabolite aspergillic acid and in dihydro-form in the luciferins of several beetles, including the firefly, *Cypridina hilgendorfii*, and is responsible for chemiluminescence of this ostracod.[5] Quite many simple methoxypyrazines are very important components of the aromas of many fruits and vegetables, such as peas and Capsicum peppers, and also wines. Although present in very small amounts, they are extremely odorous and can be detected at concentrations as low as 0.00001 ppm.[5] Several polyalkylpyrazines are insect pheromones, for example 2-ethyl-3,6-dimethylpyrazine is the major component of the trail pheromone of the South American leaf-cutting ant. A lot of research involving pyrazines derivatives has been made. As for example, 2-(allylthio)pyrazine (2-AP), a synthetic pyrazine derivative with an allylsulfur moiety has hepatoprotective effects against toxicants. The result shows that 2-AP reduced the volume of liver occupied by GST-P foci by 65–96%.[6] Moreover,

derivatives of imidazo[1,2-α]pyrazines exhibit various pharmacological activities such as antibacterial, anti-inflammatory, uterine relaxing activity, antibronchospastic, antiulcer, cardiac stimulating, antidepressant, hypoglycemic activity, antiproliferative activity, controlling allergic reactions, smooth muscle relaxant properties and phosphodiesterase inhibitory activity. Recently, the compound also shows to inhibit the receptor tyrosine kinase, EphB4.[7] Another research on pyrazine is, cis- and trans-$[Pt(pz)_2(Ypy)_2]^{2+}$ (pz = pyrazine). The ionic pyrazine-bridged dimer cis-$[Pt(NH_3)_2Cl(\mu\text{-}pz)\text{-}Pt(NH_3)_2Cl]Cl_2$ has been reported to possess good antitumor properties.[8] Some pyrazine derivatives are also being known to exhibit a wide variety of aromas in food. For instance, 2-methoxy-3-isopropylpyrazine produces a green pea odor, 2-acetylpyrazine contributes a popcorn-like odor, and dimethyl and trimethylpyrazines exhibit the roast aroma of nuts and coffee respectively.[9] *Chuanxiong* is a frequently used Chinese herb. Alkaloid ligustrazine is one of the active constituents in *chuanxiong*.[10] The chemical name for ligustrazine is tetramethylpyrazine **[3].** *Chuanxiong* has been used in China as medicinal agents for 30 years. The initial applications were based on traditional use of the crude herb in decoctions and pills basically for vitalizing blood circulation in the treatment of cardiovascular diseases and for treatment of headache and vertigo. In fact, trimethylpyrazine also has been used in making artificial flavored syrups that substitute for maple syrup.[11]

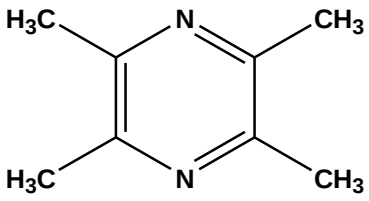

[3]

1.2 Quinoxaline

Quinoxaline **[4],** also called benzopyrazine, is a heterocyclic compound containing a ring complex made up of a benzene ring and a pyrazine ring. It is isomeric with quinazoline **[5],** phthalazine **[6]** and cinnoline **[7].**

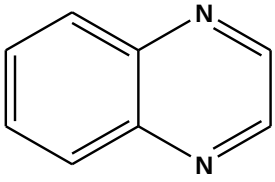

[4]

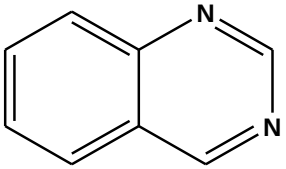

[5]

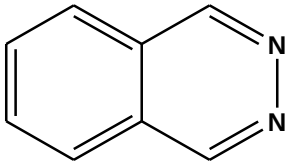

[6]

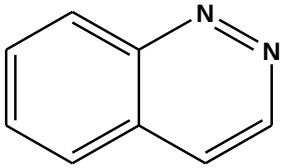

[7]

Quinoxalines are used as dyes, pharmaceuticals and antibiotics such as echinomycin, levomycin and actinoleutin. Some studies were carried out in order to explore the antitumoral properties of quinoxaline compounds.[12] Recently, quinoxaline and its analogues have been investigated as the catalyst's ligands.[13] They can be formed by condensing *ortho*-diamines with 1,2-diketones. The parent substance of the group, quinoxaline, results when glyoxal is condensed with 1,2-diaminobenzene. Substituted derivatives arise when α-ketonic acids, α-chlorketones, α-aldehyde alcohols and α-ketone alcohols are used in place of diketones. Quinoxaline and its analogues may also be form by reduction of amino acids substituted 1,5-difluoro-2,4-dinitrobenzene (DFDNB). 2-

Iodoxybenzoic acid (IBX) has been used as a catalyst in the reaction of benzil with 1,2-diaminobenzene as shown in **Figure 1.2** below.[14]

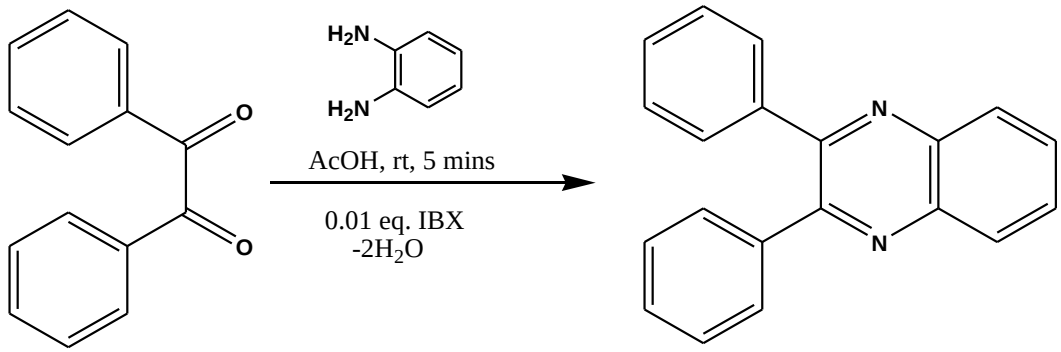

Figure 1.2: Reaction of benzil with 1,2-diaminobenzene

The primary synthesis of quinoxalines may be accomplished by cyclization of benzene substrates already bearing appropriate substituents such as by cyclocondensation of benzene substrates with acyclic synthons to provide one or more of the ring atoms required to complete the pyrazine ring, by analogous processing of preformed pyrazine substrates or by rearrangement, ring expansion/contraction, degradation, or modification of appropriate derivatives of other heterocyclic systems.[15] Quinoxaline derivatives ligands has been studied extensively because its coordination chemistry is rich in structural types and coordination modes.[16] As for example, the new macrocyclic ligands from heterocyclic groups provide rigidity and are able to participate, in some cases, in complexation through their soft donor atoms such as nitrogen and oxygen. This is also applicable to many macrocyclic compounds containing heterocycles such as pyridine, bipyridine, pyrimidine, triazole, pyrazole, imidazole and thiophene have been synthesized and studied. The study of quinoxaline derivatives has become of much interest in recent years due to

their antibacterial, antiviral, anticancer, antifungal, antihelminthes and insecticidal activities.[17] In particular, the di-*N*-oxide derivatives of quinoxaline show a dramatically increase of the diversity of biological properties. For example, some of these organic derivatives have shown hypoxia-selective cytotoxicity and they could be potentially useful for the treatment of solid tumors. Besides, some derivatives have presented excellent *M. tuberculosis* growth inhibition values, leading generally the lack of the two *N*-oxide groups to the loss of the antimycobacterial activity.[18] Although excellent *in vitro* biological results have been obtained with some 3-amino-2-carbonitrile-quinoxaline *N1*, *N*4-dioxide derivatives, they were not useful for therapy owing to too short *in vivo* half lives and low solubility in physiological media.[19] The continued interest in designing new macrocyclic ligands stems mainly from their use as models of protein–metal binding sites in biological systems, as synthetic ionophores, as therapeutic reagents in chelate therapy, as cyclic antibiotics, to study host–guest interactions and in catalysis.[20] Recognition of the importance of macrocyclic compounds and their complexes with metal cations as well as uncharged molecules has led to considerable effort being invested in developing reliable inexpensive synthetic routes to these compounds. Ahmed H. M. Elwahy, in one of his research has produced macrocyclic ligands from another heterocyclic group such as from quinoxaline subunit.[21] Quinoxaline derivatives has been done recently and the compounds were tested against intracellular forms of Leishmania peruviana.[22] Another quinoxaline derivatives compound, quinoxaline-N-acylhydrazones **[8],** has been designed as inhibitors candidates to represent a target for the potential trypanocidal drugs for Chagas disease[23]. Chagas disease is one of the most important medical problems in South America. It is caused by the intracellular protozoan Trypanosoma cruzi, which infects about 9 –12 million people in Central and South America.[24]

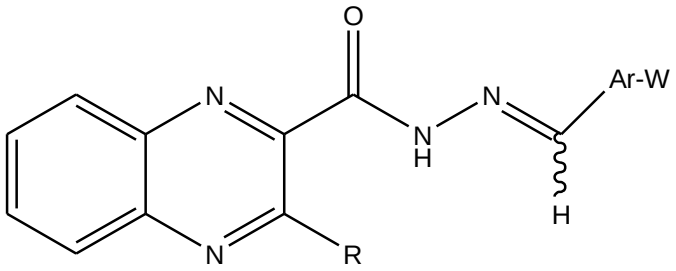

[8]

In recent years, structurally diverse cannabinoid receptor type 2, abbreviated as CB_2, is a G protein-coupled receptor from the cannabinoid receptor family that in humans is encoded by the *CNR2* gene. It is responsible for the efficacy of endocannabinoid-mediated presynaptic-inhibition, the psychoactive properties of tetrahydrocannabinol, the active agent in marijuana,and other phytocannabinoids. CB2 selective agonists exhibiting analgesic activity in various pain models have been discovered and recently reviewed. Phenoxyquinolines **[9]** were synthesized using microwave irradiation and its ability to act as CB2 receptor-dependent G-protein has been studied.[25]

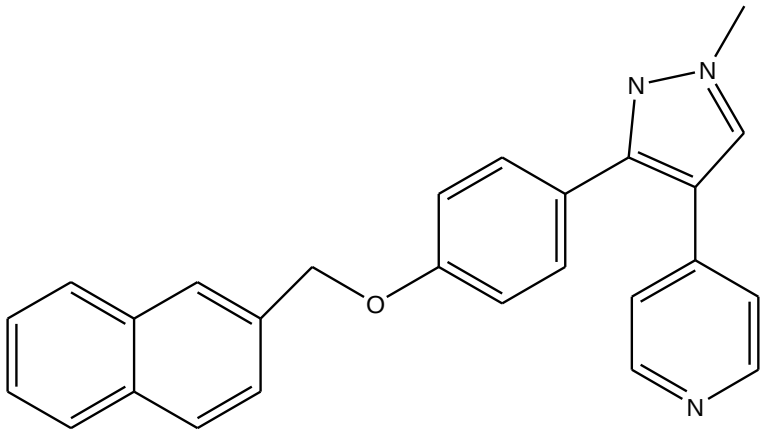

[9]

1.3 Copper

A transition metal complex is species consisting of a transition metal coordinated to one or more ligands (neutral or anionic non-metal species). The design and construction of supramolecular structures from transition metals and organic ligands has attracted considerable interest due to their potential applications and structural diversity. Non-covalent interactions such as metal–ligand coordination, hydrogen bonding and π–π stacking are powerful tools in this field. Transition metal complexes are important in catalysis, materials synthesis, photochemistry, and biological systems. Transition metal ions usually form complexes with a well defined number of ligands. Complexes with coordination numbers four and six are the most common, although two and five coordination are also very well established. Coordination number and geometry are determined by a combination of metal ion size, ligand size and electronic factors such as electronic configuration and ligand type.[26] Copper ions (Cu^{2+}) are very important for correct functions of living organisms. They are necessary as a cofactor for many important enzymes, like cytochrome c oxidase and tyrosinase.[27] Despite their crucial roles in the proper functioning of enzymes, copper can be also toxic to organisms. Concentrations of copper higher than physiological amounts could be a reason for different disorders. Humans can uptake larger amounts with Cu-contaminated food and water. It may cause development of gastrointestinal symptoms.[28] Copper ions are also responsible for development of such pathological states as liver cirrhosis, damage of renal tubules, hemolysis, brain damage and others. Cu-poisoning can results in coma, vascular collapse, hepatic necrosis and death.[29] Intoxication by copper ions can be also observed in patients after dialysis via Cu tubing.[30] Copper is also responsible for etiology of some neurodegenerative diseases like Alzheimer (a disease cause by an increase in Cu, Fe and Zn ions level, an increase in amyloidal β proteins level

in the brain tissue, degeneration of neurons), Parkinson and amyotrophic lateral sclerosis.[31] Moreover, copper also an important element present in several cell types with essential functions in the human body, participating in various biochemical and biological cycles. It is present in important enzymes including cytochrome oxidase,[32] CuZn-superoxide dismutase (catalyzes the dismutation of superoxide into oxygen and hydrogen peroxide),[33] lysyl oxidase (catalyses formation of aldehydes from lysine residues in collagen and elastin precursors),[34] and dopamine hydroxylase. Two genetic disorders produce abnormal levels of copper in humans are Menkes disease (MD) characterized by deficiency of Cu(II) and Wilson disease (WD) with an incidence of about 1 per 30,000 people. The illness is treated with permanent use of chelating agents such as trientine hydrochloride and drugs that help remove copper from tissue.[35] A variety of recent observations indicated that copper complexes when administered in conjunction with anti-inflammatory drugs exhibit synergistic activity.[36] It had also been found that the Cu complexes of some anti-arthritic drugs are themselves more active as anti-inflammatory agents than their parent compounds.[37] Previous study by G. Mohamed Gehad and E.A. El-Gamel Nadia on copper complexes of piroxicam ligand **[10]** can be coordinated in human biological systems.[38] Recently, there was a study on 2,3-bis(diphenylphosphino)quinoxaline (dppQx) and its copper(I) complexes. It has been reported and the complexes showed interesting luminescent properties.[39] Another copper complexes are a series of quinoxaline N1,N4-dioxide derivatives that can act as bioreductive drugs and has been previously described by several studies.[40]

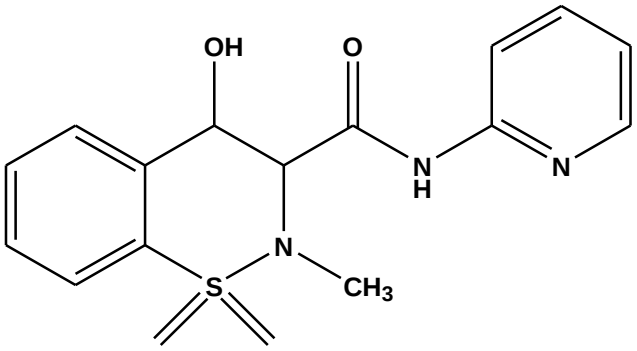

[10]

Different organic compounds and transition metal complexes can be recognized as hypoxia-selective tumor activated prodrugs. Among carbon-based compounds that are bioactivated under hypoxic conditions, a number of heterocyclic N-oxides have been developed. Macrocyclic copper complexes have been found to react with DNA by different binding modes and to exhibit effective nuclease activity. In 2004, a research on three novel Cu(II) complexes of quinoxaline *N*1, *N*4-dioxide derivatives has been made and as the result, been found that the complexes can act as bioreductive prodrugs and also has ability to act as selective antitumoral agents.[41] In view of the literature search done above, we chose to study copper complexes of pyrazine and quinoxaline due to their potential applications and structural diversity as an antitumoral agents, prodrugs, anti-inflammatory agents, antibacterial, antiviral, anticancer, antifungal, antihelminthes and insecticidal activities.

CHAPTER TWO:

FLUORESCENCE STUDIES

2.1 Introduction

Photoluminescence is a luminescence stimulated by light absorption in UV-Vis-NIR spectral region. It represents any process in which material absorbs electromagnetic energy at a certain wavelength and then emits part of it at a different (usually longer) wavelength. Therefore, only a part of the absorbed energy is transformed into luminescent light. The rest of it ends up as molecular vibrations or simply as heat. Based on practical observations, two types of photoluminescence were established, i.e. fluorescence and phosphorescence. The major distinction between fluorescence and phosphorescence is the time scale of emission, with fluorescence being prompt and phosphorescence being delayed. Time between the moment when the material absorbed the higher energy photon and the moment when the secondary lower energy photon was re-emitted is called delay time. This delay is defined by the lifetime of excitation states or simply speaking by the fact for how long atom or molecule is able to stay in excited high-energy condition. Delay time is shorter for fluorescence and much longer for phosphorescence. Fluorescence is a photoluminescence process in which atoms or molecules are excited to ion electronically excited state by absorption of electromagnetic radiation. The excited molecule or electron then return to the electronic ground state and loses its excess energy as photon by emission of light. Once the molecule is excited, several processes can occur that cause the molecule to lose its energy. Two of the most important of these mechanisms are nonradioactive and fluorescence emission. Nonradioactive processes leads to release of energy in the form of heat rather than light. Other sample of constituents may interact with an excited molecule in such a way

as to prevent it from fluorescing. This process called quenching. An electronically excited molecule can also undergo chemical reaction. The short-lived emission that occurs is called fluorescence, while luminescence that is much longer lasting is called phosphorescence. In fluorescence, the molecule is in high vibrational state after electronic excitation. The molecule excites from a vibrational level in the electronic ground state to one of many vibrational levels in the electronic excited state. This excited state is usually the first excited singlet state. The vibrational energy is converted to kinetic energy and appears as heat in the sample. Such transfer between energy levels is referred to as 'raditionless'. The molecule will also partition the excess energy to other possible modes of vibration and rotation. Fluorescence occurs when the molecule returns to the electronic ground state, from the excited singlet state, by emission of a photon. During the past 20 years, there has been remarkable growth in use of fluorescence. Fluorescence is now has been used widely in biotechnology, flow cytometry, medical diagnostics, DNA sequencing, forensics and genetic analysis. Fluorescence is a spectrochemical method of analysis where the molecules of the analyte are excited by irradiation at a certain wavelength and emit radiation of a different wavelength. The emission spectrum provides information for both qualitative and quantitative analysis. When light of an appropriate wavelength is absorbed by a molecule (i.e., excitation), the electronic state of the molecule changes from the ground state to one of many vibrational levels in one of the excited electronic states as shown in **Figure 2.1** below.[42]

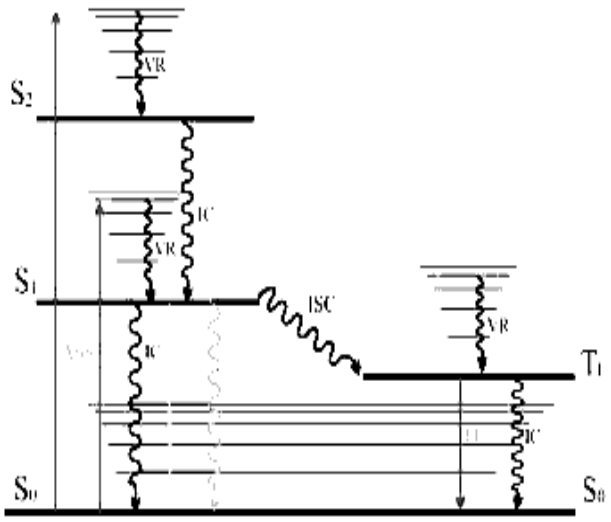

Figure 2.1: Jablonski diagram

For example, fluorescence measurement reveals ligand-induced conformational changes in proteins, as fluorescence is often sensitive to subtle environmental changes of chromophores such as tryptophan and tyrosine, sensitivity to protonation or deprotonation reactions, solvent relaxation and local conformational changes.[43] Luminescence is the emission of light from any substance and occurs from electronically excited states.[44] Luminescent compounds are attracting much current research interest because of their many applications including emitting materials for organic light emitting diodes, light harvesting materials for photo catalysis and fluorescent sensors for organic or inorganic analyses. The fluorescence of a molecule is the light emitted spontaneously due to the transitions from excited singlet states to various vibrational levels of the electronic ground state. It can be characterized by several parameters. The most important among them are the fluorescence intensity at a given wavelength $F(\lambda)$, the emission spectrum, quantum yield, lifetime and polarization.[45]

2.2 Instrumentation

The light from an excitation source passes through a filter or monochromator, and strikes the sample. A proportion of the incident light is absorbed by the sample, and some of the molecules in the sample fluoresce. The fluorescent light is emitted in all directions. Some of this fluorescent light passes through a second filter or monochromator and reaches a detector, which is usually placed at 90° to the incident light beam to minimize the risk of transmitted or reflected incident light reaching the detector. Various light sources may be used as excitation sources, including lasers, photodiodes, and lamps; xenon arcs and mercury-vapor lamps in particular. A laser only emits light of high irradiant at a very narrow wavelength interval, typically under 0.01 nm, which makes an excitation monochromator or filter unnecessary. The disadvantage of this method is that the wavelength of a laser cannot be changed by much. A mercury vapor lamp is a line lamp, meaning it emits light near peak wavelengths. By contrast, a xenon arc has a continuous emission spectrum with nearly constant intensity in the range from 300-800 nm and a sufficient irradiance for measurements down to just above 200 nm. Filters and/or monochromators may be used in fluorimeters. A monochromator transmits light of an adjustable wavelength with an adjustable tolerance. The most common type of monochromator utilizes a diffraction grating, that is, collimated light illuminates a grating and exits with a different angle depending on the wavelength. The monochromator can then be adjusted to select which wavelengths to transmit. For allowing anisotropy measurements the addition of two polarization filters are necessary which are after the excitation monochromator or filter, and one before the emission monochromator or filter. As mentioned before, the fluorescence is most often measured at a 90° angle relative to the excitation light. This geometry is used instead of placing the sensor at the line of the excitation light at a 180° angle in order to avoid interference of the transmitted excitation light. No monochromator is

perfect and it will transmit some stray light, that is, light with other wavelengths than the targeted. An ideal monochromator would only transmit light in the specified range and have a high wavelength-independent transmission. When measuring at a 90 angle, only the light scattered by the sample causes stray light. This results in a better signal-to-noise ratio, and lowers the detection limit by approximately a factor 10000,[46] when compared to the 180° geometry. Furthermore, the fluorescence can also be measured from the front, which is often done for turbid or opaque samples.[47] The detector can either be single-channeled or multichanneled. The single-channeled detector can only detect the intensity of one wavelength at a time, while the multichanneled detects the intensity at all wavelengths simultaneously, making the emission monochromator or filter unnecessary. The different types of detectors have both advantages and disadvantages. The most versatile fluorimeters with dual monochromators and a continuous excitation light source can record both an excitation spectrum and a fluorescence spectrum. When measuring fluorescence spectra, the wavelength of the excitation light is kept constant, preferably at a wavelength of high absorption, and the emission monochromator scans the spectrum. For measuring excitation spectra, the wavelength passing though the emission filter or monochromator is kept constant and the excitation monochromator is scanned. The excitation spectrum generally is identical to the absorption spectrum as the fluorescence intensity is proportional to the absorption.[48] The intensity of fluorescence can be decreased by a wide variety processes. Such decreases in intensity are called quenching. Quenching can occur by different mechanisms. Collisional quenching occurs when excited state fluorophore is deactivated upon contact with some other molecules in solution, which is called the quencher. Oxygen, halogens, amines and electron-deficient molecules can act as quencher. Nevertheless, the phenomenon of quenching provides a valuable context for understanding the role of the excited state lifetime in allowing fluorescence measurements to detect dynamic processes in solution. The basic idea is that the absorption is an instaneous event.

According to the Franck-Cordon principle, absorption occurs so fast that there is no time for molecular motion during the absorption process. As a result, absorption spectroscopy can only yield information on the average ground state of the molecules that absorb light. In contrast to absorption, emission occurs over longer period of time. The length of time fluorescent molecules remain in the excited state provides opportunity for interactions with other molecules in solutions.

2.3 Recent studies on fluorescence

An important feature of fluorescence is high sensitivity detection. The sensitivity of fluorescence was used in 1877 to demonstrate that the rivers Danube and Rhine were connected by underground streams.[49] It is interesting to notice that the first known fluorophore, quinine **[11]** was responsible for stimulating the development of the first spectrofluorometers that appeared in the 1950s. Some other substituted organic compounds such as 1,4-bis(5-phenyloxazol-2-yl)benzene (POPOP) is used in scintillation counting and acridine orange is often used as DNA stain. Pyridine 1 and rhodamine are frequently used in dye lasers.[50]

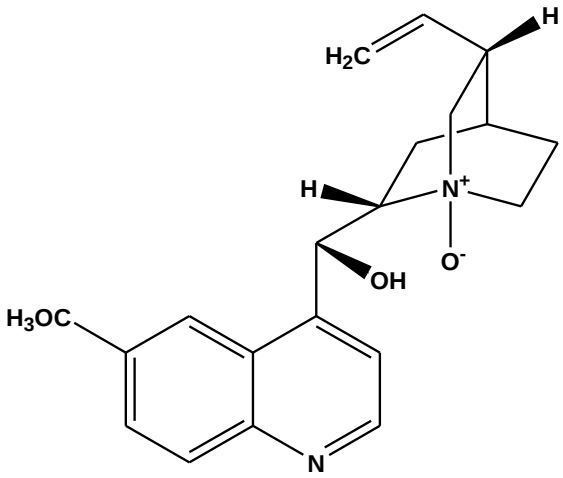

[11]

Fluorescence spectroscopy can be applied to a wide range of problems in the chemical and biological sciences. The measurements can provide information on a wide range of molecular processes, including the interactions of solvent molecules with fluorophores, rotational diffusion of biomolecules, and distances between sites on biomolecules, conformational changes and binding interactions. Fluorescence spectroscopy will continue to contribute to rapid advances in biology, biotechnology and nanotechnology. Pyrazine derivatives have a chromophoric system and perform strong fluorescence. One of the typical examples of pyrazine derivatives is coelenterazine **[12]** that was found and isolated from aequorin and is widely used as a probe to monitor intracellular levels of free calcium. Pyrazole derivatives are also applied in photography and fluorescent sensor, nonlinear optical materials, dyes and organic light emitting devices.[5]

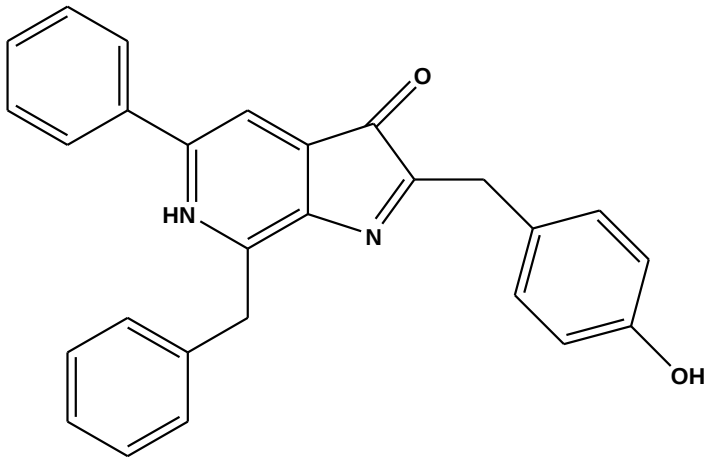

[12]

Another fluorescence studies is on azaphthalocyanines (AzaPc) which are well known as synthetic dyes. AzaPc is able to quench the fluorescence of different fluorophores in DNA hybridization probes and they were shown to be highly efficient as modern type of non emitting quenchers, so called "dark quenchers".[50] AzaPc produced from the reaction between 5,6-bis(diethylamino)pyrazine-2,3-dicarbonitrile and 6-(5,6-dicyano-3-(diethylamino)pyrazin-2-ylamino)hexanoic. The specific spectroscopic properties of metal ions have made them one of the essential components in the preparation of new materials and ideal as probes in studies of biological systems. A copper complex of a naringenin Schiff-base ligand, 4', 5, 7-trihydroxy-flavanoe benzoyl hydrazone (H3L) has certain cytotoxic activity, and can bind to CT-DNA by intercalation. The DNA-binding properties of copper complexes have been investigated and have been proved by fluorescence spectroscopy, ultraviolet spectroscopy and by viscosity measurements that the complexes do exhibit the cytotoxic activity.[52] Multidimensional fluorescence techniques, such as total luminescence and synchronous scanning fluorescence are particularly useful for the analysis of complex food matrices.[53] Fluorescence spectral data and lifetimes in diluted beers have been explored recently.[54] Total luminescence spectroscopy (TLS) which involves simultaneous acquisition at multiple excitation and emission wavelengths and synchronous fluorescence spectroscopy techniques have been successfully used in the analysis of crude oils, pharmaceuticals, polycyclic aromatic hydrocarbons, motor oils, and humic matter in water.[55] Recently, much attention has been paid to the fluorescent metal complexes because of their particular luminescence properties. Fluorescence properties of many zinc complexes of pyrazine and its derivatives such as pyrazine-2-carboxylate and prazine-2,3-dicarboxylate has been published recently.[56]

2.4 Objectives

The objectives of this research are to:

1) Synthesize selected pyrazine and quinoxaline based ligands.
2) Synthesize copper complexes of pyrazine and quinoxaline based ligands.
3) Characterize ligands and their copper complexes.
4) Study the fluorescence characteristics with respect to:
    - Effects of substituents in ligands
    - Effect of solvents
    - Effects of metal coordination
    - Effect of concentrations
    - Effect of oxygen quenching

CHAPTER THREE:

EXPERIMENTAL

4.1 Chemicals

All solvents and reagents were commercially available and used as obtained without further purifications unless otherwise stated.

4.2 Spectral data

4.2.1 ^{1}H and ^{13}C-NMR Spectroscopic Analysis

^{1}H and ^{13}C-NMR spectrum were carried out using a Lambda JEOL 400 MHz FT-NMR and ECA 400 MHz FT-NMR Spectrometer using deuterated $CHCl_3$ as solvent for the ligands. Chemical shifts are reported in ppm on δ scale, and the coupling constant is given in Hz.

4.2.2 Infrared Spectroscopic Analysis

The IR absorption spectra of all samples were recorded by Shimadzu 1600 spectrophotometer and Perkin Elmer RX1 spectrophotometer. The IR absorption spectra of solid samples were dispersed in KBr salt and pressed into thin pellets before measurement. The IR frequency range of interest was 400 cm^{-1} to 4000 cm^{-1}.

4.2.3 Mass Spectroscopic Analysis

Mass spectroscopic analyses were performed at a Hewlett- Packard HP 6890 Series of GC System with mass selective indicator and GCMS QP5050A Shimadzu.

4.2.4 Melting Point

Melting point was carried out in glass capillaries recorded on a melting point apparatus Fargo MP-ID and uncorrected.

4.2.5 CHN Analysis

In elemental analysis, samples are decomposed at high temperature in a combustion tube. The resulting gaseous is measured by using a thermal conductivity detector or IR detector. The carbon, hydrogen and nitrogen elemental compositions of samples were obtained from a Perkin Elmer 2400 CHN Elemental Analyzer. For each analysis 1mg to 10mg of weighted samples needed.

4.2.6 X-Ray Crystallography

The crystal data was collected from a Bruker SMART APEX CCD diffractometer. The structure was solved by direct method, an approach based on statistical analyses of intensities, using the SHELXTL software package for structure refinement.

4.4 Fluorescence

The fluorescence measurement was carried out in a quartz cell, using Fluorescence Spectrophotometer Model F-2000 Hitachi at room temperature with the same instrument and settings.

4.4.1 Effect of Substituent on the Ligands

Fluorescence properties for all ligands were studied based on effect of substituent attached to pyrimidine ring. All samples were prepared in methanol and DMSO with the same concentration which is $\approx 2.5 \times 10^{-4}$ M.

4.4.2 Influence of Solvents

All the compounds with the same concentration as ≈ 2.5 x 10^{-4} M were prepared in methanol and DMSO.

4.4.3 Quenching by Oxygen

Fluorescence characteristics for each of the ligand and its metal complexes were studied under the condition of capped and uncapped samples. All the compounds with the same concentration ≈ 2.5 x 10^{-4} M, ≈ 2.5 x 10^{-4} M were prepared in methanol and DMSO.

4.4.4 Quenching by Metal

Each ligand and their metal complexes with the same concentration ≈ 2.5 x 10^{-4} M, were prepared in methanol and DMSO. Fluorescence properties for each ligand and its metal complexes were recorded.

4.2 Preparation of pyrazine and quinoxaline derivatives

5.2.1 Preparation of 2-*N*-anilinopyrazine **(L1)**

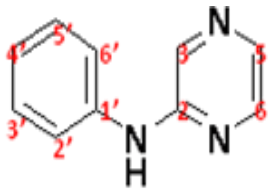

2-chloropyrazine (1.20 ml, 0.01 moles) was added to aniline (2.40 ml, 0.02 moles) for 3 hours at 120 – 140 °C. The mixture was cooled and extracted with diethyl ether for two times (2 x 10 ml). The organic layer then washed with water and dried over anhydrous sodium sulphate. The mixture was then re-crystallized with chloroform. Evaporation of chloroform gave the product, 2-*N*-anilinopyrazine **(L1).** Yield: 1.6890 g, 75%; m.p 126 – 129 °C; IR (cm^{-1}) : 3307 ($\nu_{\text{N-H stretching}}$), 1583 ($\nu_{\text{C=N stretching}}$), 1583 ($\nu_{\text{N-H bending}}$), 1419 ($\nu_{\text{C=C stretching}}$); ^{1}H-NMR δ_H ppm (400 MHz, $CDCl_3$) : 8.18 (1H, d, J= 1.3 Hz, H-3), 8.04 (1H, dd, J= 2.6 Hz, 1.4 Hz, H-5), 7.91 (1H, d, J = 2.5 Hz, H-6), 7.37 (2H, d, J=7.8 Hz, H-2', H-6'), 7.18 (2H, t, J=7.4 Hz, H-3', H-5'), 7.04 (1H, t, J= 7.4 Hz, H-4'), 6.68 (1H, s, N-H); ^{13}C-NMR δ_C ppm (100.4 MHz, $CDCl_3$) : 152.3 (C-2), 141.9 (C-3), 139.1 (C-1'), 134.9 (C-5), 132.9 (C-6), 129.4 (C-2', C-6'), 123.6 (C-4'), 120.3 (C-3', C-5') GCMS: Found M^+ =170; $C_{10}H_9N_3$ requires M^+ = 170.21

5.2.2 Preparation of 2-*N*-(*m*-methyl)anilinopyrazine **(L2)**

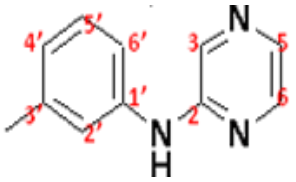

2-chloropyrazine (0.20 ml ml, 2.24 mmoles) was added to 3-methylaniline (0.24 ml, 2.24 mmoles) for 8 hours at 120 – 140 °C in an oil bath. The mixture was cooled and extracted twice with diethyl ether (2 x 10 ml). The organic layer washed with water and dried over anhydrous sodium sulphate. The mixture was then re-crystallized with chloroform. Evaporation of chloroform gave the product, 2-*N*-(*m*-methyl)anilinopyrazine **(L2),** a dark brown liquid. Yield: 0.1989 g, 46%; IR (cm^{-1}) : 3296 ($\nu_{\text{N-H stretching}}$), 1616 ($\nu_{\text{C=N stretching}}$), 1585 ($\nu_{\text{N-H bending}}$), 1411 ($\nu_{\text{C=C stretching}}$); ^{1}H-NMR δ_H ppm (400 MHz, $CDCl_3$) : 8.17 (1H, d, J= 1.4 Hz, H-3), 8.02 (1H, dd, J= 2.6 Hz, 1.4 Hz, H-5), 7.88 (1H, d, J = 2.5 Hz, H-6), 7.13 (3H, m, H-2', H-5', H-6'), 6.84 (1H, d, J=7.4 Hz, H-4'), 6.60 (1H, s, N-H), 2.28 (3H, s, CH_3); ^{13}C-NMR δ_C ppm (100.4 MHz, $CDCl_3$) : 152.4 (C-2), 141.9 (C-3), 139.3 (C-1'), 139.2 (C-3'), 134.7 (C-5), 132.8 (C-6), 129.2 (C-6'), 124.5 (C-2'), 121.3 (C-5'), 117.5 (C-4'), 21.5 (CH_3); GCMS: Found M^+ =184.00; $C_{11}H_{11}N_3$ requires M^+ = 184.23

5.2.3 Preparation of 2-*N*-(*p*-methyl)anilinopyrazine **(L3)**

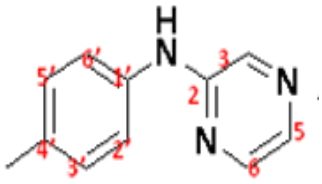

2-chloropyrazine (0.20 ml ml, 2.24 mmoles) was added to 4-methylaniline (0.24 ml, 2.24 mmoles) for 9 hours at 120 – 140 °C in an oil bath. The mixture was cooled and extracted twice with diethyl ether (2 x 10 ml). The organic layer washed with water and dried over anhydrous sodium sulphate. The mixture was then re-crystallized with chloroform. Evaporation of chloroform gave the product, 2-*N*-(*m*-methyl)anilinopyrazine **(L3),** a dark brown crystal. Yield: 0.1989 g, 46%; m.p 102 – 104 °C; IR (cm^{-1}) : 3293 ($\nu_{\text{N-H stretching}}$), 1618 ($\nu_{\text{C=N stretching}}$), 1580 ($\nu_{\text{N-H bending}}$), 1411 ($\nu_{\text{C=C stretching}}$); ^{1}H-NMR δ_H ppm (400 MHz, $CDCl_3$) : 8.19 (1H, d, J= 1.3 Hz, H-3), 8.08 (1H, dd, J= 2.6 Hz, 1.4 Hz, H-5), 7.94 (1H, d, J = 2.5 Hz, H-6), 7.30 (2H, d, J=7.8 Hz, H-2', H-6'), 7.18 (2H, d, J=7.8 Hz, H-3', H-5'), 6.59 (1H, s, N-H), 2.30 (3H, s, CH_3); ^{13}C-NMR δ_C ppm (100.4 MHz, $CDCl_3$): 152.6 (C-2), 142.0 (C-1'), 136.3 (C-4'), 134.6 (C-3), 133.7 (C-5), 132.5 (C-6), 129.9 (C-2', C-6'), 121.1 (C-3', C-5'), 20.8 (CH_3); (GCMS: Found M^+ =184.00; $C_{11}H_{11}N_3$ requires M^+ = 184.23

5.2.4 Preparation of 2-*N*-(*p*-chloro)anilinopyrazine **(L4)**

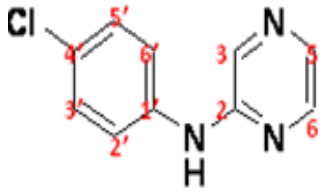

2-chloropyrazine (1.79 ml, 0.02 moles) was added to *p*-chloroaniline (2.5506 g, 0.02 moles) for 5 hours at 120 – 140 °C in an oil bath. The mixture was cooled and extracted with diethyl ether for two times (2 x 10 ml). The organic layer then washed with water and dried over anhydrous sodium sulphate. The mixture was then re-crystallized in chloroform. Evaporation of chloroform gave the product, 2-*N*-(*p*-chloro)anilinopyrazine **(L4).** Yield: 2.3420 g, 58%; m.p 143 – 145 °C; IR (cm^{-1}) : 3296 ($\nu_{\text{N-H stretching}}$), 1625 ($\nu_{\text{C=N stretching}}$), 1585 ($\nu_{\text{N-H bending}}$), 1458 ($\nu_{\text{C=C stretching}}$); ^{1}H-NMR δ_H ppm (400 MHz, $CDCl_3$) : 8.19 (1H, d, J= 1.3 Hz, H-3), 8.12 (1H, dd, J= 2.6 Hz, 1.4 Hz, H-5), 8.01 (1H, d, J = 2.5 Hz, H-6), 7.44 (2H, d, J=7 Hz, H-2', H-6'), 7.30 (2H, d, J=7 Hz, H-3', H-5'), 6.54 (1H, s, N-H); ^{13}C-NMR δ_C ppm (100.4 MHz, $CDCl_3$) : 151.9 (C-2), 141.8 (C-3), 137.8 (C-4'), 135.2 (C-5), 133.2 (C-6), 129.3 (C-3',C-5'), 121.2 (C-2',C-6') GCMS: Found M^+ = 205.0 ; $C_{10}H_8ClN_3$ requires M^+ = 205.6

5.2.5 Preparation of 2-*N*-anilinoquinoxaline **(L5)**

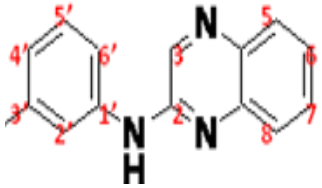

2-chloroquinoxaline (0.3295 g, 0.002 moles) was added to aniline (0.18 ml, 0.002 moles) for 2 hours at 120 - 140 °C. The mixture was cooled and extracted twice with diethyl ether (2 x 10 ml). The organic layer washed with water and dried over anhydrous sodium sulphate. The mixture was then re-crystallized in chloroform. Evaporation of chloroform gave the yellowish solid product, 2-*N*-anilioquinoxaline **(L5).** Yield: 0.3340 g, 65%; m.p 132 – 134 °C; IR (cm^{-1}) : 3201 ($\nu_{\text{N-H stretching}}$), 1585 ($\nu_{\text{C=N stretching}}$), 1518 ($\nu_{\text{N-H bending}}$), 1458 ($\nu_{\text{C=C stretching}}$); ^{1}H-NMR δ_H ppm (400 MHz, $CDCl_3$) : 8.45 (1H, s, H-3), 8.14 (1H, dd, J= 8 Hz, 1.4 Hz, H-8), 8.02 (1H, d, J = 7.8 Hz,1.4 Hz, H-5), 7.92 (2H, d, J=8 Hz, H-2', H-6'), 7.65 (1H, m, H-7), 7.42 (1H, m, H-6), 7.26 (2H, t, J=8 Hz, H-3', H-5'), 7.13 (1H, t, J= 7.8 Hz, H-4'), 6.88 (1H, s, N-H); ^{13}C-NMR δ_C ppm (100.4 MHz, $CDCl_3$) : 149.2 (C-2), 141.1 (C-1'), 139.1 (C-10), 138.3 (C-9), 137.8 (C-3), 130.3 (C-8), 129.2 (C-2', C-6'), 128.8 (C-5), 126.8 (C-7), 125.7 (C-6), 123.7 (C-4'), 119.9 (C-3',C-5'); Found M^+ = 221.0 ; ($C_{14}H_{11}N_3$) requires M^+ = 221.3

5.2.6 Preparation of 2-*N*-(*m*-methyl)anilinoquinoxaline **(L6)**

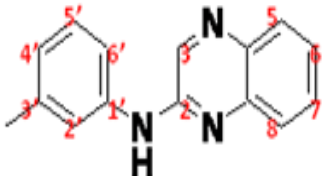

2-chloroquinoxaline (0.3260 g, 0.002 moles) was dissolved in ethanol (3.00 ml) and added to *m*-toluidine (0.21 ml, 0.002 moles). The mixture was refluxed for 5 hours at 120 - 140 °C and cooled to room temperature. The solvent was evaporated off and a minimum volume of water was added to the residue. The residual slurry was extracted with diethyl ether (2 x 10 ml). The diethyl ether extracts were washed with water for two times and dried over anhydrous sodium sulphate. The mixture was then re-crystallized in chloroform. Evaporation of chloroform gave a crude product, pure 2-*N*-(*m*-methyl)anilinoquinoxaline **(L6).** Yield: 0.1232 g, 42%; m.p 90 – 91 °C; IR (cm^{-1}) : 3295 ($\nu_{\text{N-H stretching}}$), 1616 ($\nu_{\text{C=N stretching}}$), 1544 ($\nu_{\text{N-H bending}}$), 1412 ($\nu_{\text{C=C stretching}}$); ^{1}H-NMR δ_H ppm (400 MHz, $CDCl_3$) : 8.42 (1H, s, H-3), 7.92 (1H, dd, J= 8 Hz, 1.2 Hz, H-8), 7.76 (1H, dd, J = 8 Hz, J=1.2 Hz, H-5), 7.61 (1H, m, H-7), 7.47 (1H, m, H-6), 7.43 (1H, s, H-2'), 7.26 (2H, d, J=6 Hz, H-6'), 7.21 (2H, t, J=7.8 Hz, 1.8 Hz, H-4', H-5'), 6.85 (1H, d, J=8 Hz, N-H), 2.36 (3H, s, CH_3); ^{13}C-NMR δ_C ppm (100.4 MHz, $CDCl_3$) :149.4 (C-2), 141.1 (C-1'), 139.3 (C-3'), 138.9 (C-10), 138.2 (C-3), 137.5 (C-9), 130.1 (C-8), 129.1 (C-5), 128.7 (C-7), 126.7 (C-6), 125.4 (C-2'), 124.5 (C-6'), 120.6 (C-5'), 117.1 (C-4'), 21.6 (CH_3); GCMS Found M^+ = 234.00; ($C_{15}H_{13}N_3$) requires M^+ = 234.28

5.2.7 Preparation of 2-*N*-(*p*-methyl)anilinoquinoxaline **(L7)**

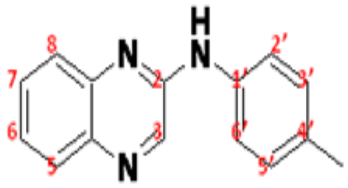

2-chloroquinoxaline (0.3297 g, 0.002 moles) was dissolved in ethanol (3.00 ml) and added to *p*-toluidine (0.21 ml, 0.002 moles). The mixture was refluxed for 5 hours at 120 - 140 °C and cooled to room temperature. The solvent was evaporated off under vacuum. The minimum volume of water was added to the residue. The residual slurry was extracted with diethyl ether two times (2 x 10 ml). The diethyl ether extracts were washed twice with water and dried over anhydrous sodium sulphate. The mixture was then re-crystallized in chloroform. Evaporation of chloroform gave dark brown crystal product, 2-*N*-(*p*-methyl)anilinoquinoxaline **(L7).** Yield: 0.2203 g, 49%; m.p 148 – 149 °C; IR (cm^{-1}) : 3296 ($\nu_{\text{N-H stretching}}$), 1617 ($\nu_{\text{C=N stretching}}$), 1584 ($\nu_{\text{N-H bending}}$), 1412 ($\nu_{\text{C=C stretching}}$); ^{1}H-NMR δ_H ppm (400 MHz, $CDCl_3$) : 8.42 (1H, s, H-3), 7.90 (1H, dd, J=8 Hz, J= 1.2 Hz, H-8), 7.64 (1H, dd, J=8 Hz, 1.2 Hz, H-5), 7.62 (1H, m, H-7), 7.47 (2H, d, J=8 Hz, H-2', H-6'), 7.43 (1H, m, H-6), 7.19 (2H, d, J=8 Hz, H-3', H-5'), 6.83 (1H, s, N-H), 2.36 (3H, s, CH_3); ^{13}C-NMR δ_C ppm (100.4 MHz, $CDCl_3$): 149.6 (C-2), 141.3 (C-1'), 138.3 (C-3), 137.7 (C-10), 136.4 (C-9), 133.5 (C-4'), 130.2 (C-8), 129.8 (C-2', C-6'), 128.7 (C-5), 126.7 (C-7), 125.4 (C-6), 120.4 (C-3', C-5'), 20.9 (CH_3); GCMS Found M^+ = 234.00; ($C_{15}H_{13}N_3$) requires M^+ = 234.28

5.2.8 Preparation of 2-*N*-(*p*-chloro)anilinoquinoxaline **(L8)**

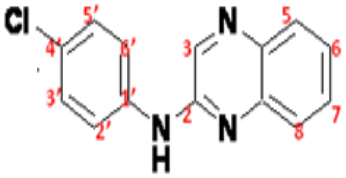

2-chloroquinoxaline (0.3286 g, 0.002 moles) was dissolved in ethanol (3 ml) and *p*-chloroaniline (0.2510 g, 0.002 moles) was added to the reaction mixture refluxed for 5 hours at 120 - 140 °C. The mixture was cooled and extracted twice with diethl ether (2 x 10 ml). The organic layer washed with water and dried over anhydrous sodium sulphate. The mixture was then re-crystallized in chloroform. Evaporation of chloroform gave the dark brown solid product, 2-*N*-*(p*-chloro)anilinoquinoxaline **(L8)**. Yield: 0.3550 g, 68%; m.p 191 – 192 °C; IR (cm^{-1}) : 3299 ($\nu_{N-H\ stretching}$), 1605 ($\nu_{C=N\ stretching}$), 1587 ($\nu_{N-H\ bending}$), 1458 ($\nu_{C=C\ stretching}$); ^{1}H-NMR δ_H ppm (400 MHz, $CDCl_3$) : 8.40 (1H, s, H-3), 7.94 (1H, dd, J=8 Hz, J= 1.2 Hz, H-8), 7.66 (2H, d, J=8 Hz, 1.2 Hz, H-3', H-5'), 7.62 (1H, m, H-7), 7.48 (1H, m, H-6), 7.36 (2H, d, J=8 Hz, H-2', H-6'), 6.98 (1H, s, N-H); ^{13}C-NMR δ_C ppm (100.4 MHz, $CDCl_3$): 148.8 (C-2), 140.9 (C-1'), 138.4 (C-3), 137.8 (C-10), 130.4 (C-9), 129.2 (C-5, C-8), 128.8 (C-3', C-5'), 128.2 (C-4'), 126.9 (C-7), 125.9 (C-6), 120.7 (C-3', C-5'); GCMS Found M^+ = 254.00; ($C_{10}H_8ClN_3$) requires M^+ = 254.75

5.3 Preparation of Copper Complexes

5.3.1 Tetra-μ-acetato-κ^8O: O-bis{[N-(pyrazine-2-yl)aniline- κN]copper(II)} **(CuL1)**

A solution of copper(II) acetate (0.1000 g) in acetonitrile (15.00 cm^3) was added dropwise to a solution of L1 (0.1883 g) in acetonitrile (15.00 cm^3) and trimethylorthoformate (9.00 cm^3) with continuous stirring and heated at 50 – 60 °C. A green precipitate was formed straight away. The precipitate was filtered and the dark blue powder was dried over silica gel in vacuum desiccators for overnight. It was then recrystallized from acetonitrile to give blue solid, **CuL1**. Yield: 0.1223 g, 48%; m.p: 230 - 233°C; *Anal.* Calc. (%) for $[Cu_2(C_2H_3O_2)_4\ (C_{10}H_9N_3)_2]$: C, 47.66; H, 4.26; N, 11.92; Found (%) : C, 47.55; H, 4.05; N, 11.34 **:** IR (cm^{-1}) : 3367 ($\nu_{\text{N-H stretching}}$), 1606 ($\nu_{\text{C=N stretching}}$), 1508 ($\nu_{\text{N-H bending}}$), 1420 ($\nu_{\text{C=C stretching}}$), 499 ($\nu_{\text{Cu-N}}$).

5.3.2 Tetra-μ-acetato- κ^8O: O-bis{[N-(pyrazine-2-yl)3-methylaniline- κN]copper(II)} **(CuL2)**

A solution of copper(II) acetate (0.1000 g) in acetonitrile (15.00 cm^3) was added dropwise to a solution of L1 (0.2038 g) in acetonitrile (15.00 cm^3) and trimethylorthoformate (9.00 cm^3) with continuous stirring and heated at 50 – 60 °C. A green precipitate was formed straight away. The precipitate was filtered and the dark blue powder was dried over silica gel in vacuum desiccators for overnight. It was then recrystallized from acetonitrile to give blue solid, **CuL2**. Yield: 0.1223 g, 48%; m.p: 235 - 237°C; *Anal.* Calc. (%) for $[Cu_2(C_2H_3O_2)_4\ (C_{11}H_{11}N_3)_2]$: C, 49.86; H, 4.71; N, 11.63; Found (%) : C, 49.04; H, 4.55; N, 11.08 **:** IR (cm^{-1}) : 3312 ($\nu_{\text{N-H stretching}}$), 1624 ($\nu_{\text{C=N stretching}}$), 1508 ($\nu_{\text{N-H bending}}$), 1426 ($\nu_{\text{C=C stretching}}$), 517 ($\nu_{\text{Cu-N}}$).

5.3.3 Tetra-μ-acetato- κ^8 O: O-bis{[N-(pyrazine-2-yl)4-methylaniline- κN]copper(II)} **(CuL3)**

A solution of copper(II) acetate (0.1000 g) in acetonitrile (15.00 cm^3) was added dropwise to a solution of L3 (0.2038 g) in acetonitrile (15.00 cm^3) and trimethylorthoformate (9.00 cm^3) with continuous stirring and heated at 50 – 60 °C. A green precipitate was formed after one day. The precipitate was filtered and the dark blue powder was dried over silica gel in vacuum desiccators for overnight. It was then recrystallized from acetonitrile to give blue crystals, **CuL3**. Yield: 0.0853 g, 56%; m.p: 221 - 223°C; *Anal.* Calc. (%) for $[Cu_2(C_2H_3O_2)_4\ (C_{11}H_{11}N_3)_2]$: C, 49.86; H, 4.11; N, 11.89; Found (%) : C, 49.77; H, 4.58; N, 11.49 **:** IR (cm^{-1}) : 3311 ($\nu_{\text{N-H stretching}}$), 1618 ($\nu_{\text{C=N stretching}}$), 1516 ($\nu_{\text{N-H bending}}$), 1414 ($\nu_{\text{C=C stretching}}$), 501 ($\nu_{\text{Cu-N}}$).

5.3.4 Tetra-μ-acetato- κ^8 O: O-bis{[N-(pyrazine-2-yl)4-chloroaniline- κN]copper(II)} **(CuL4)**

A solution of copper(II) acetate (0.1000 g) in acetonitrile (15.00 cm^3) was added dropwise to a solution of L3 (0.2114 g) in acetonitrile (15.00 cm^3) and trimethylorthoformate (9.00 cm^3) with continuous stirring and heated at 50 – 60 °C. A green precipitate was formed straight away. The precipitate was filtered and the dark green powder was dried over silica gel in vacuum desiccators for overnight. It was then recrystallized from acetonitrile to give **CuL4**. Yield: 0.0674 g, 75%; m.p: 227 - 229°C; *Anal.* Calc. (%) for $[Cu_2(C_2H_3O_2)_4\ (C_{10}H_8ClN_3)_2]$: C, 43.41; H, 3.62; N, 10.85; Found (%) : C, 42.88; H, 3.22; N, 10.12 **:** IR (cm^{-1}) : 3309 ($\nu_{\text{N-H stretching}}$), 1624 ($\nu_{\text{C=N stretching}}$), 1585 ($\nu_{\text{N-H bending}}$), 1421 ($\nu_{\text{C=C stretching}}$), 502 ($\nu_{\text{Cu-N}}$).

5.3.5 Tetra-μ-acetato- κ^8O: O-bis{[N-(quinoxaline-2-yl)aniline- κN]copper(II)} **(CuL5)**

A solution of copper(II) acetate (0.1000 g) in acetonitrile (15.00 cm^3) was added dropwise to a solution of L5 (0.2213 g) in acetonitrile (15.00 cm^3) and trimethylorthoformate (9.00 cm^3) with continuous stirring and heated at 50 – 60 °C. A dark green precipitate was formed straight away. The precipitate was filtered and the dark blue powder was dried over silica gel in vacuum desiccators for overnight. It was then recrystallized from acetonitrile to give product, **CuL5**. Yield: 0.1125 g, 69%; m.p: 245 - 248°C; *Anal.* Calc. (%) for $[Cu_2(C_2H_3O_2)_4\ (C_{14}H_{11}N_3)_2]$: C, 53.66; H, 4.22; N, 10.45; Found (%) : C, 53.11; H, 3.96; N, 10.22 **:** IR (cm^{-1}) : 3312 ($\nu_{\text{N-H stretching}}$), 1624 ($\nu_{\text{C=N stretching}}$), 1540 ($\nu_{\text{N-H bending}}$), 1426 ($\nu_{\text{C=C stretching}}$), 517 ($\nu_{\text{Cu-N}}$).

5.3.6 Tetra-μ-acetato- κ^8O: O-bis{[N-(quinoxaline-2-yl)3-methyaniline- κN]copper(II)(**CuL6)**

A solution of copper(II) acetate (0.1000 g) in acetonitrile (15.00 cm^3) was added dropwise to a solution of L6 (0.2589 g) in acetonitrile (15.00 cm^3) and trimethylorthoformate (9.00 cm^3) with continuous stirring and heated at 50 – 60 °C. A green precipitate was formed straight away. The precipitate was filtered and the dark blue powder was dried over silica gel in vacuum desiccator. It was then re-crystallized from acetonitrile to give blue crystals, **CuL6.** Yield: 0.0653 g, 72%; m.p: 221 - 222°C; *Anal.* Calc. (%) for $[Cu_2(C_2H_3O_2)_4\ (C_{15}H_{13}N_3)_2]$: C, 54.74; H, 4.56; N, 10.08; Found (%) : C, 54.12; H, 4.08; N, 9.65 **:** IR (cm^{-1}) : 3322 ($\nu_{\text{N-H stretching}}$), 1625 ($\nu_{\text{C=N stretching}}$), 1547 ($\nu_{\text{N-H bending}}$), 1417 ($\nu_{\text{C=C stretching}}$), 508 ($\nu_{\text{Cu-N}}$).

5.3.7 Tetra-μ-acetato- κ^8O:O-bis{[N-(quinoxaline-2-yl)4-methyaniline- κN]copper(II) **(CuL7)**

A solution of copper(II) acetate (0.1000 g) in acetonitrile (15.00 cm^3) was added dropwise to a solution of L7 (0.2589 g) in acetonitrile (15.00 cm^3) and trimethylorthoformate (9.00 cm^3) with continuous stirring and heated at 50 – 60 °C. A green precipitate was formed straight away. The precipitate was filtered and the dark blue powder was dried over silica gel in vacuum desiccators for three days. It was then re-crystallized from acetonitrile to give green solid, **CuL7**. Yield: 0.0657 g, 43%. m.p: 215 – 217 °C; *Anal.* Calc. (%) for $[Cu_2(C_2H_3O_2)_4\ (C_{15}H_{13}N_3)_2]$: C, 54.07; H, 4.66; N, 10.88; Found (%) : C, 54.21; H, 4.11; N, 10.12 **:** IR (cm^{-1}) : 3310 ($\nu_{\text{N-H stretching}}$), 1624 ($\nu_{\text{C=N stretching}}$), 1585 ($\nu_{\text{N-H bending}}$), 1421 ($\nu_{\text{C=C stretching}}$), 503 ($\nu_{\text{Cu-N}}$).

5.3.8 Tetra-μ-acetato- κ^8O:O-bis{[N-(quinoxaline-2-yl)4-chloroaniline- κN]copper(II)}(**CuL8*)***

A solution of copper(II) acetate (0.1000 g) in acetonitrile (15.00 cm^3) was added dropwise to a solution of L8 (0.2765 g) in acetonitrile (15.00 cm^3) and trimethylorthoformate (9.00 cm^3) with continuous stirring and heated at 50 – 60 °C. A green precipitate was formed straight away. The precipitate was filtered and the dark blue powder was dried over silica gel in vacuum desiccators. It was then re-crystallized from acetonitrile to give green solid, **CuL8**. Yield: 0.1023 g, 87%; m.p: 228 - 230°C; *Anal.* Calc. (%) for $[Cu_2(C_2H_3O_2)_4\ (C_{10}H_8ClN_3)_2]$: C, 49.43; H, 3.66; N, 9.61; Found (%) : C, 48.98; H, 3.26; N, 9.08 **:** IR (cm^{-1}) : 3308 ($\nu_{\text{N-H stretching}}$), 1622 ($\nu_{\text{C=N stretching}}$), 1586 ($\nu_{\text{N-H bending}}$), 1445 ($\nu_{\text{C=C stretching}}$), 502 ($\nu_{\text{Cu-N}}$).

CHAPTER FOUR:

RESULTS AND DISCUSSION

3.1 Characterization of 2-chloropyrazine based ligands

Reaction of 2-chloropyrazine with aniline, *m*-toluidine, *p*-toluidine, and *p*-chloroaniline were studied. **Figure 3.1** shows a diagrammatic representation of various reactions.

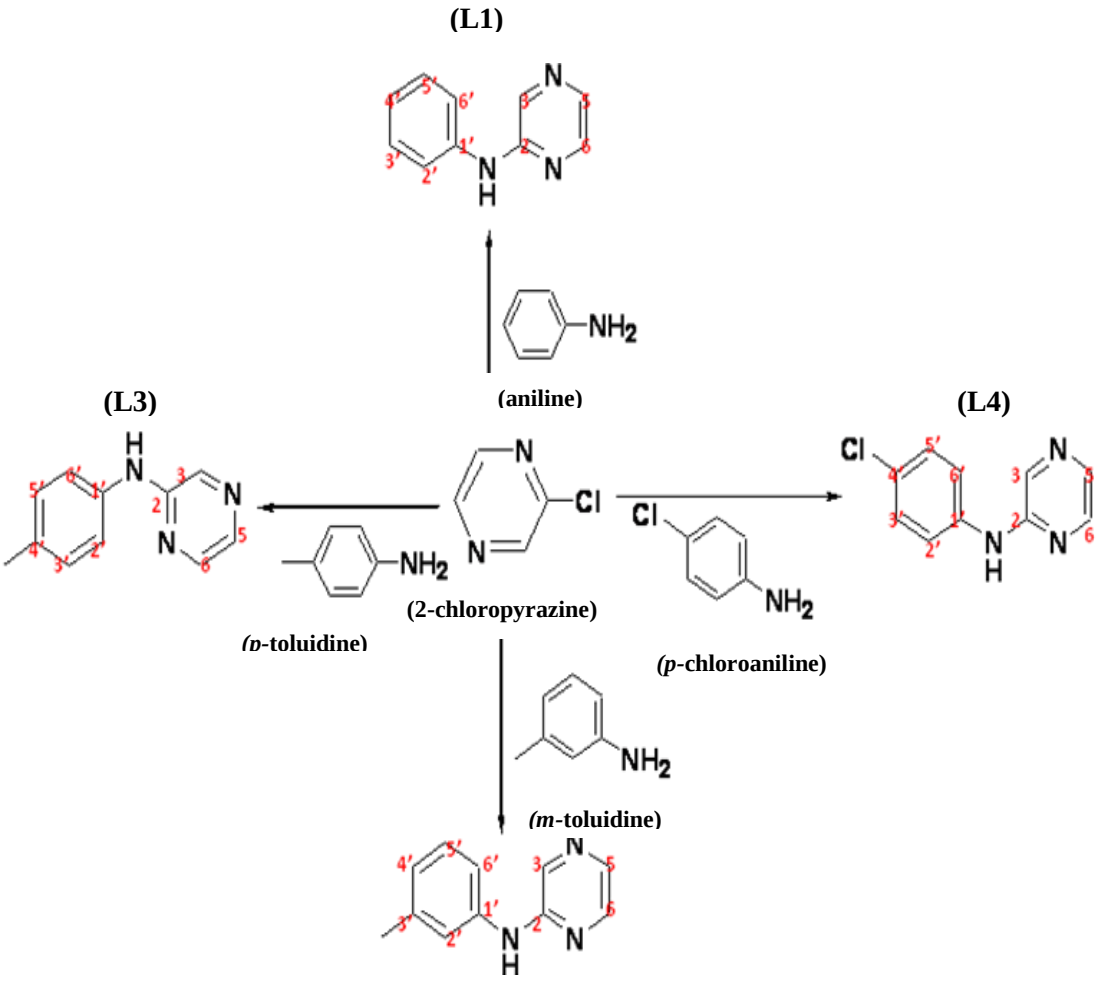

Figure 3.1: Preparation of pyrazine based ligands

3.1.1 2-*N*-anilinopyrazine **(L1)**

The reaction of 2-chloropyrazine with aniline gave 75% yield when the mixture of two compounds were refluxed in an oil bath for 3 hours at 120 °C – 140 °C. The product was extracted with diethyl ether followed by washing with water. Re-crystallization from chloroform gave light brown crystal of **L1**. The infrared spectrum of compound **L1** showed medium absorption bands at 3307 cm^{-1} indicating N-H stretching of the secondary amine. Medium absorption bands at 1624 cm^{-1} and 1419 cm^{-1} was due to C=N stretching and C=C stretching. Meanwhile medium absorption at 1583 cm^{-1} indicates the N-H bending. The GCMS spectrum showed a molecular ion peak at *m/z* 170, which corresponded with the molecular formula $C_{10}H_9N_3$.

The ^{1}H NMR spectrum of **L1** shows three absorption peaks at δ 8.18 ppm, δ 8.04 ppm, and δ 7.19 ppm, which were due to H-3, H-5 and H-6 of pyrazine ring. A doublet at δ 7.37 ppm with *J* value of 8 Hz and a triplet at δ 7.18 ppm with *J* value of 7.3 Hz were attributed to H-2', H-6' and H-3', H-5' respectively. A triplet which is observed at δ 7.06 ppm with coupling constant of 7 Hz is assigned to H-4' of the aniline ring. A singlet observed at δ 6.68 was assigned to N-H peak.

The ^{13}C NMR spectrum of **L1** showed relatively low intensity absorption peaks at δ 152.3 ppm and δ 139.1 ppm which were due to quaternary carbon resonances of C-2 and C-1' respectively. Three medium peaks at δ 141.9 ppm, δ 134.9 ppm and δ 132.9 ppm were recorded due to the carbon resonance of C-3, C-5 and C-6 of the pyrazine ring while C-4' of the aniline ring was recorded at δ 123.6 ppm. In addition, two relatively high intensity peaks at δ 129.4 ppm and δ 120.3 ppm were recorded due to the two carbons resonances of C-2', C-6' and C-3', C-5' of the aniline ring. **Table 3.1** shows the ^{1}H-NMR and ^{13}C-NMR shifts of 2-*N*-anilinopyrazine.

Table 3.1: ^{1}H-NMR and ^{13}C-NMR shifts of 2-*N*-anilinopyrazine (L1)

	Chemical Shifts in ppm (δ)	
Proton / Carbon Number Assignments	^{1}H-NMR	^{13}C-NMR
3	8.18 (d, 1H)	141.9
5	8.04 (dd, 1H)	134.9
6	7.91 (d, 1H)	132.9
2’	7.37 (d, 2H)	129.4
3’	7.18 (t, 2H)	120.3
4’	7.04 (t, 1H)	123.6
5’	7.18 (t, 2H)	120.3
6’	7.37 (d, 2H)	129.4
N-H	6.68 (s, 1H)	-

The light brown crystal from the crystallization of **L1** in chloroform, was analyzed by X-ray diffraction method. **Figure 3.2** below shows the crystal structure for **L1**. The crystal of **L1** has a monoclinic system, $P2_{1/C}$. The two aromatic rings are aligned at 15.2 (1)° these open up the angle at the amino nitrogen to 130.4 (1)°. The amino nitrogen forms a hydrogen bond to the nitrogen atom of an adjacent molecule to furnish a chain motif. Thermal ellipsoid plot (Barbour, 2001) of **L1** at the 70% probability level, hydrogen atoms are drawn as spheres of arbitrary radius. Carbon-bound H-atoms were placed in calculated positions (C—H 0.95 Å) and were included in the refinement in the riding model approximation, with *U* (H) fixed at 1.2*U*(C). The amino H-atom was located in a different Fourier map, and was refined with a distance restraint of N—H 0.88 (1) Å. **Table 3.2 and Table 3.3** indicated crystal data and structure refinement and hydrogen-bond geometry (Å, °) for 2-*N*-anilinopyrazine **(L1).**

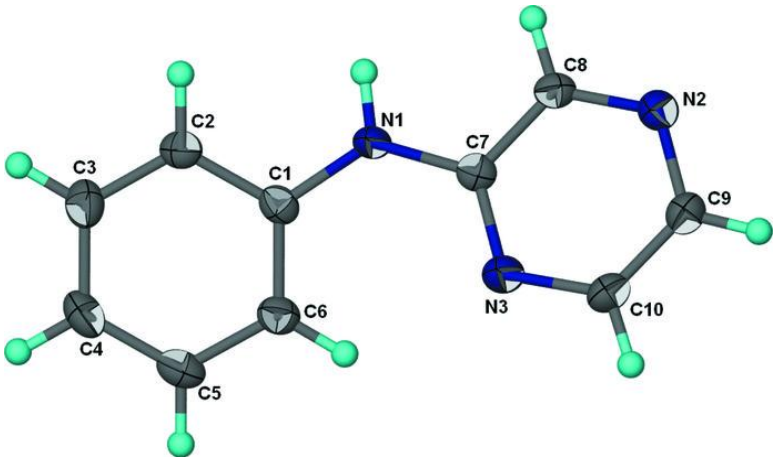

Figure 3.2: ORTEP diagram of 2-*N*-anilinopyrazine (L1)

Table 3.2: Crystal data and structure refinement for 2-*N*-anilinopyrazine (L1)

Identification code	*N*-(Pyrazin-2-yl)aniline
Empirical formula	$C_{10}H_9N_3$
Formula weight (g/mol)	171.20
Colour	Colourless
Crystal system, space group	Monoclinic, $P2_{1/C}$
Unit cell dimensions	a = 11.0644 (3) Å b = 7.8423 (3) Å c = 10.8907 (3) Å β = 116.439 (2)°
V (Å^3)	846.15 (5)
Z	4
$P_{calc.}$ (mg m^{-3})	1.344
Absorption coefficient (mm^{-1})	0.09
F_{000}	360
Crystal size (mm)	0.20 x 0.10 x 0.05
Θ_{max}	3.3–26.4
≤ h ≥	-14 to 14
≤ k≥	-10 to 10
≤ l ≥	-14 to 14
R_{int}	0.033
S	1.03
Symmetry code:(i)	$-x+1, y-1/2, -z+3/2$

Table 3.3: Hydrogen-bond geometry (Å, °) for 2-*N*-anilinopyrazine (L1)

D—H···*A*	*D*—H	H···*A*	*D*···*A*	*D*—H···*A*
N1—H1···N2i	0.89 (1)	2.12 (1)	2.977 (2)	162 (1)

3.1.2 2-*N*-(*m*-methyl)anilinopyrazine **(L2)**

The reaction of 2-chloropyrazine with *m*-toluidine gave 46% yield when the mixture of two compounds were refluxed in an oil bath for 8 hours at 120 – 140 °C. Re-crystallization from chloroform gave dark brown solid of **L2**. The structure of **L2** was confirmed by spectroscopic methods. The infrared spectrum of compound **L2** showed similar absorption bands as **L1**. The GCMS spectrum showed a molecular ion peak at *m/z* 184, which corresponded with the molecular formula $C_{11}H_{11}N_3$. The ^{1}H NMR spectrum of **L2** showed a similar observation as in **L1**. The additional peak of protons of the methyl group was indicated by the observation of a singlet at δ 2.28 in **L2** spectra. The ^{13}C NMR spectrum of **L2** showed relatively similar observations as in **L1** except there is an additional peak observed at δ 21.5 in up-field region was due to sp^3 carbon of methyl group of 3-methylaniline ring. **Table 3.4** shows ^{1}H-NMR and ^{13}C-NMR shifts of 2-*N*-(*m*-methyl)anilinopyrazine **(L2).**

Table 3.4: ^{1}H-NMR and ^{13}C-NMR shifts of 2-*N*-(*m*-methyl)anilinopyrazine (L2)

	Chemical Shifts in ppm (δ)	
Proton / Carbon Number Assignments	^{1}H-NMR	^{13}C-NMR
2	-	152.3
3	8.18 (d, 1H)	141.9
5	8.04 (dd, 1H)	134.7
6	7.91 (d, 1H)	132.8
1’	-	139.1
2’	7.37 (d, 2H)	124.5
3’	-	139.2
4’	7.04 (t, 1H)	117.5
5’	7.18 (t, 2H)	121.3
6’	7.37 (d, 2H)	129.2
N-H	6.68 (s, 1H)	-
CH_3	-	21.5

3.1.3 2-*N*-(*p*-methyl)anilinopyrazine **(L3)**

The reaction of 2-chloropyrazine with *p*-toluidine gave 46% yield when the mixture of two compounds were refluxed in an oil bath for 9 hours at 120 °C – 140 °C. Re-crystallization from chloroform gave dark brown crystal of **L3**. The structure of **L3** was confirmed by spectroscopic methods and the crystal structure was confirmed by X-ray diffraction method. The infrared spectrum of compound **L3** showed similar absorption bands as **L1**. The GCMS spectrum showed a molecular ion peak at *m/z* 184, which corresponded with the molecular formula $C_{11}H_{11}N_3$. The ^{1}H NMR spectrum of **L3** showed a similar observation as in **L1** except there was an additional peak of protons of the methyl group was indicated by the observation of a singlet at δ 2.30. The ^{13}C NMR spectrum of **L3** showed relatively similar observations as in **L1** except there is an additional peak observed at δ 20.8 in up-field region was due to sp^3 carbon of methyl group of 3-methylaniline ring. **Table 3.5** shows ^{1}H-NMR and ^{13}C-NMR shifts of 2-*N*-(*p*-methyl)anilinopyrazine **(L3).**

Table 3.5: ^{1}H-NMR and ^{13}C-NMR shifts of 2-*N*-(*p*-methyl)anilinopyrazine (L3)

	Chemical Shifts in ppm (δ)	
Proton / Carbon Number Assignments	^{1}H-NMR	^{13}C-NMR
2	-	152.6
3	8.19 (d, 1H)	134.6
5	8.08 (dd, 1H)	133.7
6	7.94 (d, 1H)	132.5
2’	7.30 (d, 2H)	129.9
3’	7.18 (d, 2H)	121.1
4’	-	136.3
5’	7.18 (d, 2H)	121.1
6’	7.30 (d, 2H)	129.9
N-H	6.59 (s, 1H)	-
CH_3	2.30 (s, 3H)	20.8

The dark brown crystal from the crystallization of **L3** in chloroform was analyzed by X-ray diffraction method. **Figure 3.2** below shows the crystal structure for **L3**. The crystal of **L3** has a monoclinic system, *C2/c*. The two aromatic systems in the title compound, $C_{11}H_{11}N_3$, are inclined by 19.1 (1)°, whilst the angle at the central amino N atom is 130.3 (2)°. The amino group forms a hydrogen bond to the pyrazine N-1 atom of an adjacent molecule, forming a chain motif. Carbon-bound H-atoms were placed in calculated positions (C—H 0.95–0.98 Å) and were included in the refinement in the riding model approximation, with *U*(H) fixed at 1.2–1.5*U*(C). The amino H-atom was located in a difference Fourier map, and was refined with a distance restraint of N–H 0.88±0.01 Å. Thermal ellipsoid plot (Barbour, 2001) of **L3** at the 70% probability level, hydrogen atoms are drawn as spheres of arbitrary radius. Carbon-bound H atoms were placed in calculated positions (C—H 0.95 Å) and were included in the refinement in the riding model approximation, with *U* (H) fixed at 1.2*U*(C). The amino H-atom was located in a difference Fourier map, and was refined with a distance restraint of N—H 0.88 (1) Å. **Table 3.6 and Table 3.7** indicate crystal data and structure refinement and hydrogen-bond geometry (Å, °) for 2-*N*-(*p*-methyl)anilinopyrazine **(L3).**

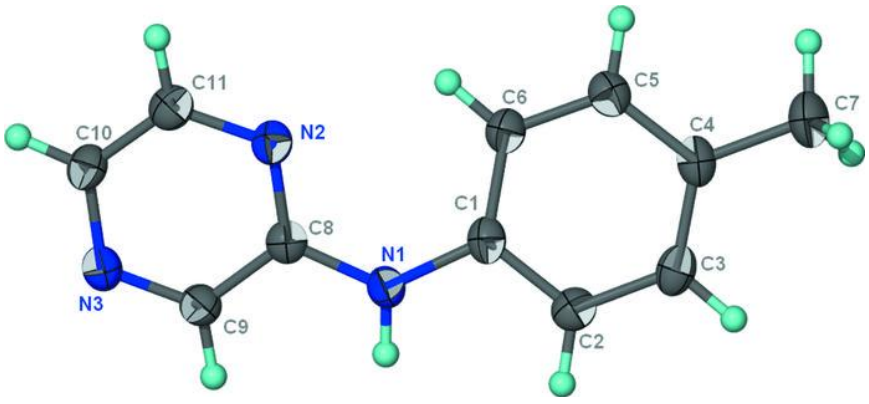

Figure 3.3: ORTEP diagram of 2-*N*-(*p*-methyl)anilinopyrazine (L3)

Table 3.6: Crystal data and structure refinement for 2-*N*-(p-methyl)anilinopyrazine (L3)

Identification code	*N*-(Pyrazin-2-yl)-4-toluidine
Empirical formula	$C_{11}H_{11}N_3$
Formula weight (g/mol)	185.23
Colour	Colourless
Crystal system, space group	Monoclinic, *C*2/*c*
Unit cell dimensions	*a* = 21.7179 (7) Å *b* = 7.5323 (3) Å *c* = 12.0073 (5) Å β = 105.790 (3)º a = 11.0644 (3)° b = 7.8423 (3)° c = 10.8907 (3)° β = 116.439 (2)
V (Å^3)	846.15 (5)
Z	8
$P_{calc.}$ (mg m^{-3})	1.302
Absorption coefficient (mm^{-1})	0.08
F_{000}	784
Crystal size (mm)	0.30 × 0.20 × 0.05
Θ_{max}	27.5º
≤ h ≥	−28 to 28
≤ k ≥	−9 to 9
≤ l ≥	−15 to 15
R_{int}	0.041
S	1.03
Symmetry code: (i)	−*x*+1/2, *y*+1/2, −*z*+1

Table 3.7: Hydrogen-bond geometry (Å, °) for 2-*N*-(*p*-methyl)anilinopyrazine (L3)

D—H···*A*	*D*—H	H···*A*	*D*···*A*	*D*—H···*A*
N1—H1···N3i	0.89 (2)	2.10 (2)	2.963 (2)	163 (2)

3.1.4 2-*N*-*(p*-chloro)anilinopyrazine **(L4)**

2-chloropyrazine was added to *p*-chloroaniline for 5 hours at 120 – 140 °C in an oil bath. Evaporation of solvent gave the product, 2-*N*-(*p*-chloro)anilinopyrazine. Re-crystallization from chloroform gave yellowish crystal of **L4.** The infrared spectrum of compound **L4** showed similar observations as in **L1**. The GCMS spectrum showed a molecular ion peak at *m/z* 205, which corresponded with the molecular formula $C_{10}H_8ClN_3$. The ^{1}H NMR spectrum of **L4** showed similar absorption peaks as in **L1.** The ^{13}C NMR spectrum of **L4** showed relatively low intensity absorption peaks as in **L1** but the C-4' peak has been shifted to lower downfield due the presence of chlorine atom. Table 3.8 shows ^{1}H-NMR and ^{13}C-NMR shifts of 2-*N*-(p-chloro)anilinopyrazine **(L4).**

Table 3.8: ^{1}H-NMR and ^{13}C-NMR shifts of 2-*N*-(p-chloro)anilinopyrazine (L4)

	Chemical Shifts in ppm (δ)	
Proton / Carbon Number Assignments	^{1}H-NMR	^{13}C-NMR
2	-	151.8
3	8.19 (d, 1H)	141.7
5	8.12 (dd, 1H)	135.2
6	8.01 (d, 1H)	133.2
1'	-	128.2
2'	7.44 (d, 2H)	121.2
4'	-	137.8
3'	7.30 (d, 2H)	129.3
5'	7.30 (d, 2H)	129.3
6'	7.44 (d, 2H)	121.2
N-H	6.54 (s, 1H)	-

The yellowish crystal from the crystallization of **L4** in chloroform, was analyzed by X-ray diffraction method. **Figure 3.4** below shows the ORTEP diagram for 2-*N*-(*p*-chloro)anilinopyrazine **(L4)**. The crystal of **L4** has a monoclinic system, $C_{2/C.}$ The two aromatic systems in the title compound, $C_{10}H_8ClN_3$, the dihedral angle between the aromatic rings is 43.0 (1) ° and the bridging C—N—C angle is 128.19 (16)°. The amino N atom of one molecule forms a hydrogen bond to the N-1 and N-2 atoms of an adjacent pyrazinyl ring, generating an inversion dimer. Carbon-bound H-atoms were placed in calculated positions (C—H 0.95 Å) and were included in the refinement in the riding model approximation, with *U* (H) set to 1.2*U*eq(C). The amino H-atom was located in a difference Fourier map, and was refined with a distance restraint of N–H 0.88±0.01 Å; its temperature factor was freely refined. Thermal ellipsoid plot (Barbour, 2001) of **L4** at the 70% probability level, hydrogen atoms are drawn as spheres of arbitrary radius. **Table 3.9 and Table 3.10** indicate crystal data and structure refinement and hydrogen-bond geometry (Å, °) for 2-*N*-(*p*-chloro)anilinopyrazine **(L4).**

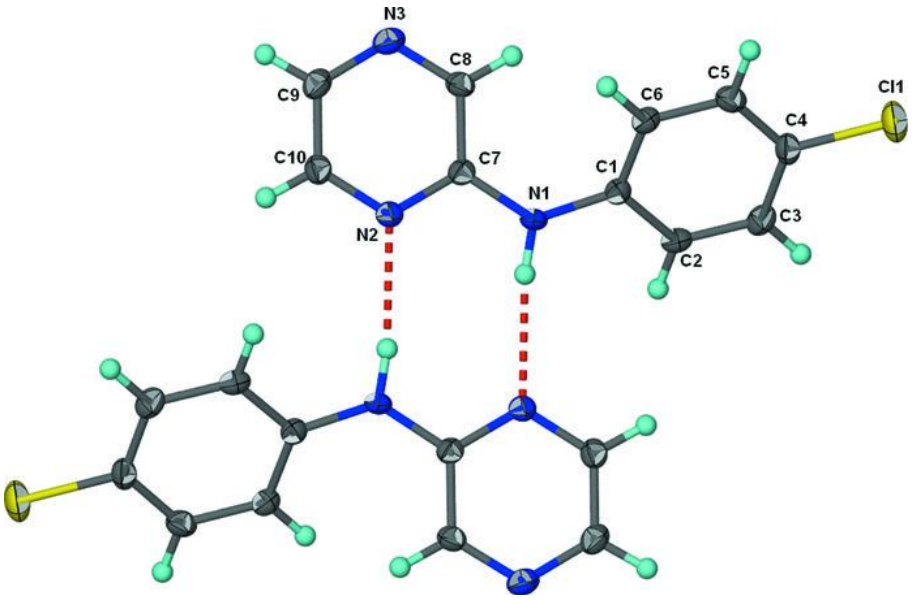

Figure 3.4: ORTEP diagram of 2-*N*-(*p*-chloro)anilinopyrazine (L4)

Table 3.9: Crystal data and structure refinement for 2-*N*-(*p*-chloro)anilinopyrazine (L4)

Identification code	2-*N*-(*p*-chloro)anilinopyrazine
Empirical formula	$C_{10}H_8ClN_3$
Formula weight (g/mol)	205.64
Colour	Colourless
Crystal system, space group	Monoclinic, *C*2/*c*
Unit cell dimensions	*a* = 12.1257 (3)
	b = 3.7944 (1) Å
	c = 19.7242 (5)
	β = 91.370 (2) º
V	907.25 (4) $Å^3$
Z	4
$P_{calc.}$ (mg m^{-3})	1.506
Absorption coefficient (mm^{-1})	0.38
F_{000}	424
Crystal size (mm)	0.25 × 0.05 × 0.01
Θ_{max}	2.6–28.1º
≤ h ≥	−15 to 15
≤ k ≥	−4 to 4
≤ l ≥	−25 to 24
R_{int}	0.033
S	1.14
Symmetry code: (i)	−*x*+1, −*y*+1, −*z*+1

Table 3.10: Hydrogen-bond geometry (Å, °) for 2-*N*-(*p*-chloro)anilinopyrazine (L4)

D—H···*A*	*D*—H	H···*A*	*D*···*A*	*D*—H···*A*
N1—H1···N2i	0.88(1)	2.15(1)	3.023(2)	171(2)

3.2 Characterization of 2-chloroquinoxaline based ligands

Reaction of 2-chloroquinoxaline with aniline, *m*-toluidine, *p*-toluidine, and *p*-chloroaniline were studied. **Figure 3.5** shows a diagrammatic representation of various reactions.

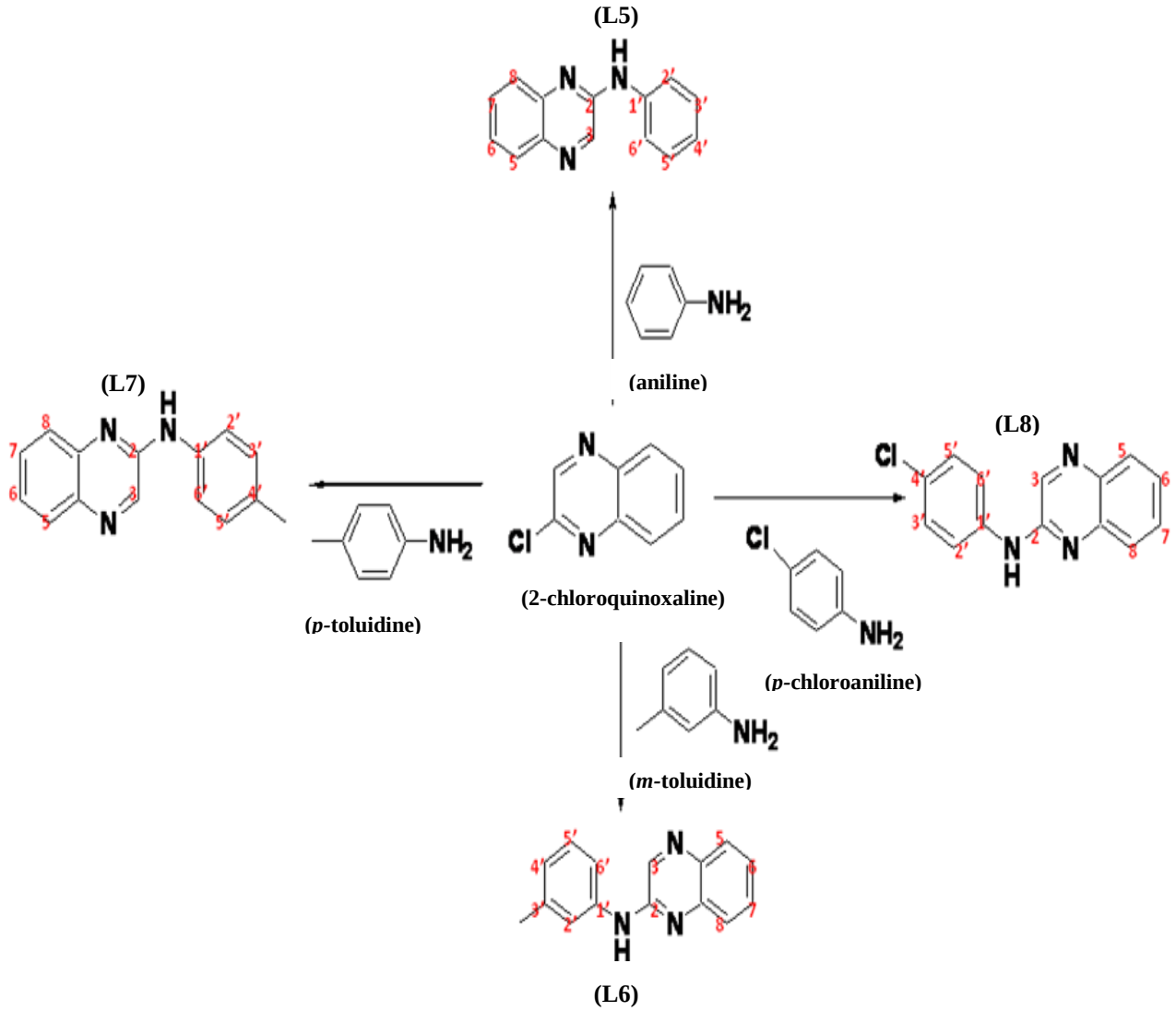

Figure 3.5: Preparation of quinoxaline based ligands

3.2.1 2-*N*-anilinoquinoxaline **(L5)**

The reaction of 2-chloroquinoxaline with aniline gave 65% yield when the mixture of two compounds were refluxed in an oil bath for 2 hours at 120 °C – 140 °C. The product was extracted with diethyl ether followed by washing with water. Re-crystallization from chloroform gave yellowish solid of **L5**.

The infrared spectrum of compound **L5** showed medium absorption bands at 3312 cm^{-1} indicating N-H stretching of the secondary amine. Medium absorption bands at 1624 cm^{-1} and 1426 cm^{-1} were due to C=N stretching and C=C stretching. The GCMS spectrum showed a molecular ion peak at *m/z* 221, which corresponded with the molecular formula $C_{14}H_{11}N_3$.

The ^{1}H NMR spectrum of **L5** showed similar peaks in the region of δ 8.45 ppm to 7.92 ppm which were due to H-3, H-8, H-5, H-7 and H-6 of quinoxaline ring. A doublet at δ 7.73 ppm with *J* value of 8 Hz and two triplets peak at δ 7.39 ppm and δ 7.11 ppm with *J* value of 8.2 Hz and 7.6 Hz were attributed to H-2', H-6, H-3', H-5'and H-4' respectively. A singlet observed at δ 6.68 ppm was assigned to N-H peak.

The ^{13}C NMR spectrum of **L5** indicated the presence of 14 carbons in the compound which is in agreement with the molecular formula. The spectrum showed absorption peaks at ranges δ 149.2 ppm and δ 125.6 ppm which were due to carbon peaks of quinoxaline ring. While carbon resonances recorded at δ 129.2 ppm to δ 120.0 ppm were due to five carbon peaks of aniline ring.

Table 3.11: ^{1}H-NMR and ^{13}C-NMR shifts of 2-*N*-anilinoquinoxaline (L5)

	Chemical Shifts in ppm (δ)	
Proton / Carbon Number Assignments	^{1}H-NMR	^{13}C-NMR
2	-	149.2
3	8.45 (s, 1H)	137.8
5	7.80 (d, 1H)	128.8
6	7.45 (m, 1H)	125.6
7	7.61 (m, 1H)	126.8
8	7.92 (dd, 1H)	130.3
9	-	138.3
10	-	139.1
1’	-	141.1
2’	7.73 (d, 2H)	129.2
3’	7.39 (t, 2H)	120.0
4’	7.11 (t, 1H)	123.7
5’	7.39 (t, 2H)	120.0
6’	7.73 (d, 2H)	129.2
N-H	6.68 (s, 1H)	-

3.2.2 2-*N*-(*m*-methyl)anilinoquinoxaline **(L6)**

The reaction of 2-chloroquinoxaline with *m*-toluidine in ethanol gave 42% yield when the mixture of two compounds were refluxed in an oil bath for 5 hours at 120 – 140 °C. Re-crystallization from chloroform gave yellow solid of **L6**. The infrared spectrum of compound **L6** showed similar absorption bands as in **L5**. The GCMS spectrum showed a molecular ion peak at *m/z* 235, which corresponded with the molecular formula $C_{15}H_{13}N_3$. The ^{1}H NMR spectrum and ^{13}C NMR spectrum of **L6** showed similar peaks pattern as in **L5.**

Table 3.12: ^{1}H-NMR and ^{13}C-NMR shifts of 2-*N*-(*m*-methyl)anilinoquinoxaline (L6)

	Chemical Shifts in ppm (δ)	
Proton / Carbon Number Assignments	^{1}H-NMR	^{13}C-NMR
2	-	149.3
3	8.45 (s, 1H)	137.9
5	8.01 (d, 1H)	128.7
6	7.45 (m, 1H)	125.6
7	7.61 (m, 1H)	126.8
8	7.93 (dd, 1H)	130.3
9	-	138.2
10	-	139.0
1’	-	141.1
2’	7.73 (d, 2H)	129.2
3’	7.38 (t, 2H)	120.0
4’	7.10 (t, 1H)	123.6
5’	7.38 (t, 2H)	120.2
6’	7.73 (d, 2H)	129.2
N-H	6.88 (s, 1H)	-

3.2.3 2-*N*-(*p*-methyl)anilinoquinoxaline **(L7)**

The reaction of 2-chloroquinoxaline with *p*-toluidine gave 49% yield when the mixture of two compounds were refluxed in an oil bath for 5 hours at 120 – 140 °C. Re-crystallization from chloroform gave orange crystal of **L7**. The structure of **L7** was confirmed by spectroscopic methods and the crystal structure was confirmed by X-ray diffraction method. The infrared spectrum of compound **L7** showed similar absorption bands as observed in **L5**. The GCMS spectrum showed a molecular ion peak at *m/z* 235, which corresponded with the molecular formula $C_{15}H_{13}N_3$ as indicates for **L5.**The ^{1}H NMR spectrum of **L7** and ^{13}C NMR spectrum of **L7** showed relatively same similar absorption peaks as in **L5.**

Table 3.13: ^{1}H-NMR and ^{13}C-NMR shifts of 2-*N*-(*p*-methyl)anilinoquinoxaline (L7)

	Chemical Shifts in ppm (δ)	
Proton / Carbon Number Assignments	^{1}H-NMR	^{13}C-NMR
2	-	149.3
3	8.38 (s, 1H)	137.8
5	7.72 (d, 1H)	128.8
6	7.41 (m, 1H)	125.4
7	7.53 (m, 1H)	128.0
8	7.85 (dd, 1H)	130.1
9	-	136.1
10	-	137.7
1’	-	141.1
2’	7.57 (d, 2H)	129.7
3’	7.18 (d, 2H)	120.4
4’	7.04 (t, 1H)	133.4
5’	7.18 (d, 2H)	120.4
6’	7.57 (d, 2H)	129.7
N-H	6.68 (s, 1H)	-
CH_3	2.34 (s, 3H)	20.8

Re-crystallization of **L7** in chloroform gave dark brown crystals which were analyzed by X-ray diffraction method. **Figure 3.6** shows the ORTEP diagram of **L7.** The crystal of **L7** has an Orthorhombic, *Pbca.* The aromatic and the aromatic fused-rings in the title compound, **L7**, open the angle at the planar N atom to 130.07 (13)° and 129.98 (13)° in the two independent molecules in the asymmetric unit. The amino N atom of one molecule forms a hydrogen bond to the 4-N atom of an adjacent quinoxalinyl ring, generating a supramolecular chain. Carbon-bound H-atoms were placed in calculated positions (C—H 0.95 to 0.98 Å) and were included in the refinement in the riding model approximation, with *U* (H) set to 1.2 to 1.5eq*U*(C). The amino H-atoms were located in a difference Fourier map, and were refined with a distance restraint of N–H 0.88±0.01 Å; their temperature factors were freely refined. Thermal ellipsoid plots (Barbour, 2001) for the two independent molecules of **L7** at the 70% probability level. Hydrogen atoms are drawn as spheres of arbitrary radius. **Table 3.14** showed crystal data and structure refinement for **(L7)** meanwhile **Table 3.15** indicated the hydrogen-bond geometry (Å, °) for **(L7).**

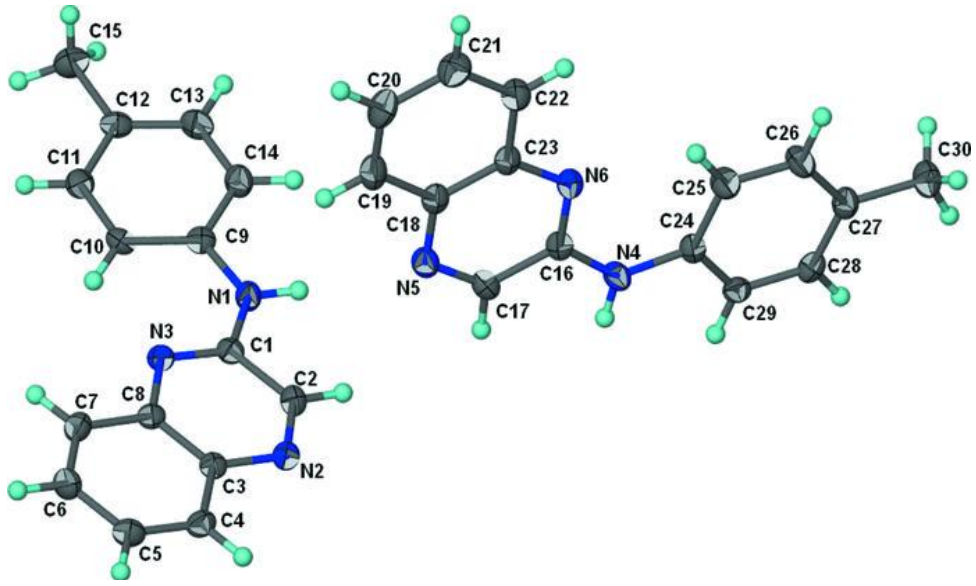

Figure 3.6: ORTEP diagram of 2-*N*-(*p*-methyl)anilinoquinoxaline (L7)

Table 3.14: Crystal data and structure refinement for 2-*N*-(*p*-methyl)anilinoquinoxaline (L7)

Identification code	*N*-(Quinoxalin-2-yl)-4-toluidine
Empirical formula	$C_{15}H_{13}N_3$
Formula weight (g/mol)	235.28
Colour	Colourless
Crystal system, space group	Orthorhombic, *Pbca*
Unit cell dimensions	*a* = 12.2081 (9) Å
	b = 11.3720 (9) Å
	c = 35.097 (3) Å
V (Å^3)	4872.5 (6) Å^3
Z	16
$P_{calc.}$ (mg m^{-3})	1.283
Absorption coefficient (mm^{-1})	0.08
F_{000}	1984
Crystal size (mm)	0.40 × 0.15 × 0.05
Θ_{max}	27.5°
≤ h ≥	−15 to 15
≤ k ≥	−14 to 9
≤ l ≥	−45 to 45
R_{int}	0.051
S	1.03
Symmetry code: (i)	−*x*+3/2, *y*+1/2, *z*

Table 3.15: Hydrogen-bond geometry (Å, °) for 2-*N*-(*p*-methyl)anilinoquinoxaline (L7)

D—H···*A*	*D*—H	H···*A*	*D*···*A*	*D*—H···*A*
N1—H1···N5i	0.89 (1)	2.26 (2)	3.114 (2)	163 (2)
N4—H4···N2i	0.87 (1)	2.19 (2)	3.017 (2)	157 (2)

3.2.4 2-*N*-(*p*-chloro)anilinoquinoxaline **(L8)**

The reaction of 2-chloroquinoxaline with *p*-chloroaniline gave 68% yield when the mixture of two compounds were refluxed in an oil bath for 5 hours at 120 – 140 °C. Re-crystallization from chloroform gave orange solid of **L8**. The infrared spectrum of compound **L8**, ^{1}H NMR spectrum and ^{13}C NMR spectrum showed similar absorptions as in L5. The GCMS spectrum showed a molecular ion peak at *m/z* 255, which corresponded with the molecular formula $C_{10}H_8ClN_3$.

Table 3.16: ^{1}H-NMR and ^{13}C-NMR shifts of 2-*N*-(*p*-chloro)anilinoquinoxaline (L8)

	Chemical Shifts in ppm (δ)	
Proton / Carbon Number Assignments	^{1}H-NMR	^{13}C-NMR
2	-	149.0
3	8.31 (s, 1H)	138.5
5	7.72 (d, 1H)	129.1
6	7.40 (m, 1H)	125.7
7	7.58 (m, 1H)	126.7
8	7.84 (dd, 1H)	129.1
9	-	130.1
10	-	138.8
1’	-	140.9
2’	7.27 (d, 2H)	120.7
3’	7.68 (d, 2H)	128.9
4’	7.04 (t, 1H)	128.3
5’	7.68 (d, 2H)	128.9
6’	7.27 (d, 2H)	120.7
N-H	6.68 (s, 1H)	-

3.3 Characterization of copper complexes

3.3.1 Physical Properties

In general, an acetonitrile solution of the copper(II) acetate was added to hot acetonitrile solution (50-60 °C) of ligands. The resulting mixture was stirred for 30 minutes. The complexes were precipitated as microcrystalline powders. They were removed by filtration, washed with acetonitrile followed by diethylether and dried in vacuum desiccators over anhydrous calcium chloride. All the complexes are coloured and obtained as powder and crystal. The complexes are insoluble in common organic solvents but soluble in chloroform, methanol, DMF and DMSO. **Table 3.17** below shows the physical properties of the synthesized compounds.

Table 3.17: Physical properties of copper complexes

Compounds	Labels	Colour	Melting point (°C)	Percentage yield (%)
2-*N*-anilinopyrazine	**L1**	light brown	126 - 129	75
$[Cu_2(C_2H_3O_2)_4\ (C_{10}H_9N_3)_2]$	**CuL1**	blue	230 – 233	48
2-*N*-(m-methyl)anilinopyrazine	**L2**	dark brown liquid	-	46
$[Cu_2(C_2H_3O_2)_4\ (C_{11}H_{11}N_3)_2]$	**CuL2**	blue	233 – 237	56
2-*N*-(p-methyl)anilinopyrazine	**L3**	dark brown	102 – 104	46
$[Cu_2(C_2H_3O_2)_4\ (C_{11}H_{11}N_3)_2]$	**CuL3**	blue	221 – 223	56
2-*N*-(p-chloro)anilinopyrazine	**L4**	yellowish	143 – 145	58
$[Cu_2(C_2H_3O_2)_4\ (C_{10}H_8ClN_3)_2]$	**CuL4**	dark green	237 – 239	75
2-*N*-anilinoquinoxaline	**L5**	yellow	132 – 134	65

$[Cu_2(C_2H_3O_2)_4\ (C_{14}H_{11}N_3)_2]$	**CuL5**	dark blue	245 – 248	69
2-*N*-(m-methyl)anilinoquinoxaline	**L6**	yellow	90 -91	42
$[Cu_2(C_2H_3O_2)_4\ (C_{15}H_{13}N_3)_2]$	**CuL6**	dark blue	221 – 222	72
2-*N*-(p-methyl)anilinoquinoxaline	**L7**	orange	148 – 149	49
$[Cu_2(C_2H_3O_2)_4\ (C_{15}H_{13}N_3)_2]$	**CuL7**	green	215 – 217	43
2-*N*-(p-chloro)anilinoquinoxaline	**L8**	orange	191 – 192	68
$[Cu_2(C_2H_3O_2)_4\ (C_{10}H_8ClN_3)_2]$	**CuL8**	green	228 – 230	87

Based on **Table 3.17**, the melting point of all complexes ranges between 220 – 250 °C. It can be seen that the melting point of the complexes are higher than in free ligands. Copper has been coordinated to ligand through Lewis acid – Lewis base coordination. In coordination method, every ligand must have at least one unshared pair of valence electrons. Pyrazine and quinoxaline derivatives have three nitrogen atoms to be coordinated with copper ion. The nitrogen atoms of pyrazine and quinoxaline ring donate the electrons to the empty *d* orbital in copper ion. As the result, the ligands play the role as Lewis base meanwhile copper acts as Lewis acid.[57] The highest melting point among the copper complexes were from $[Cu_2(C_2H_3O_2)_4\ (C_{10}H_8ClN_3)_2]$, **CuL4** and $[Cu_2(C_2H_3O_2)_4\ (C_{10}H_8ClN_3)_2]$, **CuL8.** The differences in melting point can be explained by the size of the compound and also the type of bonding. The larger molecular mass for **CuL4** and **CuL8** compared to other copper complexes gave higher melting point. The attractive orbital interactions between copper with pyrazine and quinoxaline ligands arise mainly from σ donation from ligand to copper (Cu ← ligand). But in some complexes of pyrazine and quinoxaline, it is been noted that there were significant contributions of π back-donation by copper to ligand (Cu → ligands), but the σ donation from ligand to copper (Cu ← ligand) still remains as the dominant orbital interaction.

The relative contributions of σ donation and π back-donation are only slightly altered when substituent changes from a good π donor to a poor π donor or π withdrawer. Electrostatic forces between the metal ion and the ligand are always attractive, and they are very strong. The electrostatic arise from the attraction between the local negative charge concentration at the overall positively charged donor atom of pyrazine and quinoxalines based ligands which act as the Lewis base ligands with the positive charge of the copper nucleus.

3.3.2 Elemental Analysis (CHN Analysis)

Table 3.18 shows the elemental analyses of the complexes obtained from the reaction of the pyrazine and quinoxaline based ligands with copper(II) acetate.

Table 3.18: Percentage elemental analysis in complexes

Compounds	C Found Calc.	H Found Calc.	N Found Calc.
$[Cu_2(C_2H_3O_2)_4\ (C_{10}H_9N_3)_2]$ **CuL1**	48.35 47.66	4.05 4.26	11.34 11.92
$[Cu_2(C_2H_3O_2)_4\ (C_{11}H_{11}N_3)_2]$ **CuL2**	49.06 49.86	4.55 4.71	11.08 11.63
$[Cu_2(C_2H_3O_2)_4\ (C_{11}H_{11}N_3)_2]$ **CuL3**	49.77 48.86	4.58 4.11	11.49 13.89
$Cu_2(C_2H_3O_2)_4\ (C_{10}H_8ClN_3)_2]$ **CuL4**	42.88 43.41	3.22 3.62	10.12 10.85
$[Cu_2(C_2H_3O_2)_4\ (C_{14}H_{11}N_3)_2]$ **CuL5**	53.11 53.66	3.96 4.22	10.22 10.45
$[Cu_2(C_2H_3O_2)_4\ (C_{15}H_{13}N_3)_2]$ **CuL6**	54.12 54.74	4.08 4.56	9.65 10.08
$[Cu_2(C_2H_3O_2)_4\ (C_{15}H_{13}N_3)_2]$ **CuL7**	54.21 53.07	4.11 4.66	10.12 11.88
$[Cu_2(C_2H_3O_2)_4\ (C_{10}H_8ClN_3)_2]$ **CuL8**	48.98 49.43	3.26 3.66	9.08 9.61

The calculated values for carbon, nitrogen and hydrogen atomic compositions agreed satisfactorily to the theoretical values.

3.3.3 Infrared Spectroscopy (IR)

Table 3.19 shows the IR spectroscopy of the free ligands and its copper complexes carried out in the 4000 – 400 cm^{-1} range.

Table 3.19: Characteristics IR bands of ligands and complexes

Compounds	N-$H_{stretching}$	C=$N_{stretching}$	C=$C_{stretchin}$	Cu-N
2-*N*-anilinopyrazine (**L1**)	3299	1605	1434	-
$[Cu_2(C_2H_3O_2)_4\ (C_{10}H_9N_3)_2]$ **(CuL1)**	3307	1583	1419	501
2-*N*-(*m*-methyl)anilinopyrazine **(L2)**	3312	1624	1426	-
$[Cu_2(C_2H_3O_2)_4\ (C_{11}H_{11}N_3)_2]$ **(CuL2)**	3296	1616	1411	504
2-*N*-(*p*-methyl)anilinopyrazine **(L3)**	3293	1618	1411	-
$[Cu_2(C_2H_3O_2)_4\ (C_{11}H_{11}N_3)_2]$ **(CuL3)**	3311	1618	1414	501
2-*N*-(*p*-chloro)anilinopyrazine **(L4)**	3296	1625	1458	-
$[Cu_2(C_2H_3O_2)_4\ (C_{10}H_8ClN_3)_2]$ **(CuL4)**	3309	1607	1421	502
2-*N*-anilinoquinoxaline **(L5)**	3312	1624	1426	-
$[Cu_2(C_2H_3O_2)_4\ (C_{14}H_{11}N_3)_2]$ **(CuL5)**	3321	1591	1417	521
2-*N*-(*m*-methyl)anilinoquinoxaline **(L6)**	3322	1625	1417	-

$[Cu_2(C_2H_3O_2)_4\ (C_{15}H_{13}N_3)_2]$ **(CuL6)**	3295	1616	1412	507
2-*N*-(*p*-methyl)anilinoquinoxaline **(L7)**	3310	1624	1421	-
$[Cu_2(C_2H_3O_2)_4\ (C_{15}H_{13}N_3)_2]$ **(CuL7)**	3296	1617	1412	507
2-*N*-(*p*-chloro)anilinoquinoxaline **(L8)**	3308	1622	1445	-
$[Cu_2(C_2H_3O_2)_4\ (C_{10}H_8ClN_3)_2]$ **(CuL8)**	3310	1587	1416	508

A substantial part of the knowledge concerning the mode of bonding in metal complexes can be gained by applying IR spectroscopy. A verification of the structure of the complexes of the organic ligands can be achieved by comparing the IR spectra of the free ligands with those of the copper complexes. N-H stretching for free pyrazine ligands and copper complexes appeared in ranges between 3296 cm^{-1} to 3322 cm^{-1}.[58] It can be seen that in free ligands and copper complexes the vibrational bands recorded at almost the same wavelength. This observation indicated that the N-H does not involve in the coordination with metal cation. The presence of sharp bands with high frequency in free ligands and in copper complexes corresponding to non-hydrogen bonded N–H to the metal cation. Based on X-Ray crystallography structure of the copper complexes it can be seen that the metal cation only coordinated to the C=N in the pyrazine or quinoxaline ring instead of N-H of aniline ring.[59] The infrared spectra of the complexes exhibited C=N stretching in the range of 1580 – 1630 cm^{-1} which showed a shifting to the lower frequencies compared with its free ligand. The shifts were due to the coordination of azomethine nitrogen atom to empty *d* orbital of metal cation that would reduce the electron density in the azomethine link and thus alter the C=N absorption to the lower wavelength. [60] The spectra of free ligands and copper complexes showed

the presence of medium absorption peak in the region 1600-1585 cm^{-1} along with the sharp peaks with high intensity in the 1500-1400 cm^{-1} region, corresponds to the skeletal vibration, involving C-C stretching vibration in the ring. Meanwhile, the IR stretching frequency observed at 1410 to 1426 cm^{-1} in the complexes has been attributed to the presence of acetate group.[61] Another evident to prove the existence of acetate ion is a sharp and strong band in the 817-829 cm^{-1} region in every IR spectra of copper complex. This band is similar to those reported earlier.[62]

New bands at 499, 517, 501, 502, 517, 508, 502 and 502 cm^{-1} for **CuL1, CuL2, CuL3, CuL4, CuL5, CuL6, CuL7** and **CuL8** complexes respectively observed in the spectra of complexes are corresponding to νM-N.[63] These peaks support the involvement of N atoms in complexation with metal ions under investigation.[64] The band ranges from 490 – 520 cm^{-1} in spectrums were for the M-N complexation in divalent metal ion, such as copper ion.[65]

3.3.4 UV-Visible

Table 3.20 shows the electronic spectroscopic data of the free ligands and its copper complexes. The absorption spectra of the Cu(II) complexes were recorded in 10^{-4} M $CHCl_3$ solutions in the range 200–800 nm using a quartz cuvette of 1 cm path length.

Table 3.20: Electronic spectra of ligands and complexes

		Wavelength (nm)			
Compounds	**Labels**	**Intraligand**		**Charge transfer**	**d-d transition**
2-N-anilinopyrazine	**L1**	324	417	-	-
$[Cu_2(C_2H_3O_2)_4\ (C_{10}H_9N_3)_2]$	**CuL1**	326	424	465	630
2-N-(m-methyl)anilinopyrazine	**L2**	355	398	-	-
$[Cu_2(C_2H_3O_2)_4\ (C_{11}H_{11}N_3)_2]$	**CuL2**	358	385	432	675
2-N-(p-methyl)anilinopyrazine	**L3**	341	382	-	-
$[Cu_2(C_2H_3O_2)_4\ (C_{11}H_{11}N_3)_2]$	**CuL3**	340	395	428	652
2-N-(p-chloro)anilinopyrazine	**L4**	358	395	-	-
$[Cu_2(C_2H_3O_2)_4\ (C_{10}H_8ClN_3)_2]$	**CuL4**	360	405	420	680
2-N-anilinoquinoxaline	**L5**	340	383	-	-
$[Cu_2(C_2H_3O_2)_4\ (C_{14}H_{11}N_3)_2]$	**CuL5**	341	392	415	665
2-N-(m-methyl)anilinoquinoxaline	**L6**	345	402	-	-
$[Cu_2(C_2H_3O_2)_4\ (C_{15}H_{13}N_3)_2]$	**CuL6**	340	370	412	660
2-N-(p-methyl)anilinoquinoxaline	**L7**	340	392	-	-
$[Cu_2(C_2H_3O_2)_4\ (C_{15}H_{13}N_3)_2]$	**CuL7**	341	395	442	665
2-N-(p-chloro)anilinoquinoxaline	**L8**	325	380	-	-
$[Cu_2(C_2H_3O_2)_4\ (C_{10}H_8ClN_3)_2]$	**CuL8**	326	382	412	680

Organic ligands **L1, L2, L3, L4, L5, L6, L7** and **L8** acting as Lewis bases coordinate or bond with the Cu^{2+} which acts as a Lewis acid. Historically this kind of attachment has been called either a coordinate covalent bond or a dative bond. The distinguishing characteristic of such bonds is that the shared electron pairs which constitute the bonds come from only one of the bonded species. The number of ligand attachments to the metal ion is called the coordination number. Ligands which can only make one bond with an ion are called monodentate ligands. The pyrazine and quinoxaline substituted ligands that has been used in this reaction are monodentate ligands. The UV-visible spectra for free ligands showed two bands which indicate the intraligands transition. Meanwhile, the complexes showed the presence of three bands which indicate intraligand transition (π–π* and n - π* transition), charge transfer states (*d*- π* transition or π*-*d*) and metal transition (*d-d* transition). Generally all electronic spectra of free ligands showed the presence of two bands around 290 nm and 380 nm. These two bands indicated the intraligand transitions. Intraligand transition usually occur in ligands compound which have π-systems of their own such as pyridine, bipyridine and phenanthroline.[66] In all the electronic spectra of free ligands, the π–π* intraligand transitions falls in the ultraviolet region around 190-380 nm and n - π* intraligand transition appear in the visible region around 380-430 nm. The transitions are the π–π* and n - π* intraligand transition between the pyrazine and quinoxaline with the aniline ring in the free ligands. Most n - π* transitions are forbidden therefore these transitions showed lower intensity compared to π to π * transitions.[67] It is also observed that there were hypsochromic effects in copper complexes as compared with the spectra of free ligands. In all spectra of metal complexes, the absorption bands due to π–π* and n - π* intaligand transitions that are observed in the spectrum of the free ligand have shifted to lower frequencies due to the coordination of the ligand with Cu^{2+} ion.[68] The third bands that occurred in all complexes are due to the charge transfer bands. Intense charge transfer bands observed at 400 – 450 nm assigned as a charge transfer band from nitrate

group to the metal ion. Charge transfer bands chromopohores absorb more UV- Visible and gave higher intensity of absorption compared to intensity of *d-d* transition which ranges between 600 nm to 800 nm. This explained why in all copper complexes the intensity of the *d-d* transition is lower compared to the intensity of charge transfer transitions in all spectra of copper complexes. The electronic spectra of all the copper complexes display a weak shoulder whose maximum absorption lies in the visible region at approximately ranges between 630 – 680 nm. The absorption in the ranges is expected for a distorted octahedral geometry for *d-d* transition. [69] For d^9 complexes we might expect each absorption band will correspond to excitation of an electron from t_{2g} to e_g. These coordination compounds are believed to exhibit two closely overlapping absorption bands rather than single band. **Figure 3.7** shows the electron excitation from t_{2g} to e_g level in the d^9 complexes, such as in copper complexes.

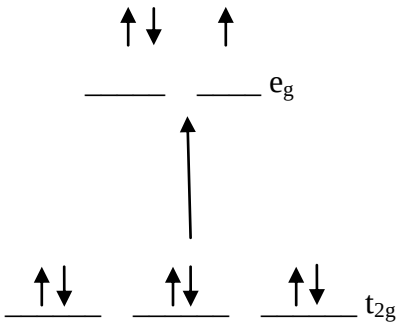

Figure 3.7: Electron excitation from t_{2g} to e_g in d^9 complexes

The John Teller theorem explains the apparent splitting of bands in these complexes. Based on the theorem, it states that there cannot be unequal occupation of orbitals with identical energies. To avoid such unequal occupation, the molecules distort so that these orbitals are no longer degenerate.[70] For a free copper ion, the *d*-orbitals are equi-energetic, that is they are "degenerate."

In an octahedral complex, this degeneracy is lifted. The d_z2 and $d_{x^2-y^2}$, the so-called e_g set, which are aimed directly at the ligands are destabilized. On the other hand, the d_{xz}, d_{xy}, and d_{yz} orbitals, the so-called t_{2g} set, are not. The labels t_{2g} and e_g refer to irreducible representations, which describe the symmetry properties of these orbitals. The loss of degeneracy upon the formation of an octahedral complex from a free ion is called crystal field splitting or ligand field splitting. The energy gap is labeled Δ_o, which varies according to the nature of the ligands. If the symmetry of the complex is lower than octahedral, the e_g and t_{2g} levels can split further.[66] The nonlinear molecules having a degenerate electronic should distort to lower the symmetry of the molecule and to reduce the degeneracy. This phenomenon is applicable for simple metal ion such as d^9 metal ion i.e. copper. For copper complexes which are d^9 complexes, the electron configuration is t_{2g}^6 to e_g^3 and the complexes should distort according to John Teller theorem.[71] The distortion is possible to take the form of an elongation along the *z* axis which is the most common distortion observed experimentally, the t_{2g} and e_g orbitals are affected. Distortion from O_h to D_{4h} symmetry results in stabillazation of the copper complexes. The e_g orbital is splitting into a lower a_{1g} level and higher b_{1g} level as shown in **Figure 3.8** below.

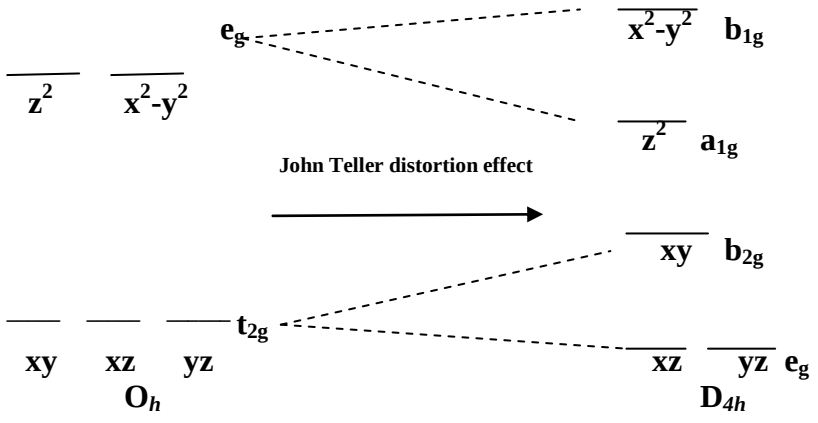

Figure 3.8: Distortion from O_h to D_{4h} symmetry

The weak shoulder band is believed to appear as a result of domination of intense intraligand and charge transfer bands. Since *d-d* transition is a forbidden transition, the intensity of the bands would be very low compared to intraligand and charge transfer transition. Meanwhile, the valence of the copper ions in the chelates is neutralized by the presence of acetate anions in the outer spheres. The broadness of the bands is due to John-Teller distortion which results from an odd number of electrons in the e_g orbitals.[72] All of the copper complexes of pyrazine ligands were blue and green in color. This presence of colors suggested that copper coordination is occurring through the azomethine nitrogen in pyrazine ligands. The copper complexes of pyrazine ligands invariably show significant color due to metal to ligand charge transfer absorptions in the visible spectrum.[73] From the electronic spectra data, the geometrical structure of the copper complexes were proposed and found to be distorted octahedral.

3.3.5 Thermogravimetry Analysis (TGA)

TGA measures weight changes by time. The results of the thermal analyses of the Cu(II) complexes with the coupled products of **L1, L2, L3, L4, L5, L6, L7** and **L8** are listed in **Table 3.21**.

Table 3.21: Thermal Decomposition Data

Complexes	Temperature (°C)	Weight loss (%) Found (Calculated)	Assignment
$[Cu_2(C_2H_3O_2)_4(C_{10}H_9N_3)_2]$ **(CuL1)**	110-220	33.08 (33.53)	Decomposition of acetate groups ($C_2H_3O_2$)
	220-900	47.93 (48.29)	Decomposition of ligands ($C_{10}H_9N_3$)
$[Cu_2(C_2H_3O_2)_4(C_{11}H_{11}N_3)_2]$ **(CuL2)**	110-220	32.86 (32.24)	Decomposition of acetate groups ($C_2H_3O_2$)
	220-900	50.08 (50.27)	Decomposition of ligands ($C_{11}H_{11}N_3$)
$[Cu_2(C_2H_3O_2)_4(C_{11}H_{11}N_3)_2]$ **(CuL3)**	110-220	32.98 (32.24)	Decomposition of acetate groups ($C_2H_3O_2$)
	220-900	51.24 (50.27)	Decomposition of ligands ($C_{11}H_{11}N_3$)
$[Cu_2(C_2H_3O_2)_4(C_{10}H_8ClN_3)_2]$ **(CuL4)**	110-220	28.67 (30.49)	Decomposition of acetate groups ($C_2H_3O_2$)
	220-900	53.21 (52.97)	Decomposition of ligands ($C_{10}H_8ClN_3$)
$[Cu_2(C_2H_3O_2)_4(C_{14}H_{11}N_3)_2]$ **(CuL5)**	110-220	29.00 (29.28)	Decomposition of acetate groups ($C_2H_3O_2$)

	220-900	56.02 (54.84)	Decomposition of ligands ($C_{14}H_{11}N_3$)
$[Cu_2(C_2H_3O_2)_4(C_{15}H_{13}N_3)_2]$ **(CuL6)**	110-220	28.66 (28.29)	Decomposition of acetate groups ($C_2H_3O_2$)
	220-900	55.16 (56.35)	Decomposition of ligands ($C_{15}H_{13}N_3$)
$[Cu_2(C_2H_3O_2)_4(C_{15}H_{13}N_3)_2]$ **(CuL7)**	110-220	27.04 (28.29)	Decomposition of acetate groups ($C_2H_3O_2$)
	220-900	54.83 (56.35)	Decomposition of ligands ($C_{15}H_{13}N_3$)
$[Cu_2(C_2H_3O_2)_4(C_{10}H_8ClN_3)_2]$ **(CuL8)**	110-220	27.49 (27.00)	Decomposition of acetate groups ($C_2H_3O_2$)
	220-900	60.33 (58.35)	Decomposition of ligands ($C_{10}H_8ClN_3$)

TGA studies for Cu(II) complexes under study are carried out within the temperature range from room temperature up to 40^{o}C to 900^{o}C. The thermogram for the ligands and its complexes were shown in appendix section. Generally, all complexes decomposed in two stages. The first stage of decomposition began around 120°C and complete at 220°C. This is referred to the decomposition of acetate molecules attached to the copper ions. **CuL1** was found to decompose as much as 36.95 % (calc. 34.04 %), **CuL2** decomposed as much as 32.86 % (calc. 32.82 %), and **CuL3** shows as much as 32.98 % (calc. 32.82 %) meanwhile **CuL4** decomposed as much as 28.67 % (calc. 30.93 %) during the first stage of decomposition. The actual percentage decomposition of the sample for these complexes was slightly lower compared to the theoretical values. The decomposition in the second stage is attributed to the breakage of ligands molecules in the respective complexes. At this stage, **CuL1** was found to decompose as much as 53.09 % (calc. 52.97 %), **CuL2** decomposed as much as 55.06 % (calc. 55.25 %), and **CuL3** showed decomposition degree as much as 54.02 %

(calc. 57.82 %) meanwhile **CuL4** decomposed as much as 60.15 % (calc. 59.63 %) at the second stage of decomposition. The leftover mass of the CuO residue gave as much as 9.96% (calc. 12.99%), 12.08% (calc. 11.93%), 13.00% (calc. 11.93%) and 11.18% (calc. 11.25%) in the respective complexes. For quinoxaline derivatives complexes, **CuL5** was found to decompose as much as 29.00 % (calc. 28.67 %), **CuL6** decomposed as much as 28.66 % (calc. 28.55 %), and **CuL7** shows as much as 26.03 % of decomposition (calc. 28.55 %) meanwhile **CuL8** decomposed as much as 28.49 % (27.12 %) within the first stage of decomposition. In second stage of decomposition, the ligands molecules were decomposed in the respective complexes. **CuL5** was found to be decomposing as much as 58.60 % (calc. 59.63 %), **CuL6** decomposed as much as 61.31 % (calc. 61.06 %), and **CuL7** shows as much as 59.98 % of decomposition (calc. 61.06 %) meanwhile **CuL8** decomposed as much as 61.33 % (63.02 %) in the second stage. The mass of CuO residue gave as much as 12.64 % (calc. 10.74 %), 10.03% (calc. 10.39 %), 13.99 % (calc. 10.39 %) and 10.18 % (calc. 9.86 %) in the respective complexes. The actual percentage decomposition of the sample for these complexes was slightly differing compared to the theoretical values. From the results obtained, it has been proposed for every copper complex, the copper ion is coordinated with acetates molecules in order to stabilize the positive charge of the copper cation. The data collected from thermal studies agreed satisfactorily with the data obtained from other methods of characterization.

3.3.6 X-Ray Crystallography

3.3.6.1 Crystal structure of Tetra-μ-acetato- κ^8 O: O-bis{[N-(pyrazine-2-yl)4-methylaniline- κN]copper(II)} **(CuL3)**

Treatment of ligand **L3** with copper (II) acetate in acetonitrile and trimethylorthoformate (TMOF) gave 56% yield. Recrystallization of **CuL3** in acetonitrile gave prismatic blue crystals which were analyzed by X-ray diffraction as shown below.

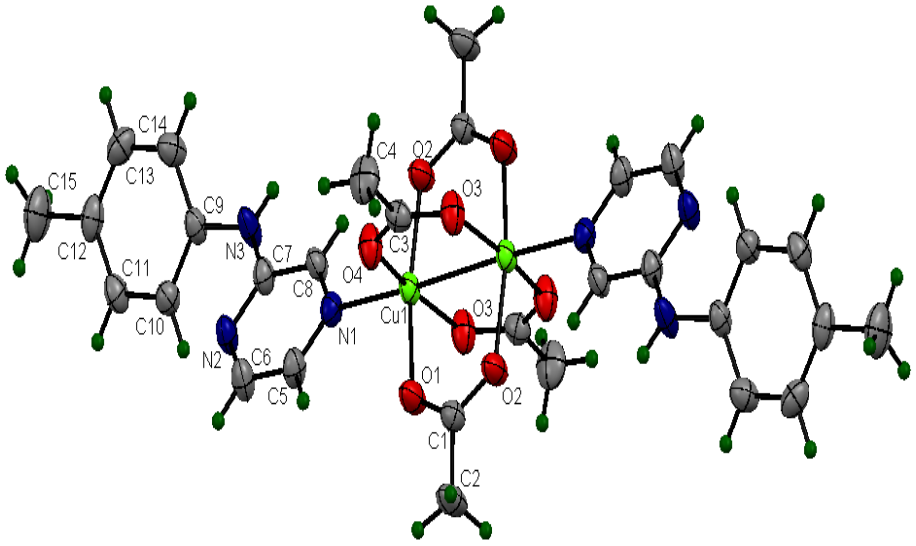

Figure 3.9: ORTEP diagram of Tetra-μ-acetato- κ^8 O: O-bis{[N-(pyrazine-2-yl)4-methylaniline- κN]copper(II)} (CuL3)

The crystals of **CuL3** crystallizes in the triclinic system, *P*-1 space group with the unit cell parameters, *a* = 7.5205(6) Å, *b* = 9.9387 (8) Å, *c* = 11.0563 (9) Å, α = 106.401 (1)°, ß = 94.441 (1)° and γ = 100.496 (1)°. In the crystal structure of Tetra-μ-acetato- κ^8 O: O-bis{[N-(pyrazine-2-yl)4-methylaniline-*κ*N]copper(II)} **(CuL3),** the four acetates groups each bridge a pair of copper atoms. The copper complex has a distorted octahedral geometry with the square planar basal plane formed by four oxygen atoms of the acetate groups and the apical positions are occupied by the

coordinating nitrogen atom in pyrazine ring. The crystal system and refinement data are shown in **Table 3.22**, meanwhile **Table 3.23** shows the selected distances and angles of **CuL3.**

Table 3.22: Crystal data and structure refinement for Tetra-μ-acetato- κ^8 O: O-bis{[N-(pyrazine-2-yl)4-methylaniline- κN]copper(II)} (CuL3)

Identification code	$Cu_2(C_2H_3O_2)_4(C_{11}H_{11}N_3)_2$
Formula weight (g/mol)	733.71
Colour	Blue
Crystal system, space group	Triclinic, *P*
Unit cell dimensions	*a* = 7.5205(6) Å *b* = 9.9387 (8) Å *c* = 11.0563 (9) Å α = 106.401 (1)° ß = 94.441 (1)° γ = 100.496 (1)°
V (Å^3)	772.19 (11) Å^3
Z	1
$P_{calc.}$ (mg m^{-3})	1.283
Absorption coefficient (mm^{-1})	1.44
F_{000}	1984
Crystal size (mm)	0.30 × 0.20 × 0.10
Θ_{max}	27.5°
≤ h ≥	−9 to 9
≤ k ≥	−12 to 12
≤ l ≥	−14 to 13
R_{int}	0.024
S	1.15
Symmetry code: (i)	−*x*+1, −*y*+1, −*z*+1

Table 3.23: Hydrogen-bond geometry (Å, °) for Tetra-μ-acetato-k^8 O: O-bis{[N-(pyrazine-2-yl)4-methylaniline-kN]copper(II)} (CuL3)

D—H···*A*	*D*—H	H···*A*	*D*···*A*	*D*—H···*A*
N3—H3···O4^i	0.848 (10)	2.385 (12)	3.221 (3)	169 (3)

3.3.6.2 Crystal structure of tetra-μ-acetato- κ^8O:O-bis{[N-(quinoxaline-2-yl)4-methyaniline-*κ*N]copper(II) **(CuL7)**

Treatment of ligand **L7** with copper (II) acetate in acetonitrile and trimethylorthoformate (TMOF) gave 43% yield. Recrystallization of **CuL7** in acetonitrile gave prismatic green crystals which were analyzed by X-ray diffraction as shown below.

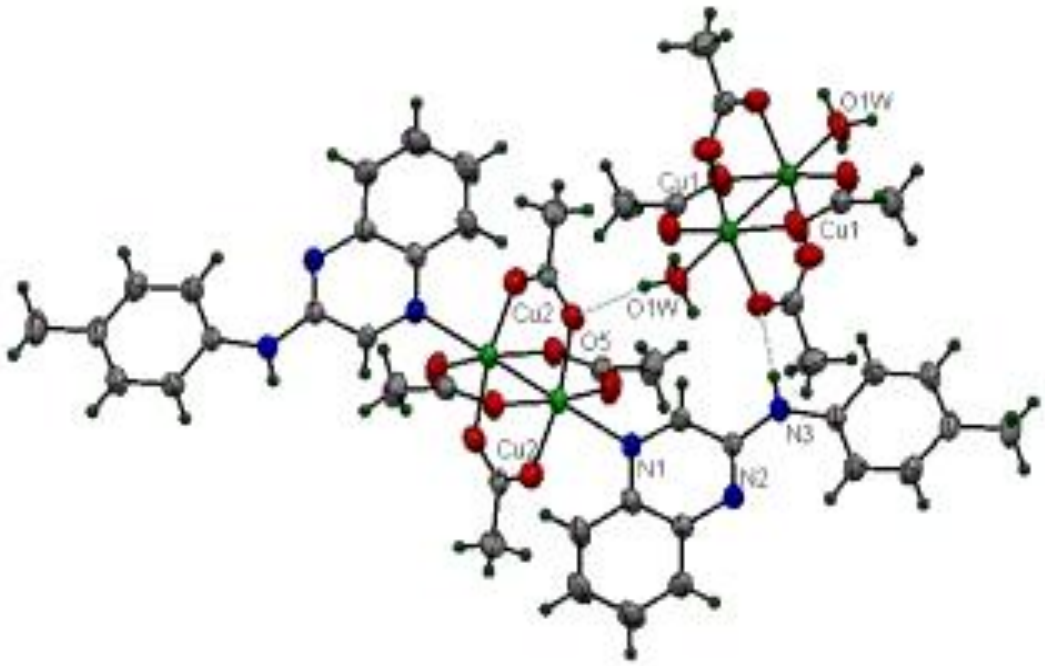

Figure 3.10: ORTEP diagram of Tetra-μ-acetato- κ^8O:O-bis{[N-(quinoxaline-2-yl)4-methyaniline-*κ*N]copper(II) (CuL7)

The crystals of **CuL7** crystallizes in the triclinic system, *P*-1 space group with the unit cell parameters, *a* = 8.4072(3) Å, *b* = 12.6120 (6) Å, *c* = 13.7993 (8) Å, α = 62.968 (5)°, ß = 82.457 (4)° and γ = 77.340 (4)°. In the crystal structure of tetra-μ-acetato-k^{8}O:O-bis{[N-(quinoxaline-2-yl)4-methyaniline-*κ*N]copper(II) **(CuL7),** the four acetates groups each bridge a pair of copper atoms. The copper complex has a distorted octahedral geometry with the square planar basal plane formed by four oxygen atoms of the acetate groups and the apical positions are occupied by the

coordinating nitrogen atom in quinoxaline ring. There is also an additional of acetate group attached to the copper ion and coordinate with the copper complexes. The crystal system and refinement data are shown in **Table 3.24**, meanwhile **Table 3.25** shows the selected distances and angles of **CuL7.**

Table 3.24: Crystal data and structure refinement for Tetra-μ-acetato- κ^{8}O:O-bis{[N-(quinoxaline-2-yl)4-methyaniline- κN]copper(II) (CuL7)

Identification code	$Cu_2(C_{15}H_{13}N_3)_2(C_2H_3O_2)_4 \cdot Cu_2(H_2O)_2(C_2H_3O_2)_4$
Formula weight (g/mol)	1233.11
Colour	Green
Crystal system, space group	Triclinic, *P*
Unit cell dimensions	*a* = 8.4072(3) Å *b* = 12.6120 (6) Å *c* = 13.7993 (8) Å α = 62.968 (5)° ß = 82.457 (4)° γ = 77.340 (4)°
V (Å^3)	1270.79 (11) Å^3
Z	1
$P_{calc.}$ (mg m^{-3})	1.283
Absorption coefficient (mm^{-1})	2.56
F_{000}	1984
Crystal size (mm)	0.25 × 0.20 × 0.15
Θ_{max}	74.3°
≤ h ≥	−10 to 10
≤ k ≥	−15 to 14
≤ l ≥	−17 to 13
R_{int}	0.040
S	1.08
Symmetry code: (i)	−*x*+1, −*y*+1, −*z*+1

Table 3.25: Hydrogen-bond geometry (Å, °) for Tetra-μ-acetato- κ^{8}O:O-bis{[N-(quinoxaline-2-yl)4-methyaniline- κN]copper(II) (CuL7)

D—H···*A*	*D*—H	H···*A*	*D*···*A*	*D*—H···*A*
O1W—H1W1···O5	0.84	1.99	2.823 (2)	169.1
O1W—H1W2···O7^i	0.84	2.38	2.932 (2)	123.9
N3—H3···O1	0.88	2.15	3.022 (3)	170.8

3.4 Fluorescence Studies of Pyrazine and Quinoxaline Based Ligands

Fluorescence is widely used for quantification of trace constituents of biological and environmental samples because of its sensitivity ability. Limits of detection is as low as 10^{-10} or lower are possible for intensely fluorescent molecule. Another advantage is the large linear concentration range of fluorescence methods, which is significantly greater than those encountered in absorption spectroscopy. The principle disadvantage of fluorescence as an analytical tool is its serious dependence on the structure and environment where the fluorescence is carried out. In this work, the fluorescence study was carried out on pyrazine and quinoxaline based ligands and its copper complexes. The fluorescence studies of heteronuclear complexes comprising *d*-transition metal is an attractive new area developed in the last decade.[74, 75]

3.4.1 Effects of substituents

The effects of substituents on pyrazine and quinoxaline system were studied under capped and uncapped condition in methanol solution. There were reports on the substituents in a conjugated system which gave profound effect on the fluorescence properties.[76] Some substituent will cause bathchromic shift i.e. the change of spectral band position of a molecule to a longer wavelength (lower frequency). The bathchromic shift also known as red shift. Meanwhile the hypsochromic shift is the change of spectral band position of a molecule to a shorter wavelength (higher frequency). This effect is also commonly called a blue shift.[77] **Table 3.26** below shows the fluorescence characteristics of pyrazine and quinoxaline derivatives in capped and uncapped conditions in methanol ($M \approx 3.0 \times 10^{-4}$ mol dm^{-3}).

Table 3.26: Fluorescence characteristics of pyrazine and quinoxaline derivatives in capped and uncapped conditions in methanol (M ≈ 3.0 x 10^{-4} mol dm^{-3})

Fluorescence Spectra(nm)					
Compounds	**Labels**	**Condition**	**E_x**	**E_m**	**Intensity**
2-*N*-anilinopyrazine	**L1**	Capped	390	425	15.33
		Uncapped	387	432	8.22
2-*N*-(*m*-methyl)anilinopyrazine	**L2**	Capped	409	473	85.33
		Uncapped	403	432	67.22
2-*N*-(*p*-methyl)anilinopyrazine	**L3**	Capped	418	468	45.35
		Uncapped	406	435	23.42
2-N-(*p*-chloro)anilinopyrazine	**L4**	Capped	346	377	6.01
		Uncapped	358	392	4.32
2-*N*-anilinoquinoxaline	**L5**	Capped	397	460	17.12
		Uncapped	387	432	13.22
2-*N*-(*m*-methyl)anilinoquinoxaline	**L6**	Capped	432	476	51.54
		Uncapped	412	452	30.89
2-*N*-(*p*-methyl)anilinoquinoxaline	**L7**	Capped	421	470	26.50
		Uncapped	428	487	13.90
2-*N*-(*p*-chloro)anilinoquinoxaline	**L8**	Capped	397	425	5.38
		Uncapped	386	434	6.08

From **Table 3.26**, it can be seen that capped samples in methanol for 2-*N*-anilinopyrazine **(L1)** fluoresced at 425 nm when excited at 390 nm. Meanwhile, both 2-*N*-(*m*-methyl)anilinopyrazine **(L2)** and 2-*N*-(*p*-methyl)anilinopyrazine **(L3)** fluoresced at longer wavelength i.e. at 473 nm and 468 nm when excited at 409 nm and 418 nm respectively compared to 2-*N*-anilinopyrazine **(L1)**. On the other hand, 2-*N*-(*p*-chloro)anilinopyrazine **(L4)** was observed to fluoresce at lowest wavelength i.e. at 377 nm when excited at 346 nm. The same trend has been observed in uncapped

samples, whereby 2-*N*-anilinopyrazine **(L1)** fluoresced at 432 nm when excited at 387 nm. Both 2-*N*-(*m*-methyl)anilinopyrazine **(L2)** and 2-*N*-(*p*-methyl)anilinopyrazine **(L3)** fluoresced at longer wavelength i.e. at 432 nm and 435 nm when excited at 403 nm and 406 nm respectively. Meanwhile, 2-*N*-(*p*-chloro)anilinopyrazine **(L4)** fluoresced at lowest wavelength i.e. at 392 nm when excited at 358 nm. The shift to the longer wavelength in 2-*N*-(*m*-methyl)anilinopyrazine **(L2)** and 2-*N*-(*p*-methyl)anilinopyrazine **(L3)** in both capped and uncapped samples is due to the presence of methyl ($-CH_3$) group, and therefore increase the delocalization of π electrons in the ring system thus resulted the shift to longer wavelength.[78] From the same table, it can also be seen that capped samples in methanol for 2-*N*-(*m*-methyl)anilinoquinoxaline **(L6)** and 2-*N*-(*p*-methyl)anilinoquinoxaline **(L7)** fluoresced at higher wavelength i.e. at 476 nm and 470 nm when excited at 430 nm and 421 nm respectively compared to 2-*N*-anilinoquinoxaline **(L5)** which fluoresced at 460 nm when excited at 397 nm. Meanwhile, 2-*N*-(*p*-chloro)anilinopyrazine **(L8)** fluoresced at lower wavelength i.e. at 425 nm when excited at 397 nm compared to 2-*N*-anilinoquinoxaline **(L5)**. Whereas in uncapped condition the same trend has been observed where 2-*N*-anilinoquinoxaline **(L5)** fluoresced at 432 nm when excited at 387 nm. Both 2-*N*-(*m*-methyl)anilinoquinoxaline **(L6)** and 2-*N*-(*p*-methyl)anilinoquinoxaline **(L7)** fluoresced at longer wavelength i.e. at 452 nm and 487 nm when excited at 412 nm and 428 nm respectively. Meanwhile, 2-*N*-(*p*-chloro)anilinopyrazine **(L8)** fluoresced at lowest wavelength i.e. at 434 nm when excited at 386 nm. The shift to the longer wavelengths observed in 2-*N*-(*m*-methyl)anilinoquinoxaline **(L6)** and 2-*N*-(*p*-methyl)anilinoquinoxaline **(L7)** are due to the presence of methyl group as discussed earlier. From **Table 3.26**, it can be observed that the fluorescence intensities for 2-*N*-(*m*-methyl)anilinopyrazine **(L2)** and 2-*N*-(*p*-methyl)anilinopyrazine **(L3)** were higher compared to 2-*N*-anilinopyrazine **(L1)** and both 2-*N*-(*m*-methyl)anilinoquinoxaline **(L6)** and 2-*N*-(*p*-methyl)anilinoquinoxaline **(L7)** also showed higher intensities compared to 2-*N*-

anilinoquinoxaline **(L5)**. The higher intensities observed in the respective compounds is due to the effects of methyl substituent on the aniline ring. The methyl group is an electron donating group, hence it, increased the intensity of fluorescence by increasing the mobility of electrons in the system. At the same time, the presence of methyl group caused the HOMO energy to be increased, thus narrowing the LUMO-HOMO energy gap of the 2-*N*-(*m*-methyl)anilinopyrazine **(L2)** and 2-*N*-(*m*-methyl)anilinoquinoxaline **(L6)**. The free mobility of the electrons enhances the π to π* transitions, thus high fluorescence intensity was observed. The fluorescence spectra for capped samples of 2-*N*-anilinopyrazine **(L1),** 2-*N*-(*m*-methyl)anilinopyrazine **(L2)** and 2-*N*-(*p*-methyl)anilinopyrazine **(L3)** in methanol at 3.0 x 10^{-4} M are as shown in **Figure 3.11** below.

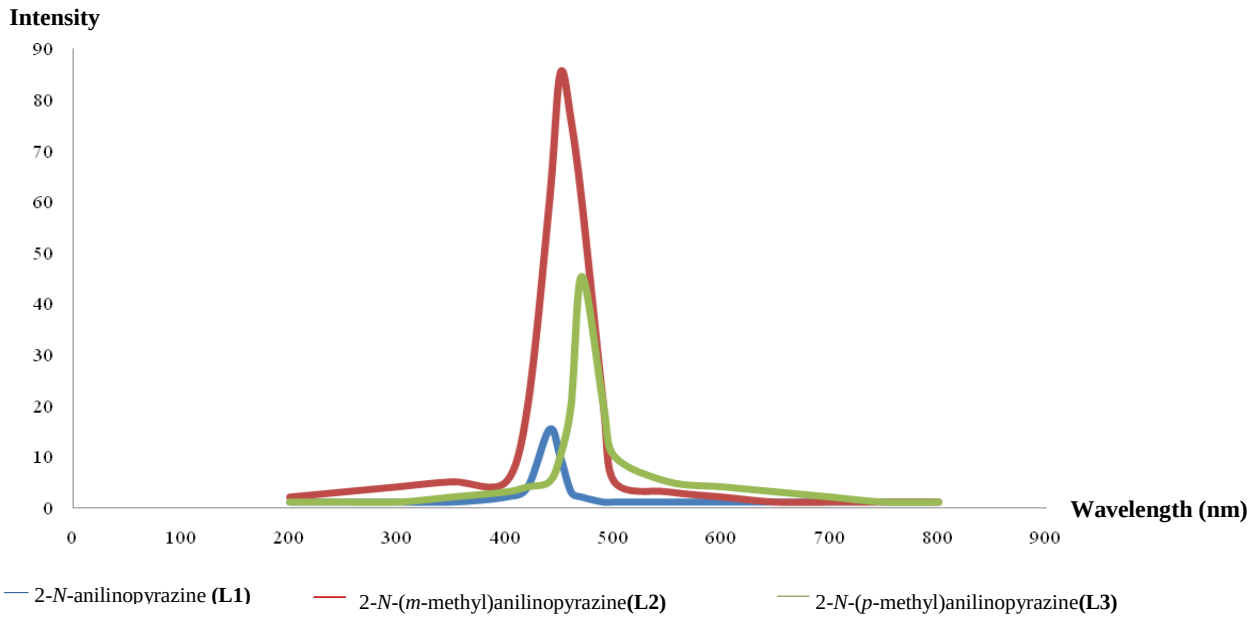

Figure 3.11: Fluorescence spectra of 2-*N*-anilinopyrazine (L1), 2-*N*-(*m*-methyl)anilinopyrazine (L2) and 2-*N*-(*p*-methyl)anilinopyrazine (L3) in capped samples in methanol (M≈3.0 x 10^{-4} M)

The fluorescence spectra for capped samples of 2-*N*-anilinoquinoxaline **(L5),** 2-*N*-(*m*-methyl)anilinoquinoxaline **(L6)** and 2-*N*-(*p*-methyl)anilinoquinoxaline **(L7)** in methanol **(M ≈ 3.0 x 10^{-4} mol dm^{-3})** are as shown in **Figure 3.12** below.

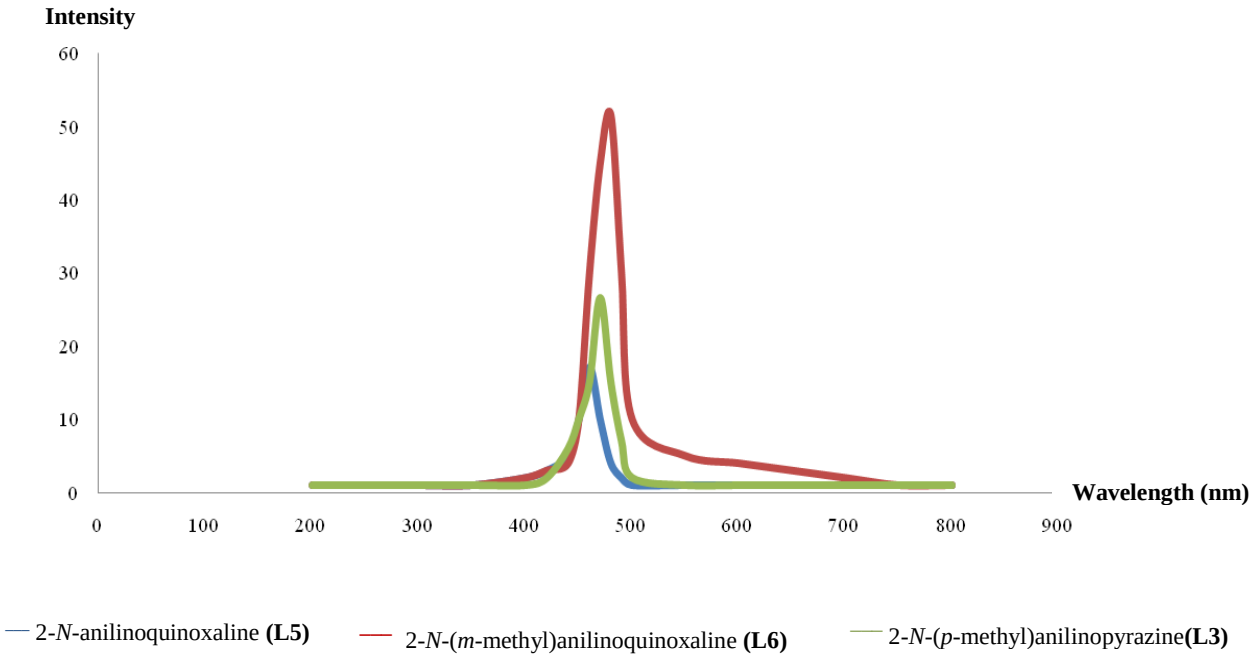

Figure 3.12: Fluorescence spectra of 2-*N*-anilinoquinoxaline (L5), 2-*N*-(*m*-methyl)anilinoquinoxaline (L6) and 2-*N*-(*p*-methyl)anilinoquinoxaline (L7) in capped samples in methanol (M≈ 3.0 x 10^{-4} M)

Meanwhile, 2-*N*-(*p*-chloro)anilinopyrazine **(L4)** showed a decrease in intensity compared to 2-*N*-anilinopyrazine **(L1)**. This observation can be explained by the presence of chlorine atom as a substituent atom on 2-*N*-(*p*-chloro)anilinopyrazine **(L4)**. Chlorine atom is an electron withdrawing group. Substitution of chlorine atom to the aromatic ring has important influence on the fluorescent signal. A decrease in fluorescence is observed with an increase in the atomic weight of the chlorine thus produced subsequent increase in phosphorescence. Chlorine atom is heavier than carbon (-CH_3) thus this is referred as the heavy atom effect. This phenomenon favor the promotion of intersystem crossing to take place.[79] Intersystem crossing is a process where fluorescence signal is

reduced and phosphorescence is generated. Within the intersystem crossing process, the relaxation of the molecule from a singlet excited state to a lower energy, triplet excitation state occured.[80] The fluorescence spectra for 2-*N*-anilinopyrazine **(L1)** and 2-*N*-(*p*-chloro)anilinopyrazine **(L4)** in capped samples in methanol (≈ M= 3.0 x 10^{-4} M) is shown in **Figure 3.13** below.

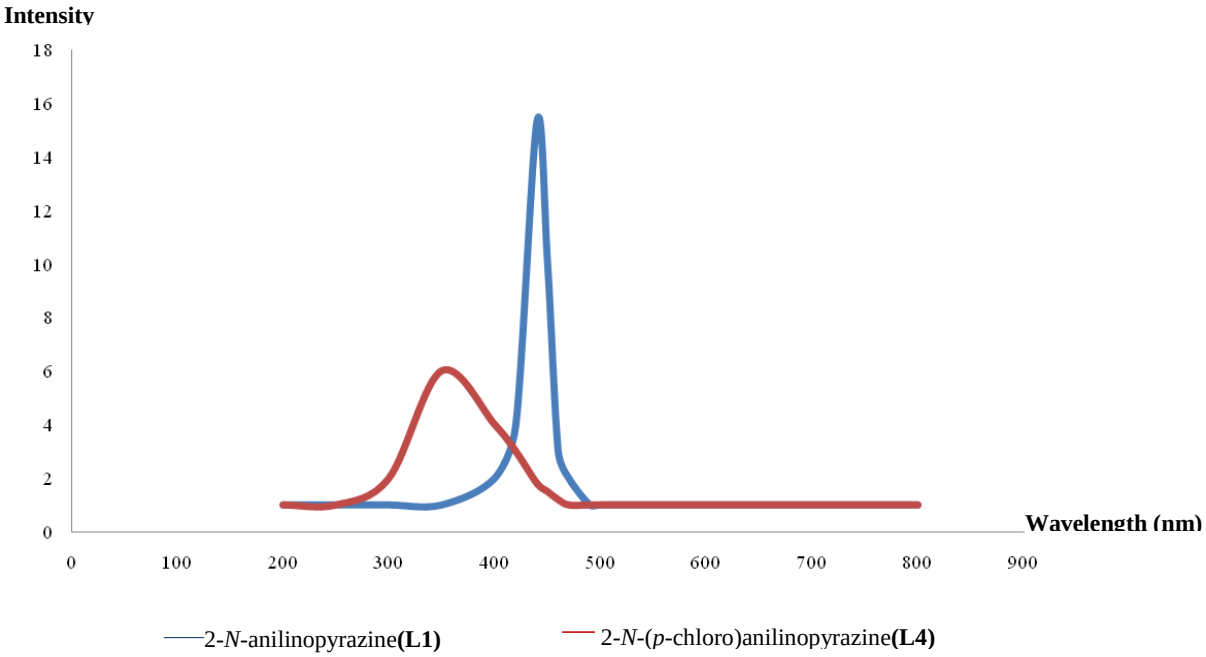

Figure 3.13: Fluorescence spectra of 2-*N*-anilinopyrazine (L1) and 2-*N*-(*p*-chloro)anilinopyrazine (L4) in capped samples in methanol (M≈ 3.0 x 10^{-4} M)

Similar observation as in 2-*N*-(*p*-chloro)anilinopyrazine **(L4)** was seen in 2-*N*-(*p*-chloro)anilinoquinoxaline **(L8).** 2-*N*-(*p*-chloro)anilinoquinoxaline **(L8)** showed a decrease in intensity compared to 2-*N*-anilinoquinoxaline **(L5)**. A decreased in fluorescence intensity in 2-*N*-(*p*-chloro)anilinoquinoxaline **(L8)** is due to the presence of substitution of chlorine to the aromatic ring as discussed earlier in 2-*N*-(*p*-chloro)anilinopyrazine **(L4).** The fluorescence spectra for 2-*N*-anilinoquinoxaline **(L5)** and 2-*N*-(*p*-chloro)anilinoquinoxaline **(L8)** in capped samples in methanol (≈ M= 3.0 x 10^{-4} M) is shown in **Figure 3.14** below.

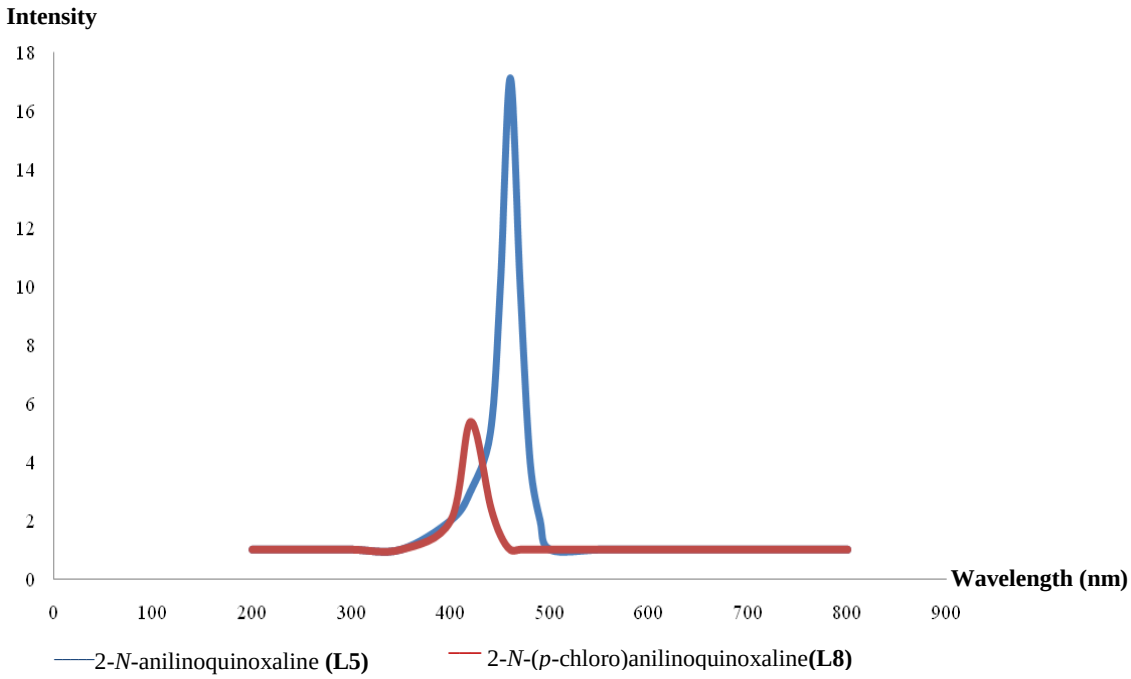

Figure 3.14: Fluorescence spectra of 2-*N*-anilinoquinoxaline (L5) and 2-*N*-(*p*-chloro)anilinoquinoxaline (L8) in capped samples in methanol (M≈3.0 x 10^{-4} M)

From **Table 3.26**, it also noted that 2-*N*-anilinoquinoxaline **(L5)** fluoresced at a higher wavelength compared to 2-*N*-anilinopyrazine **(L1).** The same phenomenon was also observed with 2-*N*-(*m*-methyl)anilinoquinoxaline **(L6)** with 2-*N*-(*m*-methyl)anilinopyrazine **(L2)**, 2-*N*-(*p*-methyl)anilinoquinoxaline **(L7)** with 2-*N*-(*p*-methyl)anilinopyrazine **(L3)** and 2-*N*-(*p*-chloro)anilinoquinoxaline **(L8)** with 2-*N*-(*p*-chloro)anilinopyrazine **(L4)**. In general, it is observed that the quinoxaline derivatives fluoresced at higher wavelength compared to pyrazine derivatives. The shifting of emission towards higher wavelength is due to the addition of benzene ring fused with pyrazine which enhanced the mobility of electrons through the π system in the benzene ring in quinoxaline compounds.[81] Based on the previous studies, better fluorescence signal was observed for molecules with π bonds and preferably those having aromatic rings.[82] Thus, the shifting of emission in quinoxaline derivatives ligands is due to the low energy in π–π* transitions in the molecules with π bonds and aromatic rings, hence promoted the fluorescence to the higher

wavelength for quinoxaline derivatives ligands. The fluorescence intensities for pyrazine and quinoxaline derivatives in capped samples in methanol (≈ M= 3.0 x 10^{-4} M) are shown in **Figure 3.15** below.

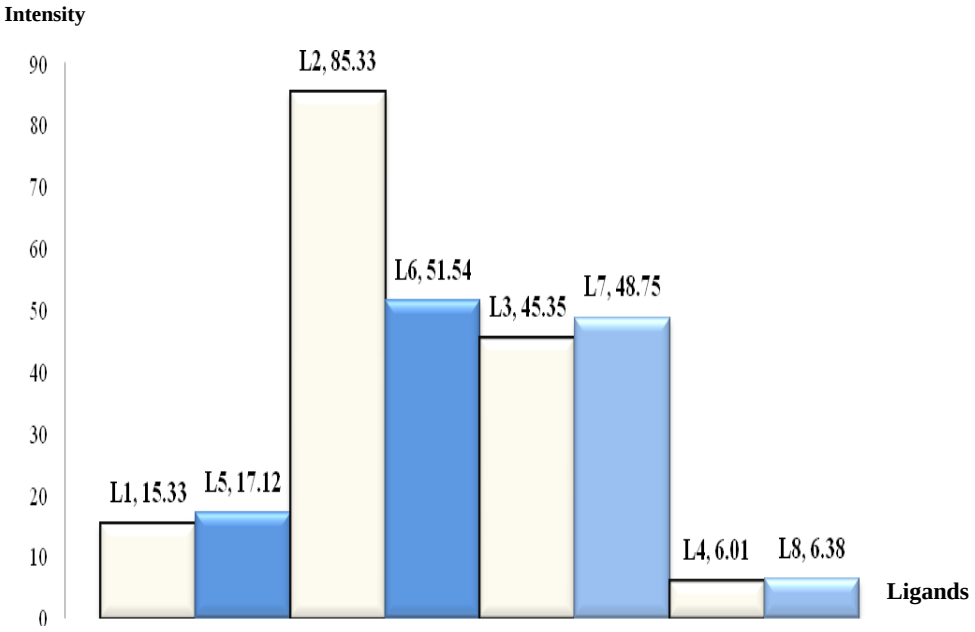

Figure 3.15: Fluorescence intensities in capped samples for pyrazine and quinoxaline derivatives in methanol (M≈ 3.0 x 10^{-4} M)

3.4.2 Effects of solvents

Fluorescence characteristics of synthesized ligands were carried out in two different solvents i.e. DMSO, as a polar aprotic solvent and methanol as a polar protic solvent. Polar protic solvents have higher dielectric constants and high polarity compared to polar aprotic solvents. The fluorescence characteristics of pyrazine and quinoxaline derivatives in capped and uncapped conditions in DMSO (M ≈ 3.0 x 10^{-4} mol dm^{-3}) are shown in **Table 3.27**.

Table 3.27: Fluorescence characteristics of pyrazine and quinoxaline derivatives in capped and uncapped samples in DMSO (M ≈ 3.0 x 10^{-4} mol dm^{-3})

Fluorescence Spectra(nm)					
Compounds	**Labels**	**Condition**	**E_x**	**E_m**	**Intensity**
2-*N*-anilinopyrazine	**L1**	Capped	408	448	26.66
		Uncapped	417	439	17.22
2-*N*-(*m*-methyl)anilinopyrazine	**L2**	Capped	412	488	205.66
		Uncapped	420	450	67.22
2-*N*-(*p*-methyl)anilinopyrazine	**L3**	Capped	428	468	56.12
		Uncapped	417	430	23.01
2-N-(*p*-chloro)anilinopyrazine	**L4**	Capped	388	420	7.01
		Uncapped	370	411	10.33
2-*N*-anilinoquinoxaline	**L5**	Capped	400	480	31.66
		Uncapped	406	463	9.22
2-*N*-(*m*-methyl)anilinoquinoxaline	**L6**	Capped	441	489	103.46
		Uncapped	449	481	5.67
2-*N*-(*p*-methyl)anilinoquinoxaline	**L7**	Capped	432	481	97.77
		Uncapped	445	478	12.22
2-*N*-(*p*-chloro)anilinoquinoxaline	**L8**	Capped	400	421	14.55
		Uncapped	406	433	9.03

From **Table 3.27** above, it can be seen that capped samples in DMSO for 2-*N*-(*m*-methyl)anilinopyrazine **(L2)** fluoresced at highest wavelength i.e. at 488 nm when excited at 412 nm followed by 2-*N*-(*p*-methyl)anilinopyrazine **(L3)** fluoresced at 468 nm when excited at 428 nm**.** Meanwhile 2-*N*-anilinopyrazine **(L1)** fluoresced at 448 nm when excited at 408 nm. 2-*N*-(*p*-chloro)anilinopyrazine **(L4)** fluoresced at lowest wavelength i.e. at 420 nm when excited at 388 nm. It is also noted that uncapped samples in DMSO for 2-*N*-(*m*-methyl)anilinopyrazine **(L2)** fluoresced at highest wavelength i.e. at 450 nm when excited at 420 nm followed by 2-*N*-(*p*-methyl)anilinopyrazine **(L3)** fluoresced at 430 nm when excited at 417 nm**.** Meanwhile 2-*N*-anilinopyrazine **(L1)** fluoresced at 439 nm when excited at 417 nm. 2-*N*-(*p*-chloro)anilinopyrazine **(L4)** fluoresced at lowest wavelength i.e. at 411 nm when excited at 370 nm. The fluorescence spectra in capped samples for pyrazine derivatives in DMSO (M ≈ 3.0 x 10^{-4} mol dm^{-3}) are shown in **Figure 3.16** below.

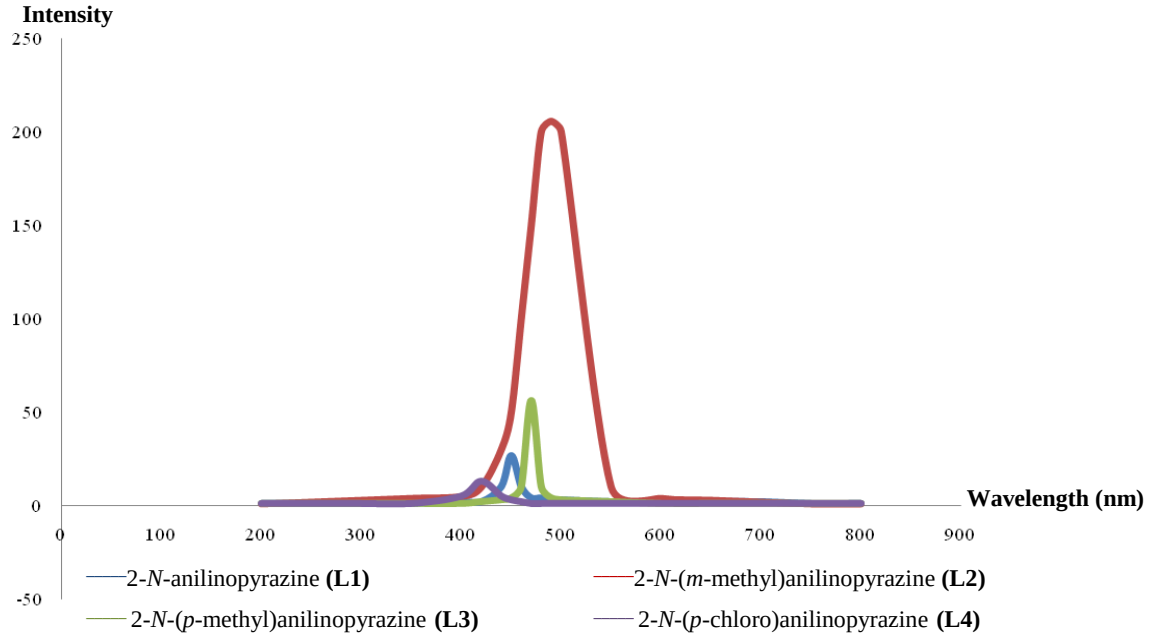

Figure 3.16: Fluorescence spectra in capped samples for 2-*N*-anilinopyrazine (L1), 2-*N*-(*m*-methyl)anilinopyrazine (L2), 2-*N*-(*p*-methyl)anilinopyrazine (L3) and 2-*N*-(*p*-chloro)anilinopyrazine (L4) in DMSO (M ≈ 3.0 x 10^{-4} mol dm^{-3})

The same trend can be seen in capped samples for quinoxaline derivatives in DMSO. 2-*N*-(*m*-methyl)anilinoquinoxaline **(L6)** and 2-*N*-(*p*-methyl)anilinoquinoxaline **(L7)** were observed to fluoresce at higher wavelength i.e. at 489 nm and 481 nm when excited at 441 nm and 432 nm respectively compared to 2-*N*-anilinoquinoxaline **(L5)** which fluoresced at 480 nm when excited at 400 nm. Meanwhile, 2-*N*-(*p*-chloro)anilinopyrazine **(L8)** fluoresced at lowest wavelength i.e. 421 nm when excited at 400 nm. It is also noted uncapped samples for 2-*N*-(*m*-methyl)anilinoquinoxaline **(L6)** fluoresced at highest wavelength i.e. at 481 nm when excited at 449 nm meanwhile, 2-*N*-(*p*-methyl)anilinoquinoxaline **(L7)** observed to fluoresce at high wavelength i.e. at 478 nm when excited at 445 nm as compared to 2-*N*-anilinoquinoxaline **(L5)** which fluoresced at 463 nm when excited at 406 nm. Meanwhile, 2-*N*-(*p*-chloro)anilinopyrazine **(L8)** fluoresced at lowest wavelength i.e. 433 nm when excited at 406 nm. The fluorescence spectra in capped samples for quinoxaline derivatives in DMSO (M ≈ 3.0 x 10^{-4} mol dm^{-3}) are shown in **Figure 3.17** below.

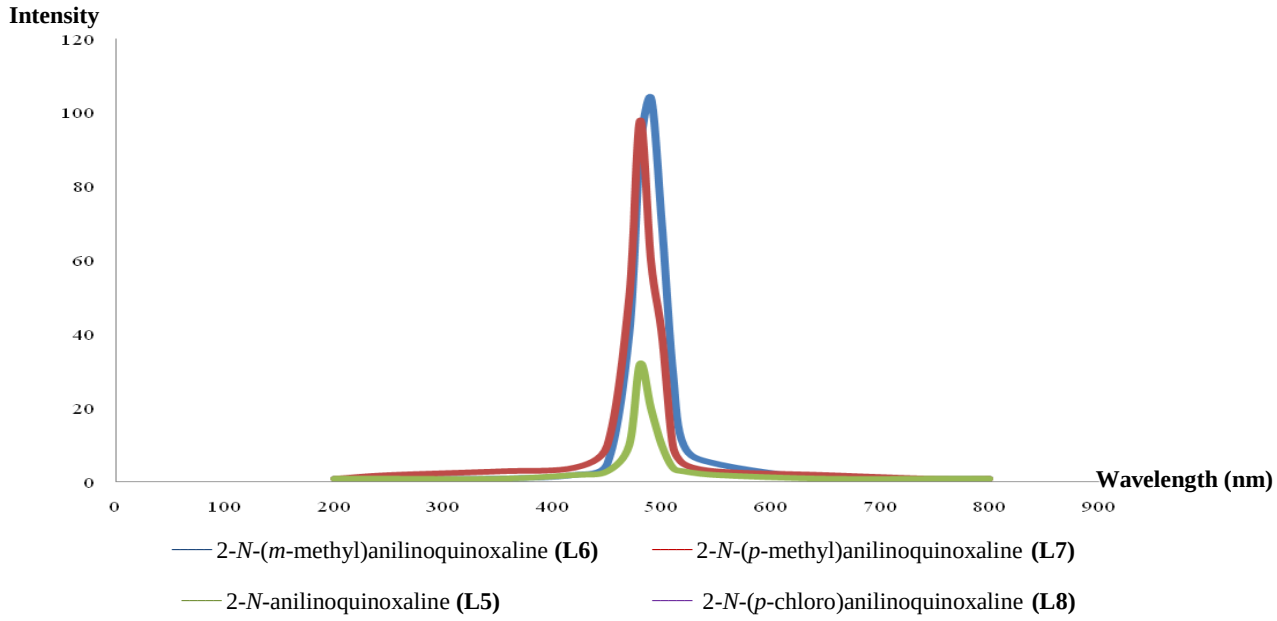

Figure 3.17: Fluorescence spectra of 2-*N*-anilinoquinoxaline (L5), 2-*N*-(*m*-methyl)anilinoquinoxaline (L6), 2-*N*-(*p*-methyl)anilinoquinoxaline (L7) and 2-*N*-(*p*-chloro)anilinoquinoxaline (L8) in DMSO (M ≈ 3.0 x 10^{-4} mol dm^{-3})

Based on **Table 3.26** and **Table 3.27** above, it can be seen that capped samples for 2-*N*-anilinopyrazine **(L1)** fluoresced to the longer wavelength of emission in DMSO i.e. at 448 nm compared to methanol i.e. at 425 nm. The shifted to the longer wavelength in capped sample for 2-*N*-anilinopyrazine **(L1)** in DMSO is due to the higher dipole moment value and higher dielectric constant in DMSO as compared to methanol. The polarity of DMSO is 3.96 D while ethyl acetate i.e. 1.78 D. Pyrazine and quinoxaline based ligands are polar compounds, and in most polar compounds, the excited state is more polar than the ground state. Hence, the increase of polarity in solvent will leading to the greater stabilization of the excited state. Thus shifted in fluorescence to the longer wavelength is observed. In general, it can be seen that the capped samples for pyrazine based ligands observed to fluoresce at longer wavelength in DMSO as compared to methanol. This observation can be explained by the same reason as discussed earlier in capped sample of 2-*N*-anilinopyrazine **(L1)**. The intensities in capped samples for 2-*N*-anilinopyrazine **(L1),** 2-*N*-(*m*-methyl)anilinopyrazine **(L2)**, 2-*N*-(*p*-methyl)anilinopyrazine **(L3**) and 2-*N*-(*p*-chloro)anilinopyrazine **(L4)** in DMSO and methanol ($M \approx 3.0 \times 10^{-4}$ mol dm^{-3}) are as shown in **Figure 3.18** below**.**

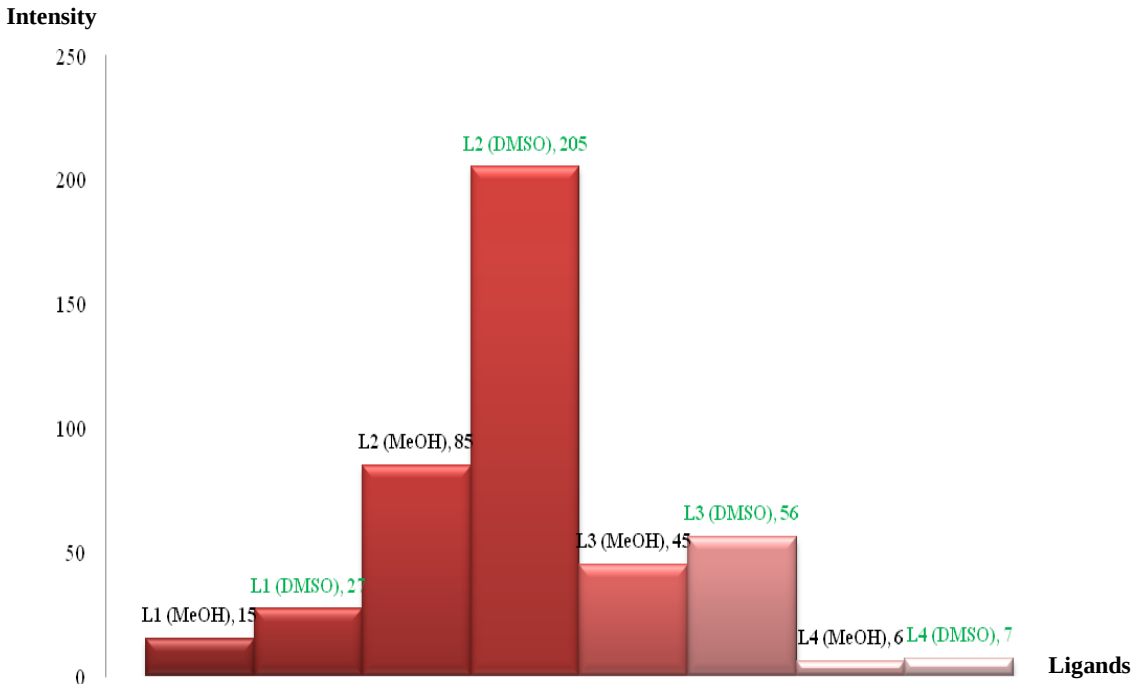

Figure 3.18: Fluorescence intensities in capped samples of pyrazine derivatives in methanol and DMSO (M ≈ 3.0 x 10^{-4} mol dm^{-3})

Similar observations have been seen in capped samples of quinoxaline derivatives. All the quinoxaline derivatives fluoresced at higher intensity in DMSO compared to methanol. The explanation is the same as been discussed earlier for capped samples of pyrazine derivatives. Fluorescence intensities in capped samples of quinoxaline derivatives in DMSO and methanol are as shown in **Figure 3.19** below.

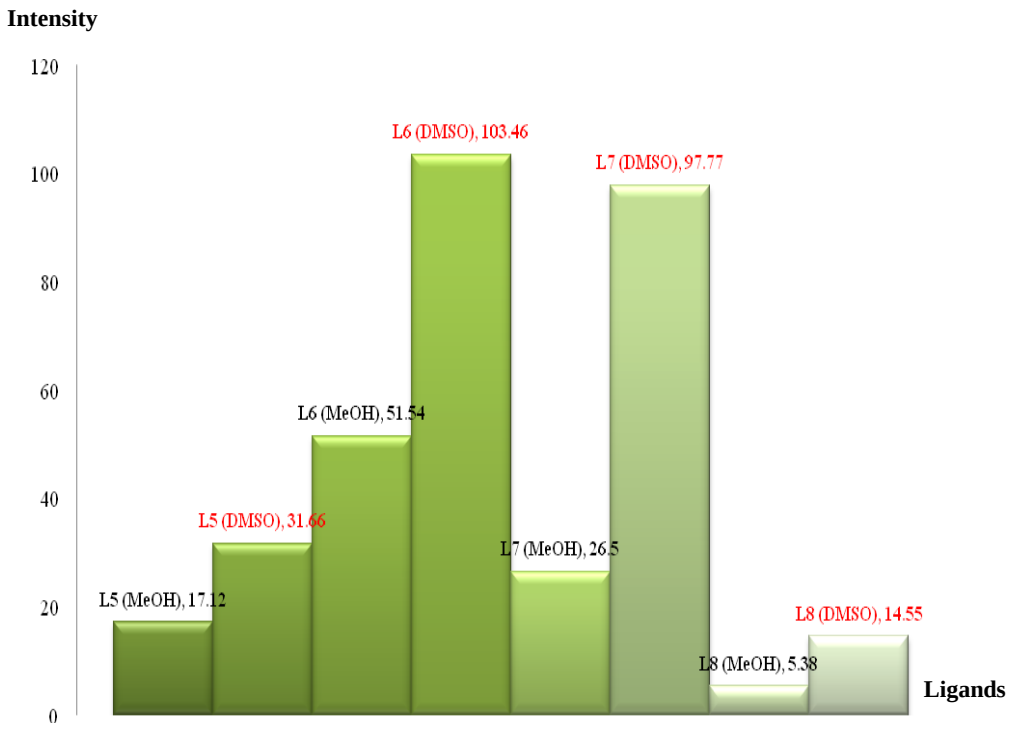

Figure 3.19: Fluorescence intensities in capped samples of quinoxaline derivatives in methanol and DMSO ($M \approx 3.0 \times 10^{-4}$ mol dm^{-3})

The second possible reason for the observations is the formation of hydrogen bonding between the lone pair on pyrazine and quinoxaline ligands with the hydrogen atom in methanol solution. The formation of hydrogen bond is capable of conjugating the π-electron system of the heterocyclic ring thus result the mobility of the π-electron to be disturbed. Thus, caused the intensity to be reduce.[83] The phenomena favors the low lying n → π* transitions which refer to the excitation of a nonbonding electron to an antibonding orbital.[84] It was reported that n → π* transitions were usually not observed in fluorescence spectra and if do present, the intensity is weak.[85] The diagram of formation of hydrogen bond between the methanol and the ligands are as shown in **Figure 3.20** and **Figure 3.21** below.

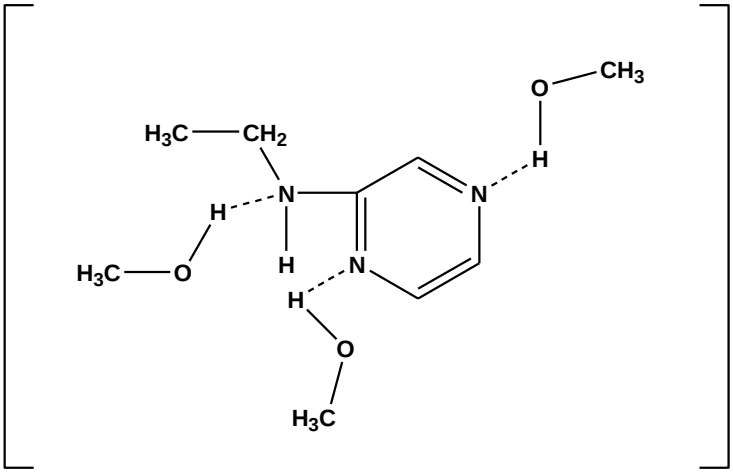

Figure 3.20: Hydrogen bond formation on pyrazine

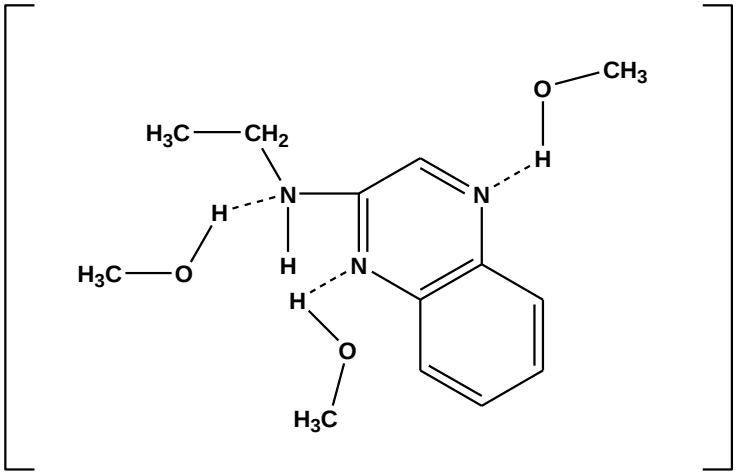

Figure 3.21: Hydrogen bond formation on quinoxaline derivatives

It is also been observed that quinoxaline derivatives fluoresced towards higher wavelength as compared to pyrazine derivatives in DMSO. The shifting of fluorescence towards higher wavelength is due to the addition of benzene ring fused with pyrazine thus enhanced the mobility of electrons through the π system in the benzene ring in quinoxaline derivatives compounds.[82]

3.4.3 Effect of Dissolved Oxygen

The fluorescence studies on dissolved oxygen have been done on **L1, L2, L3, L4, L5, L6, L7** and **L8** in methanol solution at 10^{-4} M**.** Based on **Table 3.27**, it can be seen that the fluorescence intensity of capped samples was observed to be higher than the uncapped samples. The fluorescence spectra for pyrazine and quinoxaline derivatives ligand is shown in **Figure 3.22** and **Figure 3.23** respectively.

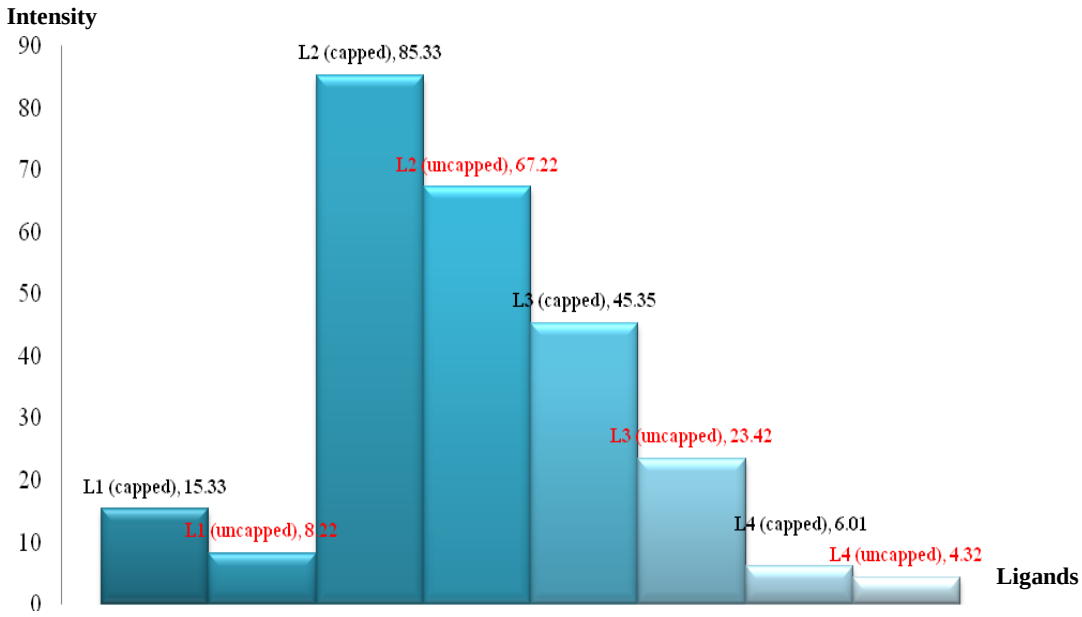

Figure 3.22: Fluorescence intensities of capped and uncapped samples of pyrazine derivatives in methanol (M ≈ 3.0 x 10^{-4} mol dm^{-3})

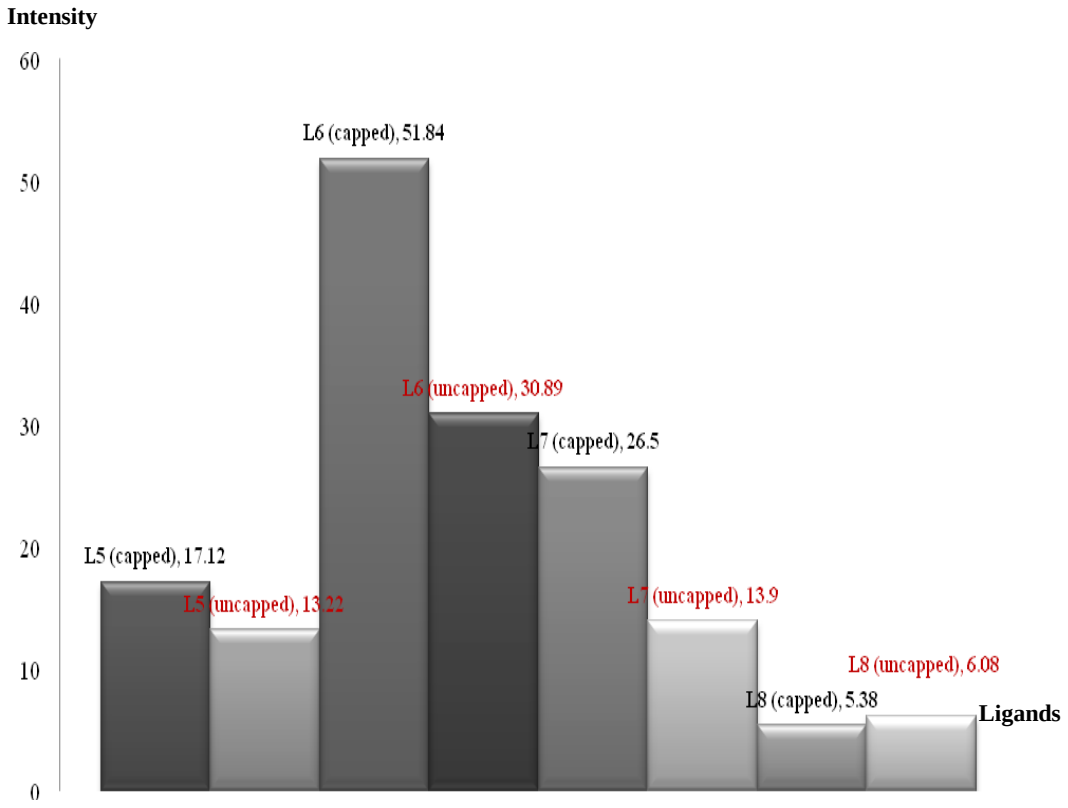

Figure 3.23: Fluorescence intensities of capped and uncapped samples of quinoxaline derivatives in methanol (M ≈ 3.0 x 10^{-4} mol dm^{-3})

From the observation, the intensity of fluorescence is eliminated and quenched in the presence of dissolved oxygen. This is due to the positions of electrons in oxygen atom. The ground state of oxygen is the triplet state and it is easier for an electron in the triplet state to transfer its energy to triplet oxygen rather than performing a flip in spin and relax to singlet state. Therefore, oxygen will be excited thus the transitions observed is actually due to oxygen emission rather than fluorescence of the compounds. This is why oxygen should be totally excluded to be able to detect fluorescence better. Moreover, oxygen has unusual large diffusion coefficient and on prolong exposure of the solution to the atmosphere could result in large quantity of oxygen diffusing into solution.[86] Dissolved oxygen largely limits fluorescence since it promotes intersystem crossing because it is paramagnetic.

However, dissolved oxygen affects phosphorescence more than it does to fluorescence. Although one would think that as far as intersystem crossing is increased in the presence of oxygen, phosphorescence is expected to increase. On the contrary, phosphorescence is completely eliminated and quenched in presence of dissolved oxygen. Oxygen is known to diminish the fluorescence of many compounds in some previous studies.[87] Weil-Malherbe and Weiss observed that the fluorescence of benzpyrene was nearly the same in several solvents from which oxygen had been removed by suction, but that on oxygenation varying degrees of quenching resulted.[88] The quenching effect was greater in oxygen than in air, and was completely and rapidly reversible.[89]

3.4.4 Effect of concentrations

Table 3.28 below shows the fluorescence characteristics for pyrazine and quinoxaline derivatives in methanol at 10^{-4} M and 10^{-5} M concentrations. Concentration effect on the fluorescence excitation and emission from various sources had thoroughly been studied. [90] Based on the results, it is emphasized that the spectra should be determined at sufficiently low concentrations of methanol because red-shift, distortion, and even quench often occur especially in the excitation and synchronous excitation spectra at relatively higher concentrations.

Table 3.28: Fluorescence characteristics of pyrazine and quinoxaline derivatives in capped and uncapped conditions in methanol and DMSO solutions at 10^{-4} M and 10^{-5} M

		Methanol solution			
Compounds	**Labels**	**E_m(10^{-4} M)**	**Intensity**	**E_m(10^{-5} M)**	**Intensity**
2-*N*-anilinopyrazine	**L1**	425	15.33	433	13.20
2-*N*-(*m*-methyl)anilinopyrazine	**L2**	473	85.33	425	43.12
2-*N*-(*p*-methyl)anilinopyrazine	**L3**	468	45.35	455	34.87
2-N-(*p*-chloro)anilinopyrazine	**L4**	377	6.01	367	4.10
2-*N*-anilinoquinoxaline	**L5**	460	17.12	443	10.03
2-*N*-(*m*-methyl)anilinoquinoxaline	**L6**	476	51.54	470	50.21
2-*N*-(*p*-methyl)anilinoquinoxaline	**L7**	480	26.50	449	12.56
2-*N*-(*p*-chloro)anilinoquinoxaline	**L8**	425	5.38	411	3.44
Compounds		**DMSO solution**			
2-*N*-anilinopyrazine	**L1**	448	26.66	401	22.00
2-*N*-(*m*-methyl)anilinopyrazine	**L2**	488	205.66	418	51.80
2-*N*-(*p*-methyl)anilinopyrazine	**L3**	468	56.12	421	23.90
2-N-(*p*-chloro)anilinopyrazine	**L4**	420	7.01	424	2.02
2-*N*-anilinoquinoxaline	**L5**	480	31.66	450	11.16
2-*N*-(*m*-methyl)anilinoquinoxaline	**L6**	489	103.46	449	58.99
2-*N*-(*p*-methyl)anilinoquinoxaline	**L7**	481	97.77	411	87.23
2-*N*-(*p*-chloro)anilinoquinoxaline	**L8**	421	43.54	378	35.55

Generally, the fluorescence intensity increases with the increasing concentrations. However there were reports stating that with increasing concentrations, the fluorescence intensity increases until it reaches its maximum value which also a limitation value. At this point, further increases in concentrations results in concentration quenching which decrease with further increases of concentrations and sometimes accompanied by shifts in wavelength.[91] Negative deviations from the linear relation between fluorescence and concentration may be observed at absorbance higher than 0.05, self-quenching whereby excited molecules lose their energies by collision with other molecules or solvent and self-absorption which occurs when an emission band overlaps with an excitation (absorption) band. In this case, emitted photons excite other molecules in the ground state which results in no net emission. As for the conclusion, the concentrations are not relatively linear with fluorescence intensity. **Figure 3.24** and **Figure 3.25** below showed the fluorescence intensity between pyrazine and quinoxaline derivatives in methanol solution at 10^{-4} M and 10^{-5} M concentrations.

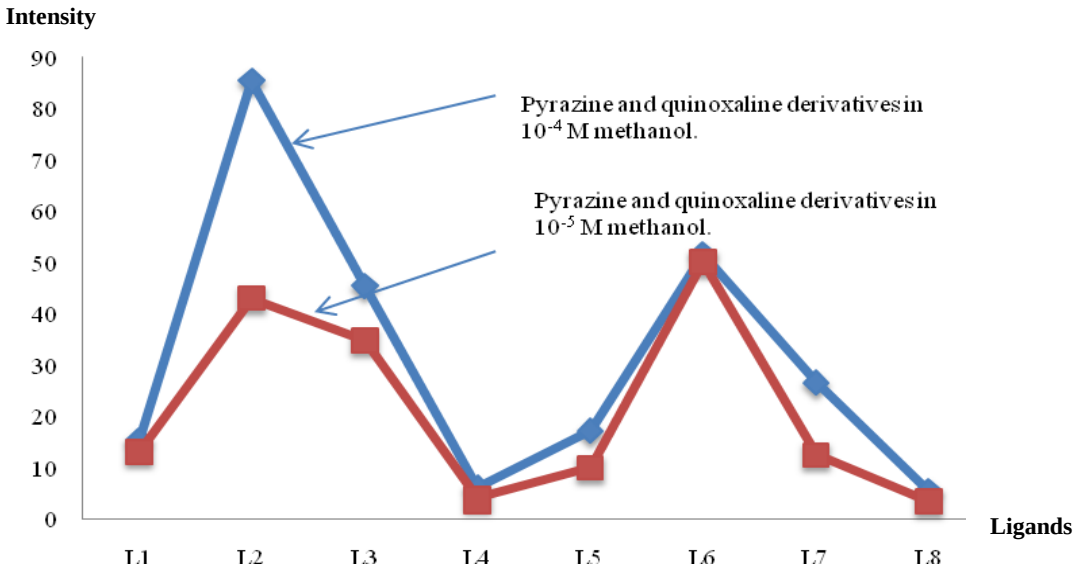

Figure 3.24: Fluorescence intensities of capped samples of pyrazine and quinoxaline derivatives in methanol solution at 10^{-4} M and 10^{-5} M

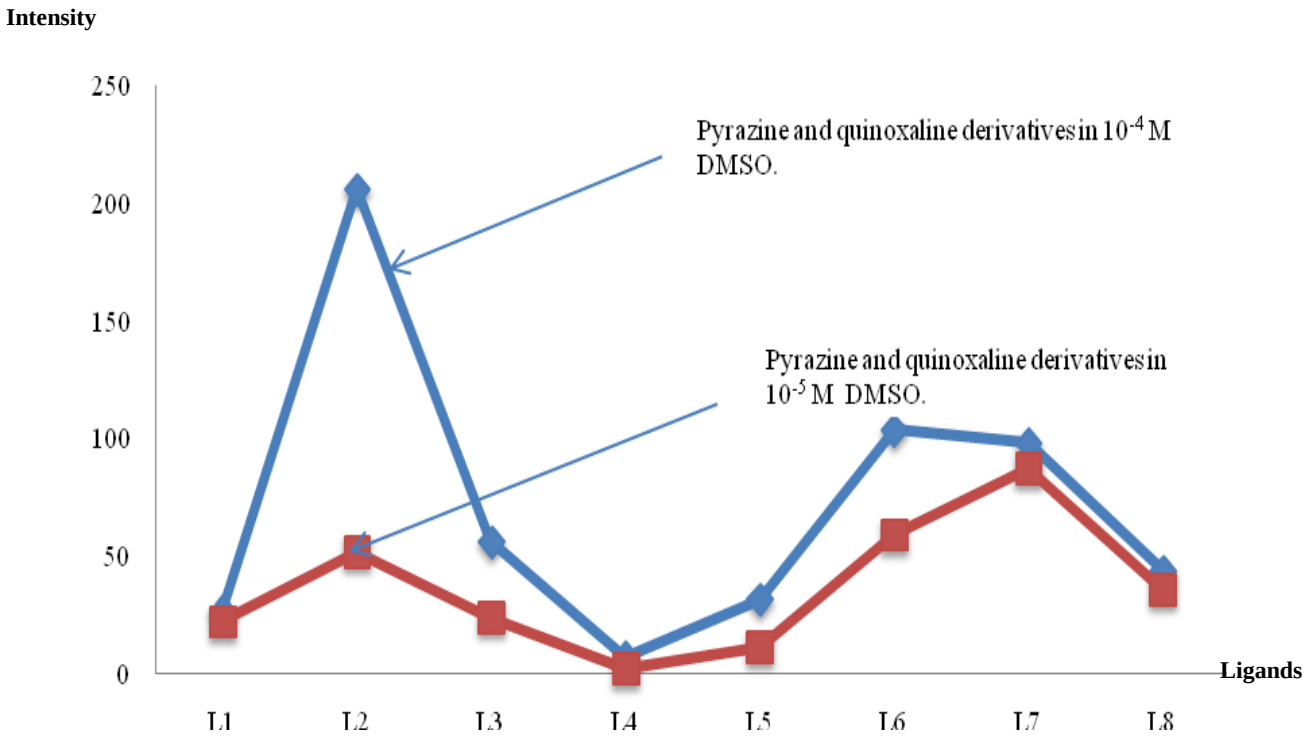

Figure 3.25: Fluorescence intensities of capped samples of pyrazine and quinoxaline derivatives in DMSO solution at 10^{-4} M and 10^{-5} M

3.4.5 Effect of metal coordination

The effect of copper metal on the fluorescence characteristics of the free ligands in methanol were studied for **L1, L2, L3, L4, L5, L6, L7** and **L8. Table 3.29** shows the fluorescence characteristics of ligands and their copper complexes in methanol (M ≈ 3.0 x 10^{-4} mol dm^{-3}).

Table 3.29: Fluorescence characteristics of ligands and their copper complexes in methanol ($M \approx 3.0 \times 10^{-4}$ mol dm^{-3})

Compounds	Labels	$E_X(10^{-4} M)$	$E_M(10^{-4} M)$	Intensity
2-*N*-anilinopyrazine	**L1**	390	435	15.33
$[Cu_2(C_2H_3O_2)_4 (C_{10}H_9N_3)_2]$	**CuL1**	405	447	7.41
2-*N*-(*m*-methyl)anilinopyrazine	**L2**	409	443	85.33
$[Cu_2(C_2H_3O_2)_4 (C_{11}H_{11}N_3)_2]$	**CuL2**	420	455	55.80
2-*N*-(*p*-methyl)anilinopyrazine	**L3**	418	468	45.35
$Cu_2(C_2H_3O_2)_4 (C_{11}H_{11}N_3)_2]$	**CuL3**	438	480	12.50
2-N-(*p*-chloro)anilinopyrazine	**L4**	346	377	6.01
$[Cu_2(C_2H_3O_2)_4 (C_{10}H_8ClN_3)_2]$	**CuL4**	360	406	11.44
2-*N*-anilinoquinoxaline	**L5**	397	460	17.12
$[Cu_2(C_2H_3O_2)_4 (C_{14}H_{11}N_3)_2]$	**CuL5**	410	471	13.88
2-*N*-(*m*-methyl)anilinoquinoxaline	**L6**	432	476	51.54
$[Cu_2(C_2H_3O_2)_4 (C_{15}H_{13}N_3)_2]$	**CuL6**	450	490	111.08
2-*N*-(*p*-methyl)anilinoquinoxaline	**L7**	421	470	26.50
$Cu_2(C_2H_3O_2)_4 (C_{15}H_{13}N_3)_2]$	**CuL7**	489	503	41.77
2-*N*-(*p*-chloro)anilinoquinoxaline	**L8**	397	425	5.38
$[Cu_2(C_2H_3O_2)_4 (C_{10}H_8ClN_3)_2]$	**CuL8**	420	465	1.55

The studies on fluorescence also involved the using of metals either as surfactant or as cation in complexation. One of the studies is the quenching of fluorescence on humic substances. The quenching of the intrinsic fluorescence of humic substances (HS) by paramagnetic metal ions is a well known phenomenon that has often been used for acquiring qualitative and quantitative information on the effect of these substances on the environmental fate of metal ions. Jones Jr. (1975) reported in his study**,** addition of aqueous solutions of metal ions (La^{3+}, Dy^{3+}, Nd^{3+}, Eu^{3+},

Lu^{3+}, Sc^{3+}, Al^{3+}, and Be^{2+}) to the fluorescence probe Quin-2 induced changes in the emission band.[92] Lanthanide metal ions showed decreasing fluorescence emission meanwhile Lu^{3+} and Sc^{3+} caused a decrease in the emission intensity and a substantial increase in emission intensity respectively. Vanderkooi reported Ni(II) and Co(II) are more effective than Mn(II) in quenching the fluorescence of ethenoadenosine phosphates. Whereas the diamagnetic ions Mg(II), Ca(II), and Zn(II) do not appear to affect the fluorescence of the ethenoadenosine phosphates directly.[75] **Table 3.29** shows the fluorescence characteristics of ligands and their copper complexes in methanol. In this work, it is been observed that both bands and intensities of the fluorescence changed after the complexation with copper. It can be seen that **CuL1** fluoresced at 447 nm when excited at 405 nm. **CuL2** and **CuL3** fluoresced at higher wavelength i.e. at 455 nm and 480 nm respectively. Meanwhile **CuL4** fluoresced at lower wavelength compared to **CuL1** i.e. at 406 nm when excited at 360 nm. On the other hand, **CuL5** fluoresced at 471 nm when excited at 410 nm. In capped condition, both **CuL6** and **CuL7** fluoresced at longer wavelength compared to **CuL5** i.e. at 490 nm and 503 nm respectively. Meanwhile, **CuL8** seems to fluoresce at slightly shorter wavelength compared to **CuL5** as stated in **Table 3.29** above. Generally, the fluorescence intensities are higher in all free ligands compared to copper complexes. This is due to the charge transfer transition that occurred during complexation process. [93] The charge transfer occurred between *d* orbital in copper cation to vacant π orbitals in free ligands. The charge transfer is a favorable process than the fluorescence. The decreasing in fluorescence intensity was also due to the paramagnetic characteristics and heavy metal effect of the copper ion. delocalization of π electrons in the system of complexes. The paramagnetic characteristics and heavy metal effect of the copper ion also contribute to the low fluorescence intensity. The spin-orbital coupling populates low lying high multiplicity states that are later deactivating by the intersystem crossing.[94] However there were two complexes show an increase in intensity i.e. **CuL6** and **CuL7. CuL6** fluoresced at 490 nm with

higher in intensity reading compared to **L6** meanwhile **CuL7** fluoresced at 503 nm with higher in intensity compared to **L7**. The increasing in intensity of copper complexes can be explained by photoinduced electron transfer (PET) phenomenon which is a common phenomenon occurs in complexes. This phenomenon happened when electrons reside as electron bands in bulk materials and electron orbitals in molecules. Thus, when a photon excites a molecule, an electron in a ground state orbital can be excited to a higher energy orbital. This excited state leaves a vacancy in a ground state orbital that can be filled by an electron donor. It produces an electron in a high energy orbital which can be donated to an electron acceptor.[95] The important part of the process is the decrease in total energy of the charge transfer hence increases the fluorescence intensity.[96] The PET reaction releases more energy if the ligand contains additional electron donating group such as methyl group as presence in both **CuL6** and **CuL7**.[97]The second possibility is the formation of hydrogen bonded in the complexes where there are the formations of a stable hydrogen bonded complex as suggested in the previous discussion. The fluorescence spectra of the pyrazine and quinoxaline derivatives and its copper complexes are shown in **Figure 3.26** and **Figure 3.27** below.

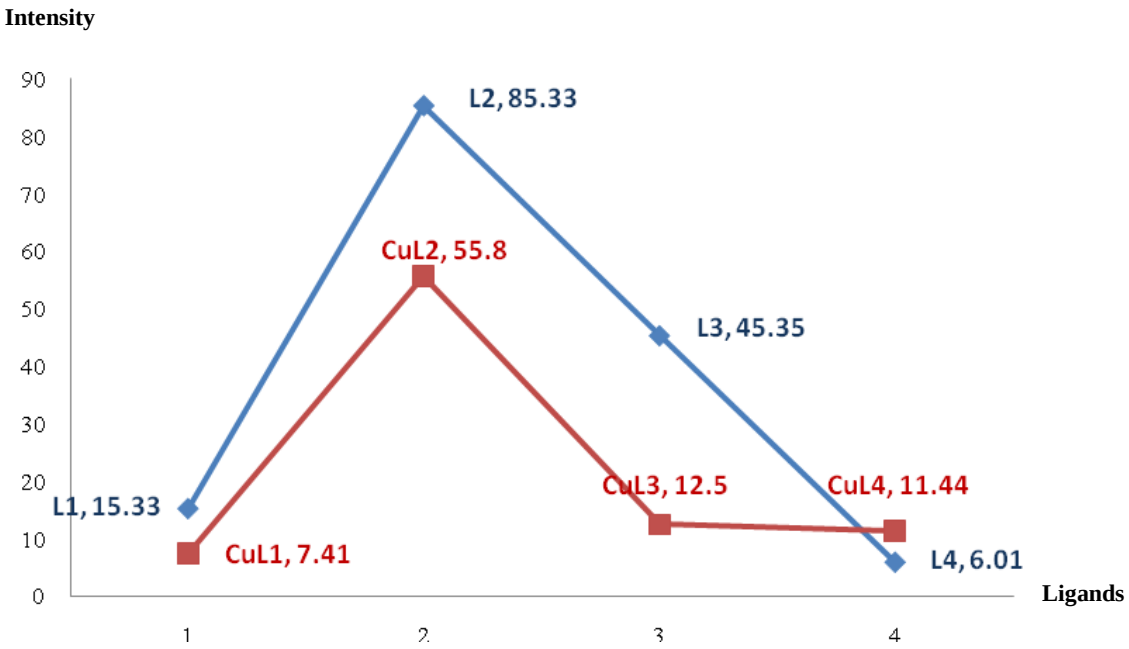

Figure 3.26: The fluorescence intensities of the pyrazine derivatives ligands and its copper complexes

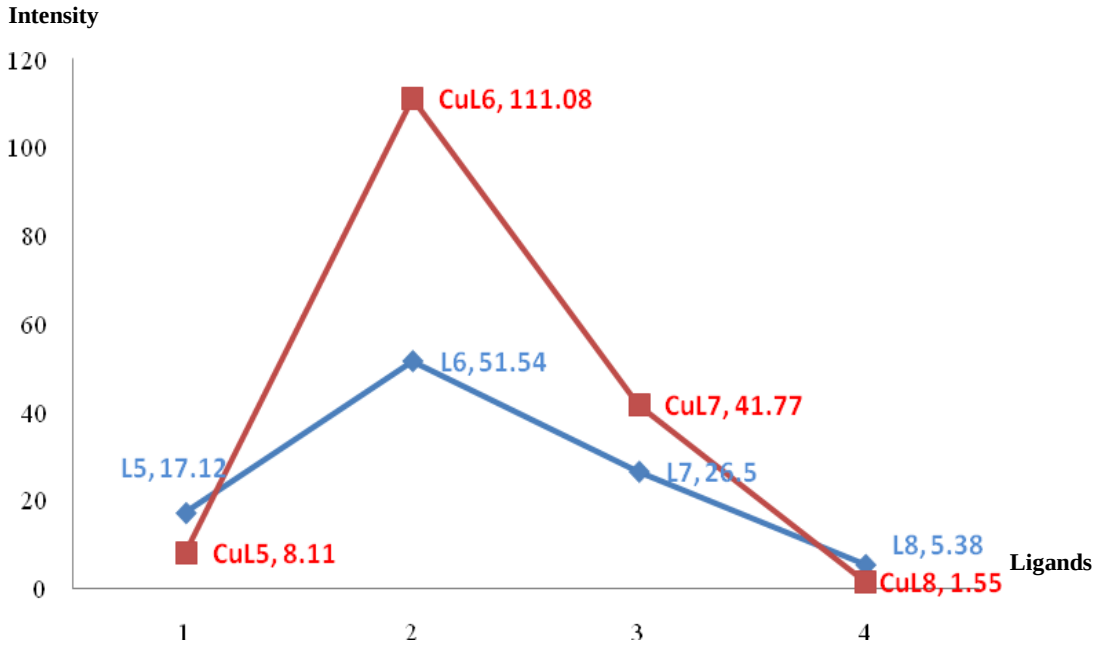

Figure 3.27: The fluorescence intensities of the quinoxaline derivatives ligands and its copper complexes

CHAPTER FIVE:

CONCLUSION

The study of the complex formation of copper(II) acetate with selected pyrazine and quinoxaline based ligands derived from the condensation reaction between 2-chloropyrazine and 2-chloroquinoxaline, respectively with selected aniline derivatives was successfuly carried out. 16 New compounds consisting of eight ligands and eight copper complexes were successfully synthesized and have been characterized with various methods. From the characterization methods, the copper complexes were proposed to form the binuclear complexes. The proposed structures for copper complexes are distorted octahedral and the structures have been confirmed by X-ray crystallography structures of tetra-μ-acetato-k^8 O: O-bis{[N-(pyrazine-2-yl)4-methylaniline-kN]copper(II)} **(CuL3)** and tetra-μ-acetato-k^8O:O-bis{[N-(quinoxaline-2-yl)4-methyaniline-kN]copper(II) **(CuL7)**. Each of the ligand molecules acts in a monodentate manner coordinating through the pyrazine and quinoxaline nitrogen, meanwhile, four acetate groups had attached to the copper ion in order to stabilize the positive charge on the cation. Each two acetates groups will produce a bridge that will connect to the copper ion. The fluorescence characteristics for complexes shown several of trends and it depend on several factors such as π system, structural rigidity, solvent polarity, substitutions effects, concentrations, dissolved oxygen and heavy metal quenching effects. As e for $\pi - \pi^*$ transition is maximum, it is advantageous that a fluorophore. Fluorophore contain π system and preferably an aromatic ring. Structural rigidity or collisional deactivation is a major fluorescence quenching mechanism. Therefore, molecules possessing rigid structures are better fluorophore than others with lack rigidity. It can be seen that the substituent effects does play a big role on fluorescence results. The compounds with withdrawal group such as

chloro group showed a decrease in intensity. On the other hand, the presence of donating groups such as methyl group showed an increase in fluorescence. The positions of the substituent also give effect on the fluorescence readings. The fluorescence intensity is slightly greater if the methyl group is located at a *meta*-position compared to *para*-position. At low concentrations the fluorescence intensity is proportional to the concentration of the fluorophore. Polar solvents with higher dielectric constant showed an increase in fluorescence intensity since the energy for π - π^* transition is lowered and may become less than n - π^* transition leading to increased absorption, and thus emission. Molecules that contain lone electron pairs (nonbonding electrons) tend to be weaker fluorophore. This is because n electrons increase intersystem crossing and thus decrease fluorescence. Molecular oxygen is paramagnetic which increases intersystem crossing through triplet - triplet interaction. Oxygen is thus a good fluorescence quencher and is sometimes determined by its quenching characteristic. Generally, the fluorescence intensity in complexes is lower compared to the intensity of ligands. This phenomenon can be explained by the heavy metal effect. Heavy metals increase the intersystem crossing which is leading to decreased in fluorescence intensity. This is most obvious with paramagnetic heavy metals such as copper(II) ion. This observation can be explained by occurrence of PET process and the formation of hydrogen bonding between the ligands and copper ion.

REFERENCES

1. Barlin G.B., (1982), *The Chemistry of Heterocyclic Compounds,* **41**, John Wiley and Sons, p. 194-196.
2. Staedel W., Rügheimer L., (1876), *die Einwirkung von Ammoniak auf Chloracetylbenzol* **1(9),** p. 563 – 564.
3. Gutknecht H., (1879), *Mittheilungen Ueber Nitrosoäthylmethylketon,* **2(12),** p. 2290-2292.
4. Cheeseman G. W. H., Ronald Frederick Cookson, (1979), *Chemistry of heterocyclic compounds,* (**35)**, Wiley-Blackwell, p. 164.
5. John Arthur, Keith Mills, (2000), *Heterocyclic chemistry*, **4,** Wiley-Blackwell, p.195-196.
6. Ha. T.G., Jang, J.J., Kim, S.G., Kim, N.D., (1999), *Chemico-Biological Interactions.* **121 (2)**, p. 209–222.
7. Myadaraboina K. S., (2010), *European Journal of Medicinal Chemistry*, **45,** p. 5208-5216.
8. Rochon F.D., Dieng P.S., (2008), *Inorganica Chimica Acta.*, **361,** p. 1222–1230.
9. Adams T.B., (2002), *Food and Chemical Toxicology*, **40**, p. 429–451.
10. Tang X., (2003), Chinese Herbal Drugs, **26(8)**, p.611-612.
11. Cao W. F, Li R. H, and Chen B. X, (1997), Chinese Journal of Integrated Chinese and Western Medicine., **17(5)**, p. 314-315.
12. Sylviane Giorgi-Renault, Jean Renault, Patricia Gebel-Servolles, Michel Baron, Claude Paoletti, Suzanne Cros, Marie Christine Bissery, Francois Lavelle, Ghanem Atassi (1981), Eur. J. Med. Chem., **16(6)**, p. 545-550.
13. Xianghong Wu, Anne E. V. Gorden, (2007), J. Org. Chem., **72**, p. 8691-8699.
14. Elwahy A. H. M., (2000), *Tetrahedron,* **56**, p. 897–907.
15. Brown D.J., (2004), *The Chemistry of Heterocyclic Compound,* Vol. 2, John Wiley and Sons, p. 224-226.
16. Garoufis A., Kasselouria S., Boyatzisb S., Raptopoulouc C.P., (1999), *Polyhedron,* **18, p.**1615 –1620.
17. Khan S. A., Saleem K., Khan Z., (2007), *Eur. J. Med. Chem*., **42**, p. 103.
18. Jaso A., Zarranz B., Aldana I., Monge A., (2003), *Eur. J. Med. Chem*, **38**, p. 791.

19. Monge A., Palop J. A., López de Ceráin A., Senador V., Martínez-Crespo F. J., Sáinz Y., Narro S., García E., De Miguel C., González M., Hamilton E., Barker A. J., Clarke E. D., Greenhow D. T., (1995), *J. Med. Chem*, **38**, p. 1786.
20. Weber, E.; Vo¨gtle, F. Ed.; Pergmon, (1996), *In Comprehensive Supramolecular,* Vol. 2, New York, p. 25.
21. A. H. M. Elwahy, (2000), *Tetrahedron,* **56**, p. 897–907.
22. Annick Estevez, Miguel Quiliano, Asunción Burguete, Billy Cabanillas, Mirko Zimic, Edith Málaga, Manuela Verástegui, Silvia Pérez-Silanes, Ignacio Aldana, Antonio Monge, Denis Castillo, Eric Deharo (2011), *Experimental Parasitology,* **127(4),** p. 745–751.
23. Nelilma C. Romeiro., Gabriela Aguirre, Paola Hernández, Mercedes González, Hugo Cerecetto, Ignacio Aldana, Silvia Pérez-Silanes, Antonio Monge, Eliezer J. Barreiro, Lídia M. Lima, (2009), *Bioorg. Med. Chem*., **17**, p. 641-652.
24. De Souza, W., (2007), *Microbes and Infection*, **9**, p. 544–545.
25. Saari R., Torma J.C., Nevalainen T., (2011), *Bioorg Med Chem*, **19**, p.939.
26. Jie Liu, Tixiang Zhang, Tongbu Lu, Lianghu Qu, Hui Zhou, Qianling Zhang, Liangnian Ji, (2002), *Journal of Inorganic Biochemistry,* **91**, p. 269 –276.
27. Turnlund J. R., Copper In., Shils M. E., Olson J. A., Shike M., Ross A. C., (Eds.), (1999). *Modern Nutrition in Health and Disease.* Lippincott Williams and Wilkins, Baltimore MD.
28. Knobeloch L., Schubert C. & Hayes J. (1998). *Wisc. Med.* **97,** 49 – 53.
29. Winge D. R. & Mehra R. K. (1990), *Int. Rev. Exp. Pathol.* **31,** 47 – 83.
30. Klein W. J., Metz Jr. E. N. & Price A. R. (1972), *Arch. Inter. Med.* **129,** 578 – 582.
31. Strausak D., Mercer J. F., Dieter H. H., Stremmel W., Multhaup G. (2001), *Brain Res. Bull.* **55,** 175 – 185.
32. Cobine P.A., Pierrel F., Winge D.R., (2006), *Biochim. Biophys. Acta,* **1763,** p. 759–772.
33. Mondola P., Serun R., Damiano S., Santillo M., (2007), *Cent. Eur. J. Biol.,* **2,** p. 337–350.
34. Szauter K.M., Cao T., Boyd C.D., Csiszar K., (2005), *Pathol. Biol.*, **53,** p. 448–456.
35. Madsen E., Gitlin J.D., (2007), *Annu. Rev. Neurosci*., **30,** p. 317–337.

36. Crouch R.K., Kensler T.W., Oberley L.W., Sorenson J.R.J., Karlin K.D., Zubieta J. (Eds.), (1985), *Biological and Inorganic Copper Cheimstry,* Vol. 1, Adenine Press, Guilderland, NY, p. 1397.
37. Brown D.H., Smith W.E., Teape J.W., Lewis A.J., (1980), *J. Med. Chem.,* **23,** p. 729.
38. Gehad G.M., Nadia E.A.E.-G., (2004), *Vibrational Spectroscopy*, **36**, p. 97–104.
39. Mark J. Cain, Anthony Cawley, Vivienne Sum, Dearg Brown, Mark Thornton-Pett, Terence P. Kee, (2011), *Inorganica Chimica Acta*, **369**, p.55–61.
40. Cerecetto, H., González, M., (2001), *Mini. Rev. Med. Chem*., **1**, p. 219.
41. Maria H. Torre, Dinorah Gambino, Jeannette Araujo, Hugo Cerecetto, Mercedes Gonzalez, Maria Laura Lavaggi, Amaya Azqueta, Adela L pez de Cerain, Antonio Monge Vega, Ulruch Abram, Antonio J. Costa-Filho., (2005), *European Journal of Medicinal Chemistry*, **40,** p. 473–480.
42. O'Reilly J. E., (1975), *J. Chem. Ed*., **52**, p. 610.
43. Ludwig Brand, Sidney P. Colowick, Michael L. Johnson, Nathan Oram Kaplan, (2008), *Fluorescence spectroscopy,* Vol. 450, Academic Press, p. 112.
44. Joseph R. Lakowicz, (2006), *Principles of fluorescence spectroscopy* (**3rd Ed**.), Vol.1, Springer, p. 24.
45. Martin Hof, Hutterer R., Vlastimil Fidler, Fidler V., (2005), *Fluorescence spectroscopy in biology*, Springer, p. 4-5.
46. Rendell, D., David Joseph Mowthorpe, (1987), *Fluorescence and Phosphorescence*, Wiley, p. 44-45.
47. Eisinger, J., Flores J., (1979). *Analytical Biochemistry* **94** (1), p. 15–21.
48. Sharma, A., Schulman, S. G., (1999), *Introduction to Fluorescence Spectroscopy*. Wiley Interscience, p. 11- 13
49. Moerner W.E, Kador L, (1989), *Phys Rev Lev*, **57(14), p.** 1699-1702.
50. Kamil Kopecky, Dalibor Šatinský, Veronika Novakova, Miroslav Miletin, Antonín Svoboda, Petr Zimcik (2011), *Dyes and Pigments,* **91**, p. 112-119.
51. Zheng, Liang-Wen, Gong, Zhong-Liang, Liu, Wen-Long, Liu, Ying-Rui, Zhao, Bao-Xiang, (2011), *Spectrochimica Acta Part A*, **81,** p. 372– 379.
52. Yan-hua Li, Bao-dui Wang, Zheng-yin Yang, (2007), *Spectrochimica Acta Part A*, **67,** p.395–401.

53. Oldham, P. B., McCarroll, M. E., McGown, L. B., Warner, I. M., (2000), *Anal. Chem.*, **72**, p. 197–209.

54. Apperson, K., Leiper, K. A., McKeown, I. P. and Birch, D. J. S., (2002), *J. Inst. Brew.*, **108**, p. 193–199.

55. Persson, T., Wedborg, M., (2001), *Anal. Chim. Acta*, **434**, p.179–192.

56. Jin-Min Li, Jing-Min Shi, Chang-Ju Wu, Wei Xu, (2003), *J. Coord. Chem*., Vol. 56:**10**, p.869-875.

57. Chang, R. and Cruickshank, B. (2005), *Chemistry* (8th Ed.), McGraw Hill, New York, p.917.

58. Coulson, E. A., Hales, J. L., Herington, E.F.G. (1951). *J. Chem. Soc*. **261**, p. 2125-2128.

59. Wan Ainna Mardhiah Wan Saffiee, Azila Idris, ZaharahAiyub, Zanariah Abdullah and Seik Weng Ng, (2011), *Acta Crystallographica Section E*, **(728).**

60. Venkateswar Rao P., S. Sammanni, A. Kalidasu, (2011), *Journal of Chemistry*, **8(1),** p. 470-478.

61. Veeraraj, A., Sami, P., Raman, N., *Proc. Indian Acad. Sci.* (*Chem. Sci.*), (2000), **112(5),** p.515–521.

62. Sudhamani, C. N., Bhojya Naik H. S., Girija, D., Aravinda, T., *International Research Journal of Pure & Applied Chemistry*, (2011), **1(2)**, p. 42-57.

63. Emsley J., Raza N. M., Dawes H. M., and Husthouse M. B., *J. Chem. Soc.*, (1986) p.313.

64. Jain A., Goyal R., and Agarwal D. D., (1981), *J. Inorganic Nuclear Chem*. **43**

65. West D.X., Swearingen J.K., Martinez J.V., Ortega S.H., El-Sawaf A.K., Meurs F.V., Castineiras A., Garcia I., Bermejo E., (1999), *Polyhedron*, **18**, p. 2919

66. Vincenzo Balzaniu, *Photophysics of Transition Metal Complexes in Solution*, Department of Chemistry .G. Ciamician, University of Bologna, Italy, p. 2-3.

67. Rao, C.N.R., (1967), *Ultraviolet and visible spectroscopy chemical applications.* (2nd Ed.), Butterworth & Co. (Publishers) Ltd, London, p. 203

68. El-Behery M. and El-Twigry H., (2007), *Spectrochimica Acta Part A*, **66**, p. 28–36.

69. Sreekanth, A. and Prathachapachandra Kurup, (2003), *Polyhedron*, **22,** p. 3321-3332.

70. Meissler, Gary L., Tarr, Donald A., *Inorganic Chemistry*, (**3**), Pearson Education Inc, 2004.

71. B. Bersucker, *Coord. Chem. Rev.*, 1975, **14**, 357
72. Allan J. R., Baillie G. M., and Baird N. D., *J. Coord. Chem. 10*, (1980) p.171.
73. Hartmut Yersin, (1997), *Electronic and Vibronic Spectra of Transition Metal Complexes*, Vol. 2, Springer, p. 5-6.
74. Ressalan S., Iyer C. S. P., (2005), *Journal of Luminescence*, **111**, p.121–129.
75. Casellato U., Guerriero P., Tamburini S., Vigato, P. A., Benelli, C., (1993), *Inorg. Chim. Acta*, 207, p.39.
76. Yadav L. D. S., (2005), Organic Spectroscopy, Springer, p.16.
77. Abdullah, Z., Tahir, M. N., Abas, M.R., Low, B.K., and Aiyub, Z. (2004), Molecules, **9**, p.520-526.
78. Stevenson, P.E., *J. Chem. Soc*., 1974, p.204.
79. Mishina S., Takayanagi M., Nakata M., Otsuki J., Araki K., (2001), *Journal of Photochemistry and Photobiology A:Chemistry*, 141(**2-3**), p.153-158.
80. Peter T.C So, Chen Y Dong, (2002), *Encyclopedia of Life Sciences*, Macmillan Publishers Ltd, Nature Publishing Group, p.2-3.
81. Guibault G. G.., *Molecular Fluorescence Spectroscopy in Comprehensive Analytical Chemistry*, Elsevier Scientific Publication Company, 1977, **(VIII),** Chapter 2.
82. Khopkar S. M., (1998), *Basic Concepts Of Analytical Chemistry*, **(2),** New Age International, p.297-302.
83. Liang Ding, Yu-Qi Din, Qi-Wen Teng and Ke Wang, *J. Chin. Chem. Soc.*, 2007, **54,** p. 853-860.
84. Weisstuch, A., and Testa, A.C., *J. Ph. Chem. Soc*., 1957, **74**, p.2999.
85. Sidman, J. W., Chem. Rev., 1958, **58,** p.689.
86. Kasha, M., Pimentel, G. C., *J. Am. Chem. Soc.*, 1957, **79**, p.3323
87. Bowen and Norton, (1939), *Trans Faraday Soc*, **38**, p.44.
88. Weil-Malherbe and Weiss, (1942), *Nature***, 149**, p.471.
89. Miller, J. A., Baumann, C. A., (1943) *J. Am. Chem. Soc.*, **65 (8),** p.1540–1546.
90. Yu hui Yang, De he Zhang, 1995, *Communications in Soil Science and Plant Analysis*, 26(15-16), p.2333-2349.
91. Joseph R. Lakowicz, (2006), *Principles of fluorescence spectroscopy*, **1(3),** Springer, p.336-338.

92. Elliot B. Jones Jr., Donald J. Nelson, Mark M. Turnbull, (1992), *Journal of Inorganic Biochemistry*, 45(**2**), p.85-92.

93. Schulman, S. G., (1997), *Fluorescence and Phosphorescence Spectroscopy,* Pergamon Press, New York, p.138- 150.

94. Hariharan, C., Vijaysree, V., Mishra, A. K., (1997), *Journal of Luminescence*, **75(3**), p.205-211.

95. Roth, H. D., (1990), *Photoinduced Electron Transfer I*,**(5)** Springer-Verlag, Heidelberg.

96. C. D. Lindstrom and X.-Y. Zhu,(**2006),** Chem. Rev.**,** 106(10), p.4281□-4300.

97. Griesbeck, A. G., Mattay, J., **(2007),** *Acc. Chem. Res.*, **40(**128).